Investigating the role of Protein Kinase D1 (PRKD1) in adipose tissue thermogenesis

By

Mark Kamau Alexander Crowder

Dissertation

Submitted to the Faculty of the

Graduate School of Vanderbilt University

in partial fulfillment of the requirements

for the degree of

DOCTOR OF PHILOSOPHY

in

Pharmacology

June 30, 2023

Nashville, Tennessee

Approved:

Joey Barnett, Ph.D. (chair)

Sheila Collins, Ph.D.

Sean Davies, Ph.D.

Ann Richmond, Ph.D.

Brian Wadzinski, Ph.D.

ACKNOWLEDGMENTS

I am deeply grateful for how much I have learned during my time at Vanderbilt. I'd like to thank my advisor, Dr. Sheila Collins and my committee, Drs. Joey Barnett, Sean Davies, Ann Richmond, and Brian Wadzinski. Many thanks also to my funding sources including the Vanderbilt Department of Pharmacology T32 training grant, Initiative for Maximizing Student Diversity, other National Institutes of Health sources, and the American Heart Association. A special thanks is owed to Dr. Lee Limbird, a longtime mentor.

Table of Contents

List of Tables

List of Figures

Chapter I: Introduction to brown adipose tissue development and signaling

The relationship between obesity and fat deposition in adipose tissue

Adipose tissue (AT) evolved as a survival organ in mammals – storing nutrients when food sources were plentiful for later use during periods when food was scarce. Understanding AT function and its regulation has become increasingly important as obesity continues to rise in the U.S. and global populations (1). In an obese person, adipocyte numbers and volume expand (2-5), but often not in sufficient amounts to accommodate the excess calories. This can lead not only to adipocyte cell death and release of triglycerides into the AT milieu and circulation (6), but the inappropriate deposition of lipid species in other organs such as liver, skeletal muscle and pancreas resulting in significant disturbances of the normal functions of these organs (7-10).

Obesity is clinically defined by the body mass index (BMI), which is calculated as weight (kg) divided by height (m^2) (11). Obesity is operationally defined as a BMI value > 30 (12), which now affects at least 1/3 of the United States population; another 1/3 of the population is overweight (BMI > 25-29) (13). The rise of obesity is a major contributor to several chronic diseases such as Type II diabetes and cardiovascular disease in the US and worldwide (14-16). Obesity and its complications have been attributed to sedentary lifestyle (lack of exercise), diet (overconsumption of calories, particularly as unhealthy fats or carbohydrates), and environmental factors (13). However, even people adherent to dietary and exercise regimes often have trouble reducing or maintaining their body weight. Indeed, in less than 50 years our modern lifestyle has little need for physical exertion, and yet we still eat three meals a day. Early efforts to study energy expenditure in humans focused on the effects of a variety of physical activities and their duration on oxygen consumption. In fact, in some early studies, duration of physical activity was considered a better indicator of expending energy than the activities themselves (17). A logical conclusion to be drawn from the aforementioned studies is that longer periods of exercise offer more metabolic benefits. While this may be true, recent work has shown that short bursts of vigorous physical movement, even in those who don't exercise, can greatly reduce mortality (which has a strong positive correlation with obesity) (18-20). Currently exercise is thought to promote weight loss by redistribution of energy stores to energy-expending tissues, thus reducing AT mass (21).

Additional efforts to curb the increasing population of overweight individuals were therapeutic in nature. Behavioral therapy to reduce food consumption was once considered a standard-of-care for individuals carrying

excess fat. Psychiatrists posited that dysfunction in the brain led to overeating and encouraged their patients to modify their eating habits as a means of both reducing and preventing weight gain (22). Other therapeutic interventions included drugs like dinitrophenol, a nonspecific mitochondrial uncoupler that killed many of those who ingested it (23), as well as more recently a role for bariatric surgery to reduce the size of the stomach and improving insulin sensitivity (24). While therapies (behavioral or pharmacological in nature) aimed to treat obesity have been largely unsuccessful, surgical interventions have a demonstrated record of success in producing rapid weight loss in the morbidly obese (25). Nonetheless, some individuals undergoing bariatric surgery eventually regain much of the weight lost after surgery (24). A key point to make here is that even when BMI remains high (>40) in patients having undergone bariatric surgery, insulin sensitivity is still significantly improved relative to the pre-surgical state (26). The methods of recourse for weight regain, though, are limited: undergo surgery again (27) or rely on diet and exercise to maintain a healthy weight. New therapeutic advances show promise as alternatives to bariatric surgery. A new drug class which mimics the actions of glucagon-like peptide 1 (GLP1) *in vivo* has shown great efficacy in improving insulin sensitivity and promoting weight loss (28). Rybelsus and Ozempic (semaglutide, administered orally or by injection respectively, Novo Nordisk) are standard examples of this drug class. Plenity (an orally administered superabsorbent hydrogel, Gelesis) induces weight loss by reducing “available” stomach volume, similar to bariatric surgery (29). Also, a new FDA-approved drug, Mounjaro (tirzepatide, an injectable glucagon-like peptide receptor 1/ glucose-dependent insulinotropic polypeptide receptor [GLPR1/ GIPR] dual receptor agonist, Eli Lilly), can reduce body weight by over 20% and improve insulin sensitivity with greater efficacy than GLPR1 agonists but requires lifelong administration (30).

Given the relationship of obesity to high morbidity diseases like Type II diabetes and cardiovascular disease, it is crucial to explore additional ways of preventing and reducing fat accumulation. In particular, obesity drives whole-body inflammation, leading to increased risk and incidence of the aforementioned co-morbidities (31-33). While there will always be an important role for a healthy and moderately portioned diet and physical activity, it is important to understand in detail the hormonal signaling pathways that regulate healthy adipose tissue physiology and how they go awry in obesity. Understanding the intracellular signaling downstream of critical hormonal pathways regulating adipose tissue biology opens the door for the discovery of novel therapeutic targets that can be pharmacologically modulated for the benefit of human health – in particular, to

eliminate the obesity epidemic and its metabolic consequences. This dissertation research has been intended to reveal some of these not yet understood regulatory mechanisms.

What is adipose tissue?

AT exists in discrete depots throughout the body; collectively, these depots have been referred to as 'the adipose organ' (34). The parenchymal cell of the adipose organ is the adipocyte of which there are three types: white, brown, and beige (Fig. 1). White and brown adipocytes exist in adipose depots specifically known as white adipose tissue (WAT) and brown adipose tissue (BAT) respectively (34). Beige adipocytes represent an adipocyte with functional plasticity. These cells are usually found in WAT but relative to white and brown adipocytes display an intermediate phenotype. Also, AT secretes adipokines such as leptin and adiponectin which regulate whole body metabolic function (35-39). Each adipocyte type possesses distinct features that facilitate its unique functions.

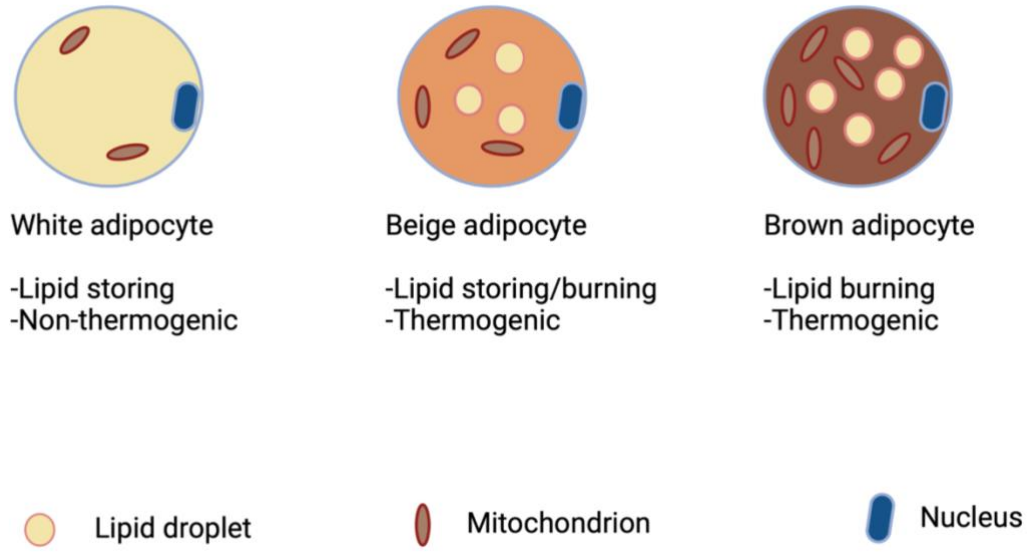

Figure 1: Types of adipocytes. White adipocytes are unilocular (one large lipid droplet), lipid storing and non-thermogenic. Brown adipocytes are lipid catabolizing (burning) cells with multiple small lipid droplets. They are also thermogenic. Beige adipocytes display an intermediate phenotype between brown and white adipocytes.

White adipose tissue. A key function of WAT is the synthesis and storage of triglycerides, which can later be released during periods of nutrient deprivation (40, 41). The parenchymal cells of WAT, called white adipocytes, have certain defining characteristics related to their energy-storing function. White adipocytes are unilocular (possess one large, single lipid droplet), a nucleus, and have a modest number of mitochondria. These

lipid-rich white adipocytes are responsible for the eponymous yellowish-white color of WAT (42, 43). Additionally, the expansion of WAT is primarily responsible for the weight gain observed in individuals with obesity, particularly, in humans the visceral WAT (44, 45).

Given the importance of AT as a fuel reserve during periods of nutrient deprivation, it is critical that the storage and release of this fuel is tightly controlled. This fuel is stored in the form of triglycerides (TGs) (46). A TG consists of a glycerol molecule (propan-1,2,3-triol) with a free fatty acid (FFA) esterified to each of the three alcohol groups. Glycerol can be found in the body as a metabolite of glucose (47). FFA molecules that are incorporated into TGs can be consumed from the diet or made endogenously via *de novo* lipogenesis (DNL) (48, 49).

DNL can occur in a variety of tissues including adipose, skeletal muscle, and the liver (49-51). The primary precursor for DNL is acetyl CoA (49), which is generated from citrate (not pyruvate as is the case for acetyl CoAs entering the TCA cycle). Citrate, produced by the TCA cycle, is exported from the mitochondria into

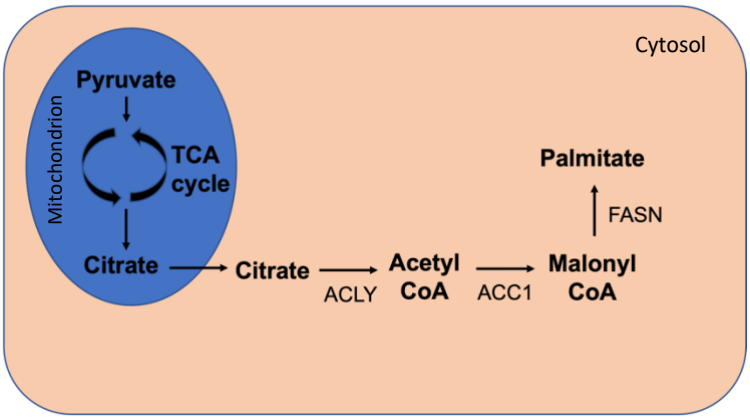

Figure 2: *De novo* lipogenesis pathway. Citrate from the TCA cycle can also produce acetyl CoA. Nonetheless, ACC1 converts acetyl CoA into malonyl CoA, which is then used as a substrate by FASN to make palmitate. Palmitate can be used to make longer chain fatty acids by the stearoyl coA desaturase (SCD) and ELOVL family of enzymes.

the cytosol and converted to acetyl CoA by the enzyme ATP citrate lyase (ACLY) for DNL (52). Next, acetyl CoA carboxylase 1 (ACC1), using citrate-derived acetyl CoA as a substrate, produces malonyl CoA (53). Finally, fatty acid synthase (FASN) catalyzes the conversion of malonyl CoA into palmitate (C16:0) (54), though longer FA chains can sometimes be made by FASN and through the action of the elongation of very long chain fatty acids (ELOVL) family of enzymes (Fig. 2) (55). These newly made FFA are then used to synthesize TGs for immediate energetic use or storage in WAT or BAT. These TGs can later be released under conditions of increased energy demand by a tightly controlled process known as lipolysis (56). Lipolysis is the hydrolysis of TGs that release

FFAs from adipocytes as needed during periods of nutrient deprivation or increased energy demand (i.e., exercise, starvation).

WAT also secretes hormones, known as 'adipokines', that play key physiological roles in modulating whole organism metabolism (39, 57, 58). Two of the most well-known hormones secreted from WAT are leptin and adiponectin (2, 59, 60). Leptin is a satiety hormone that is secreted in proportion to WAT mass (60) and is encoded by the *ob* gene (short for *obese*) for the early discovery that leptin deficiency results in obesity (36, 61, 62). In AT, leptin expression is regulated by adipose tissue mass, fasting, and re-feeding (63, 64) and its expression can be regulated by C/CAAT enhancer binding proteins (C/EBPs) (65). Leptin has been reported to also be expressed in the hypothalamus and pituitary gland (66, 67). Leptin action in the hypothalamus reduces food intake and increases sympathetic nervous system tone; loss-of-function animal models for leptin and its receptor reveal both diabetic and obesogenic phenotypes (37, 68). Adiponectin (AdipoQ), unlike leptin, is secreted in a manner inversely proportional to WAT mass (38). Transcriptionally, its expression is regulated primarily by peroxisome proliferator activated receptor γ (PPARγ) and C/EBPα (69). Plasma AdipoQ levels in rodents and humans are positively correlated with improved insulin sensitivity and high-density lipoprotein (HDL) cholesterol levels, suggesting that AdipoQ protects against both diabetes and heart disease (70).

WAT also contains other cell types including immune cells, endothelial cells, preadipocytes, neurons, and stem cells, which are collectively called the stromal vascular fraction (SVF) of AT (71). These cells play an important role in supporting adipose tissue function. Immune cells (T regulatory cells and macrophages) act as important modulators of the adipose tissue microenvironment, cleaning up dead adipocytes and cellular debris (72, 73). Immune cell migration to adipose tissue is currently seen as a major contributing factor to adipose tissue inflammation and fibrosis that are thought to drive many of the negative health effects associated with obesity (72-74).

Brown adipose tissue. The second major adipose type is BAT (75). BAT also has an important evolutionary function in mammals, non-shivering thermogenesis (heat production), which helps to maintain temperature homeostasis (76, 77). Skeletal muscle also conducts a form of thermogenesis known as shivering thermogenesis that is activated during the initial phases of cold exposure (78, 79). Thermogenesis in BAT is enhanced as a more effective means ~~secondary response when shivering thermogenesis is insufficient~~ to

maintain core body temperature (79). Nonetheless, the amount and activity of BAT in humans and rodents is associated with improved metabolic health, namely improved glucose homeostasis and insulin sensitivity (80-82). These positive metabolic benefits are attributed to the thermogenic function of BAT (81, 83). As an example, mice transplanted with mouse BAT had improved glucose homeostasis relative to sham-operated mice (84). These observed improvements in glucose handling could be further potentiated by increasing the amount of BAT transplanted. Additionally, in humans, where BAT transplantation studies are more difficult to perform, studies in which BAT was activated using cold exposure demonstrate that BAT promotes euglycemia and improved insulin sensitivity (80, 85). BAT activity also promotes lipid oxidation, suggesting that BAT promotes excess fuel uptake from the bloodstream, ultimately preventing the storage of these fuels in WAT. Due to this mechanism of fuel disposal, BAT amount and activity, despite its classification as AT, are negatively correlated with obesity risk. In aging humans, the amount and activity of BAT are reduced and this decline in BAT function is associated with the onset of a variety of metabolic diseases, including Type 2 diabetes, obesity, and their associated co-morbidities (86-88). There is still much debate as to the number and location of BAT depots in humans, but positron emission tomography (PET) imaging studies using radiolabeled glucose have revealed a prominent BAT depot in the neck or supraclavicular region (89, 90). However, there are several other “hot spots” in these studies, namely along the sternum and spine, that may represent *bona fide* BAT (91) or “beige” adipocytes, which will be discussed in the next section. In rodents, the most commonly studied BAT depot is the interscapular BAT (iBAT), though others can exist that can be found around visceral organs (34, 92). Despite the disparity in location, murine and human BAT currently appear to function in a similar manner (93), although the study of adult human brown adipocytes is only about a decade old.

Several key physiological features of BAT allow it to carry out its thermogenic function. Unlike white adipocytes, brown adipocytes have multiple, small lipid droplets within them (multilocular), hypothesized to enhance access to stored lipid for use as fuel during cellular respiration and thermogenesis (94, 95). Furthermore, to sustain high levels of thermogenesis, BAT is dense in mitochondria, the cellular “energy factory”. Along with a dense mitochondrial network, robust glucose and free fatty acid uptake into BAT, in addition to lipids stored intracellularly, enable the high levels of respiration required for thermogenesis (83, 96, 97). This mechanism of fuel uptake is thought to contribute to the beneficial metabolic effects of BAT primarily by clearing

excess glucose and fatty acids from the blood resulting in improved glucose tolerance and insulin sensitivity (80, 98).

Mitochondrial function is crucial to BAT thermogenesis. During brown adipocyte development, increases in *Pgc1α* expression primarily drive mitochondrial biogenesis (99). Given its high respiratory capacity, one might assume that the high mitochondrial density of BAT is solely responsible for its thermogenic capacity. However, thermogenesis is achieved in BAT not due to standard, electron-coupled respiration, but rather a unique mechanism known as "uncoupled respiration". BAT expresses a unique protein called uncoupling protein 1 (UCP1), a proton (H+) pump that sits in the inner mitochondrial membrane (100).

Uncoupled respiration, as the name implies, uncouples proton (H+) movement from ATP production. There are 5 mitochondrial protein complexes involved in cellular respiration: Complexes I-V (101). Importantly, complexes 1, 3, 4, and 5 act as H+ pumps (Fig. 3) (101).

Complexes 1,3, and 4, in addition to and coupled with their redox capacities, pump H+ into the inner membrane space, which produces a H+ gradient with higher [H+] in the inner membrane space and a lower [H+] in the matrix (101).

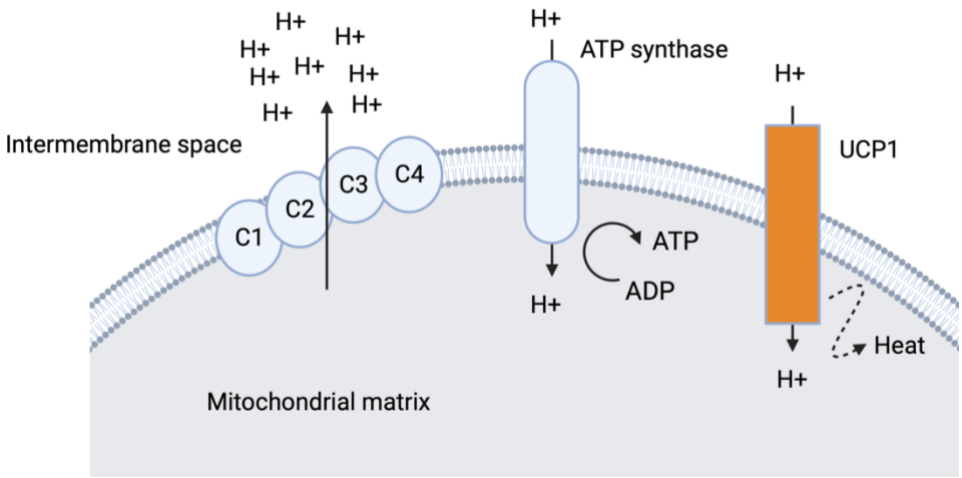

Figure 3. Role of UCP1 as an uncoupler of mitochondrial respiration. During standard (coupled) respiration, the first 4 mitochondrial complexes pump H+ from the matrix to the intermembrane space. ATP synthase then moves H+ down their concentration, harnessing this chemical energy to make ATP. UCP1 offers an alternative path to H+ movement. H+ movement through UCP1, as indicated in the diagram, is released as heat, resulting in thermogenesis.

Of the 5 mitochondrial H+ pumps, ATP synthase is the only pump that moves H+ down their concentration gradient across the inner membrane and into the matrix. ATP is subsequently produced, harnessing the chemical energy released by H+ moving down their concentration gradient (101, 102). UCP1 dissipates the H+ gradient

by moving H+ down their concentration gradient without synthesizing ATP (Fig. 3) (103). This bypass of the normal H+ movement through ATP synthase is called 'proton leak'.

The chemical energy produced by H+ movement down its concentration gradient through UCP1 is released as heat rather than being used to make ATP (104, 105). This H+ motive force (pmf) is sufficient to produce the energy needed to drive ATP synthesis and/or thermogenesis (77, 106). Brown adipocytes increase their mitochondrial oxidation of metabolic substrates (e.g., glucose, fatty acids) to maintain both thermogenesis and ATP production in the face of enhanced UCP1-mediated proton leak (107, 108).

The major physiological regulator of BAT activity is the catecholamine norepinephrine (NE) that is released from sympathetic neurons innervating the tissue (109). The heat generated in brown adipocytes can then be distributed through the body by the dense vasculature within BAT. NE regulation of brown adipocytes occurs via binding with its cognate receptors, β-adrenergic receptors (β-ARs) – of which there are three isoforms, β_1-AR, β_2-AR, β_3-AR (110). There is also a small contribution of α_1-ARs to the control of thermogenesis (111). NE enhances a gene expression program required for the primary function of BAT: thermogenesis (112, 113) (discussed in greater detail below in section, **β-AR signaling in BAT**). This neurotransmitter acts both to promote the differentiation (114) and proliferative expansion (115) of brown adipocyte precursors during cold exposure. For example, prolonged cold exposure causes BAT hyperplasia (113). NE also increases mitochondrial number in BAT by upregulating peroxisome proliferator activated receptor coactivator 1 (*Pgc1α*), a master regulator of mitochondrial biogenesis, and estrogen related receptors (*ERRs*) (116), providing the cellular infrastructure to carry out thermogenesis. Uniquely, UCP1 is activated by FFA released during lipolysis in BAT (117), indicating that β-AR signaling orchestrates a complex system of processes to drive thermogenesis by both regulating the existing brown adipocyte machinery in addition to expanding its overall mass and respiratory capacity.

Another less well-characterized mechanism of BAT activation is mild psychological stress. In one study, women were administered a mild stressor (a math test) which elevated levels of cortisol, an endogenous steroid, in the saliva (118). This elevation in saliva cortisol levels was associated with enhanced skin temperature in anatomical regions believed to house BAT in humans, namely the supraclavicular region, suggesting enhanced BAT activity (118). While this study shows association, not causation, between elevated cortisol levels and

purported BAT activity, these findings are consistent with years of *in vitro* brown adipocyte studies wherein dexamethasone, a glucocorticoid (steroid), is required for full brown adipocyte differentiation. Additionally, other work has confirmed that glucocorticoid administration in humans activates BAT (119).

Lastly, it's important to note that changes in circadian rhythm also can modulate BAT function, altering metabolic health. Genetic deletion of brain and muscle ARNT-like 1 (*Bmal1*), a primary regulator of circadian rhythm, in BAT mildly reduced thermogenesis, but did not alter core body temperature (120). The authors of this study attribute the maintenance of body temperature to sustained shivering thermogenesis. One key observation was an increase in weight gain after HFD administration in *Bmal1* BAT knockout animals (120), providing evidence for an important role for circadian rhythm in metabolic health. In humans, single nucleotide polymorphisms (SNPs) in *Bmal1* and *Clock* (circadian locomotor cycles output kaput), a transcriptional partner of Bmal1, are associated with increased risk of obesity and Type 2 diabetes (121, 122).

Beige adipocytes. In many mammals, including rodents and primates, beige adipocytes (BeAs) are found in several WAT depots after physiological SNS stimulation, such as cold exposure or after exogenous administration of β-AR agonists (123, 124). This phenomenon is known as adipose tissue 'browning' or 'beiging'. These stimuli, as previously discussed, also drive BAT activity and expansion (124). Reduced sympathetic tone to BAT results in a "whitening" phenotype, wherein UCP1 expression and mitochondrial density are reduced, largely by organelle turnover and absence of the NE stimulus to maintain their levels (125). One example of BAT "whitening" occurs in mice housed at thermoneutrality (30 °C), a temperature at which the body has no need to endogenously maintain temperature homeostasis and thereby downregulates the physiological programs that promote it (126).

BeAs display phenotypes associated with both white and brown adipocytes. BeAs, relative to WAT, have higher expression of UCP1, mitochondrial genes and other genes characteristic of brown adipocytes, and are thermogenic (127). In humans, since no single *bona fide* BAT depot has been identified as it has in rodents (92), it is postulated that many of depots identified as BAT in humans may actually consist of beige adipocytes (128). The presence of UCP1+ adipocytes as well as imaging studies measuring glucose uptake into AT suggest that humans have physiologically active brown or beige fat (129-131). Nonetheless, debate still exists as to whether this UCP1+ AT is constitutive (as it is in mouse iBAT) or primarily activated by factors such as cold exposure,

which explains the lack of consensus as to whether this AT is brown or beige. There is a perception that targeting BeAs might represent a strategy for reducing the risk of obesity and Type 2 diabetes (132).

Two primary theories have been proposed regarding the cellular origins of BeAs primarily using lineage tracing studies in mice: 1) that mature white adipocytes undergo transcriptional changes (in response to NE or similar stimuli) that increase the expression of genes normally expressed in BAT (transdifferentiation), and 2) that BeAs are derived from a unique progenitor cell type that, in response to NE, differentiates *de novo* into BeAs (133). There is evidence supporting both hypotheses and it is possible that the browning phenomenon occurs due to contributions from both mechanisms. A key experimental model that provided evidence to support the hypothesis for transdifferentiation is a tamoxifen-inducible AdipoQ-Cre tDTomato reporter system in mice (134). tdTomato labeled cells in iWAT prior to cold exposure, representing mature white adipocytes, also expressed UCP1 after 7 days of cold exposure indicating that mature white adipocytes can upregulate UCP1 and develop features of beige adipocytes. These data support the transdifferentiation hypothesis. Another study revealed that mice exposed to cold followed by a return to room temperature contained white adipocytes that had once been UCP1+ (135). Now these data only suggest that beige adipocyte can return to a white adipocyte phenotype (i.e., supporting the notion that the mature white and beige adipocyte phenotype is interconvertible). However, these white adipocytes that had once been UCP1+ could have been developed from *de novo* differentiated adipocytes.

Other work has supported the *de novo* differentiation hypothesis. Experiments using the AdipoChaser model (a tetracycline-inducible reporter system) showed that newly developed UCP1+ adipocytes in WAT arose from both *de novo* differentiated adipocytes as well as adipocytes that had long been labeled by the AdipoChaser system (136). The results of other studies also support these findings (137). Thus, it is likely that a combination of both *de novo* differentiation and mature white adipocyte transdifferentiation contribute to the appearance of BeAs in WAT. Importantly, new evidence (132) suggests beige adipocytes are also associated with positive metabolic benefits. In my view, the strongest rationale for manipulation of BeA number and function to achieve therapeutic benefit is that BeAs can be recruited by pharmacological agonists. Under laboratory conditions, BeAs also can be acutely regulated by cold exposure in animal models (133). Removal of these pharmacological or environmental stimuli return BeAs to their features of white adipocytes with limited amounts of mitochondria and no longer producing UCP1 (133, 135).

The conversion of white adipocytes to BeAs is controlled by transcription factors whose expression and activity are induced primarily by adrenergic stimulation. As in brown adipocytes, *PPAR*γ and *Pgc1*α are upregulated during the white-to-beige adipocyte transition. One example of a transcription factor that regulates white verus beige adipocyte cell identity is zinc finger protein 423 (ZFP423). ZFP423 was identified as a transcription factor that is upregulated in adipose stem cells (adipocyte precursors or preadipocytes) versus non-adipogenic fibroblasts in WAT (138). However, when *Zfp423* mRNA expression was assessed in the 3T3-L1 adipocyte cell line and other known adipocyte cell lines, its expression was not significantly modulated during differentiation, indicating that *Zfp423* is not a primary driver of adipogenesis (at least in these WAT-derived adipocyte cell culture models)(138). Studies in mice showed that *Zfp423* mRNA expression is 2-3 fold higher in WAT depots than BAT leading to the hypothesis that this transcription factor may have distinct roles in regulating the biology of WAT versus BAT depots (139). The use of a doxycycline inducible AdipoQ-Cre *Zfp423* KO mouse model revealed that loss of *Zfp423* in WAT resulted in the recruitment of beige adipocytes as assessed by H & E staining and thermogenic gene expression. This result led the authors to ask whether the recruitment of beige adipocytes observed upon *Zfp423* loss in WAT was driven by *de novo* beige adipocyte differentiation or transdifferentiation of white adipocytes to the beige phenotype? To answer this question, a GFP reporter (expressed on a *Rosa26* floxed allele) mouse was crossed with the AdipoQ-Cre inducible *Zfp423* KO mouse such that mature adipocytes were labeled with GFP, while adipose stem cells were GFP-negative. The objective was to use a doxycycline pulse-chase approach to detect whether *Zfp423* loss induced beiging via *de novo* differentiation or transdifferentiation using a 7-day doxycycline pulse and a 3-week chase period. Since doxycycline induces both GFP expression and *Zfp423* KO in this model, the appearance of GFP-negative beige adipocytes after the chase would indicate that *Zfp423* loss in mature adipocytes somehow stimulates *de novo* beige adipocyte differentiation. If large numbers of GFP-positive beige adipocytes were detected after the chase in the GFP reporter AdipoQ-Cre *Zfp423* KO model, then this would suggest that *Zfp423* loss causes white-to-beige transdifferentiation as these GFP-positive cells had to be mature adipocytes before the 3-week chase period. After 7 days of doxycycline administration at room temperature, quantitative reverse transcriptase polymerase chain reaction (qRT-PCR) measurements in isolated mature adipocytes harvested from the iWAT revealed that *Zfp423* was efficiently deleted in this cell population and GFP immunofluorescence in iWAT showed

that nearly all adipocytes were GFP-positive as expected. After the 3-week chase period, large numbers of GFP-positive multilocular adipocytes were observed in the iWAT of *Zfp423* KO mice only (139), suggesting that *Zfp423* specifically regulates the white-to-beige conversion of mature adipocytes and not *de novo* differentiation. Upon cold exposure in this model after the 3-week chase period, both GFP-positive and GFP-negative BeAs were observed. This finding is consistent with studies previously discussed in this section establishing that *in vivo*, beige adipocytes are produced by both *de novo* and transdifferentiation. Lineage tracing assays are a novel and powerful tool for studying adipocyte development and differentiation.

The adipose developmental program: Tough choices for brown fat?

Developmentally, AT is derived from the mesoderm. Though it was initially thought that brown and white adipocytes were derived from a common progenitor (140, 141), it is now known that they originate from distinct precursor cell populations (142, 143). For the sake of providing a reasonably complete picture of adipocyte differentiation, white adipocyte differentiation is discussed here, though in significantly less detail than brown adipocyte differentiation as BAT function served as primary focus of the studies presented in this thesis. Several transcription factors and co-regulators – such as the C/EBPs and PPARγ – are necessary for the development and differentiation of adipocytes into both WAT and BAT. These transcriptional regulators increase adipogenic gene expression to allow for complete maturation of adipocyte precursors via a transcriptional positive feedback mechanism (144, 145).

White adipocyte development can be characterized by three stages of differentiation. The first stage is represented by 1) an uncommitted adipocyte precursor cell, which has been shown to be multipotent in *in vitro* differentiation experiments. Upon induction of key transcription factors, these precursors become 2) committed preadipocytes and eventually 3) mature lipid-containing adipocytes. Studies of white adipocyte differentiation have largely been done using stromal vascular fraction (SVF) cells from rodent and human AT and cultured adipocyte cell lines. The SVF contains numerous cell types including uncommitted adipocyte precursors (similar to mesenchymal stem cells), committed preadipocytes, as well as endothelial and immune cells (146, 147). AT SVF served as the first model of adipocyte differentiation *in vitro* (148, 149). Soon thereafter clonal cell lines were developed from rodent AT SVF that could be differentiated *in vitro* using an adipogenic cocktail: thiazolidinediones (TZDs, a family of PPARγ agonists), steroid hormones (dexamethasone), phosphodiesterase

inhibitors (isobutylmethylxanthine [IBMX]), insulin, and other factors (150-152). Notably, these models were all WAT-derived. Some of the adipocyte cell lines entered the canon of adipocyte biology as key models for studying the transcriptional cascades driving adipocyte differentiation. The primary one was the 3T3-L1 line (153). Other groups such as Spiegelman and colleagues used primary fibroblasts to study adipogenesis (154, 155).

These studies have led to the following model of white adipocyte differentiation. In both 3T3-L1 cells and primary fibroblasts, PPARγ expression is low under non-stimulated conditions (156, 157). While early studies revealed that PPARγ agonists could stimulate adipogenesis *in vitro* (158), the mechanisms of endogenous PPARγ activation in developing adipocytes *in vivo* remains unclear. Just prior to full PPARγ induction, the expression of C/EBP-β and C/EBP-δ transiently increases, which is hypothesized to further induce PPARγ and initiate C/EBPα expression (159, 160). PPARγ also interacts with retinoid X receptor (RXR) to fulfill its transcriptional role in adipogenesis (158, 161) Next, C/EBPα and PPARγ enter a positive feedback loop whereby each factor promotes the expression of the other ultimately leading to complete differentiation of white adipocytes (154, 162-164). The key features of full white adipocyte differentiation include 1) the appearance of lipid droplets and 2) expression of adipogenic genes including fatty acid binding protein 4 and the insulin receptor among others (154-156, 164, 165).

The identification and use of adipocyte precursor cell markers has provided additional insights into the development of ATs. However, WAT SVF contains many cell populations and the ability to distinguish between these cell types, particularly adipocyte precursors and committed preadipocytes, is critical to a robust understanding of adipocyte differentiation. Determining the role of adipocyte precursors and preadipocytes in the development of obesity is, of course, the primary aim of these studies. Initial work seeking to identify adipocyte precursors indicated that these cells expressed stem cell markers such as cluster of differentiation protein 29 (CD29), PDGFRα, and CD24 (3, 166, 167). Adipocyte precursors were also identified by the lack of expression of markers associated with other cell lineages, termed lineage-negative (lin-), indicating that the cells being identified as adipocyte precursors were a true adipose progenitor cell population and not uncommitted precursors of other cell lineages in the SVF such as endothelial cells (168). A key marker that distinguishes adipocytes precursors from committed preadipocytes is CD24, which is not expressed in committed preadipocytes (3, 169). More recent work by Hong and colleagues (170) hypothesized that adipocyte precursors

and preadipocytes could be detected in developing AT. To test this, embryonic inguinal adipose tissues were immunostained with perilipin-1 (PLIN1), a protein that exists within the membranes of lipid droplets within mature adipocytes (171). Rapid expansion of PLIN1+ cells was observed at various stages of embryogenesis. While these cells initially lacked lipid deposition, boron-dipyrromethane (BODIPY), a molecule used to recognize neutral lipids, staining at postnatal day 1 revealed that these rapidly proliferating populations of PLIN1+ cells indeed contained lipid droplets. Importantly, AT isn't fully developed in rodent embryos (172), consistent with the hypothesis that these PLIN1+ cells are not mature adipocytes, but adipocyte progenitors in the process of differentiation. The eventual co-localization of PLIN1 and BODIPY staining strongly suggested that this developing cell population was representative of adipocyte precursors or preadipocytes and positions PLIN1, thought to be a mature adipocyte marker (173), as a putative marker of adipocyte precursors and/or preadipocytes.

In brown adipocytes, these factors are regulated in a similar way, but given the differences in gene expression between white and brown adipocytes, other transcription factors also regulate the differentiation of the brown fat cell. One key difference between brown and white adipocytes is that brown adipocytes and skeletal myocytes share a common myogenic factor 5 (*Myf5*)-expressing progenitor (174, 175). Other defined markers of brown adipocyte precursors include the genes *Engrailed* (*Eng*) (176) and *Paired Box 7* (*Pax7*) (177). Brown

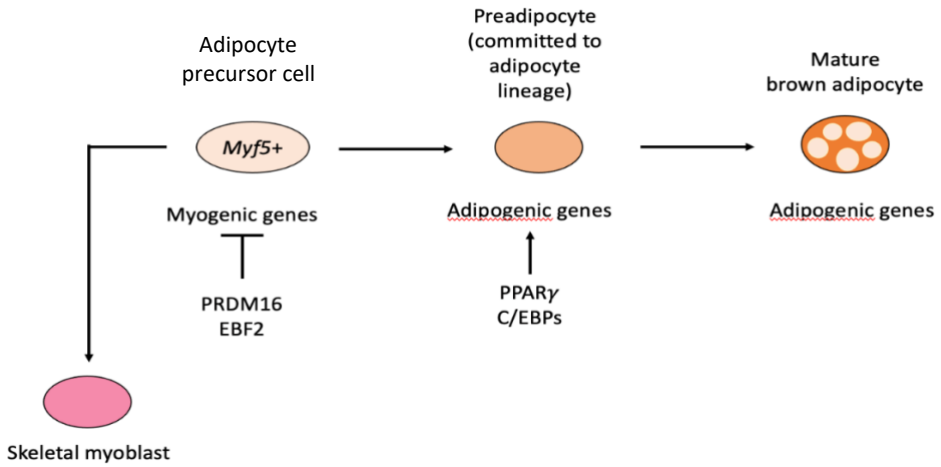

Figure 4: Brown adipocytes and skeletal myocytes share a common progenitor while white adipocytes develop from a distinct lineage. BAT and skeletal muscle are derived from *Myf5+* progenitor cells with PRDM16 being the major driver of brown adipocyte cell fate commitment over the skeletal myocyte lineage. The reasons why brown adipocyte precursor cells express a myogenic gene signature are not known or understood but may offer insights into the differences in function between brown and white adipocytes (the latter being derived from different progenitors).

adipocyte progenitors transiently express mRNAs for a host of genes that are normally expressed in the skeletal muscle (Fig. 4) (142, 175, 178). Since their discovery, key transcription factors that direct *Myf5*+ progenitors to the brown adipocyte lineage (versus the skeletal myocyte lineage) have been identified. One of the first was PRDM16.

PRDM16 was shown to drive the development and differentiation of brown adipocyte progenitor cells into mature brown adipocytes by acting as a PPARγ co-activator and does not appear to require direct binding of PRDM16 to DNA (174, 175). Reduced expression of PRDM16 in primary brown adipocyte cultures reduces adipogenic, but increases myogenic, gene expression. Furthermore, overexpression of PRDM16 in the C2C12 myoblast cell line leads to increased adipogenic gene expression and lipid droplet deposition in these cells, supporting the central role of PRDM16 (in concert with other transcription factors) as a cell fate switch for brown adipocyte vs. myocyte differentiation (174).

Early B cell factor 2 (EBF2) is another transcription factor that regulates brown adipocyte identity and cell fate. The primary function of EBF2 is to maintain brown adipocyte identity in mature brown adipocytes, similar to PRDM16 (179, 180). However, reports suggest that EBF2 also regulates beige adipocyte progenitor cell fate (179). EBF2-expressing adipocyte progenitors harvested from mouse embryonic WAT differentiate almost exclusively into brown adipocytes and express PPARγ and PRDM16. Non-EBF2 expressing cells from the same depot develop features of white adipocytes (179). Since the WAT progenitors expressing higher levels of EBF2 differentiated almost exclusively into brown adipocytes, these studies establish a critical role for EBF2 as a primary regulator of particularly beige, but also brown, adipocyte identity.

In adult WAT in mice, EBF2 expression is induced in adipocyte progenitors after 3 days of cold exposure (179). Progenitor cells from these cold-exposed mice that had higher EBF2 expression induced a BAT-selective gene expression program upon *in vitro* differentiation while cells with lower EBF2 levels again largely differentiated into white adipocytes (179). Like PRDM16, overexpression of EBF2 suppresses myogenic gene expression in brown adipocyte progenitor cells and induces adipogenic gene expression in C2C12 myoblasts (179). Thus, PRDM16 and EBF2 function to promote and maintain brown adipocyte identity by enhancing BAT-selective gene expression and reducing myogenic gene expression during critical stages of brown (and beige, for EBF2) adipocyte progenitor development.

A variety of other transcription factors also regulate brown adipocyte development. One noteworthy example is GATA2. GATA-binding protein 2 (GATA2) is established to act as a negative regulator of white preadipocyte differentiation to mature white adipocytes (181, 182) and its role is similar during brown adipocyte differentiation. Using the HIB-1B brown adipocyte cell line, Tsai and colleagues showed that *Gata2* mRNA levels are reduced significantly by day 2 of differentiation and remain suppressed through day 6, indicating that GATA2 likely regulates early adipogenesis (183). Retroviral overexpression of GATA2 in HIB-1B cells led to reduced induction of *Pgc1*α and *Ucp1* during differentiation. In fact, ectopic co-expression of *Pgc1*α in HIB-1B cells overexpressing GATA2 did not rescue *Ucp1* expression relative to differentiated wild type HIB-1B cells, while levels of fatty acid binding protein 4 (*Fabp4* or *aP2*) were not affected by GATA2 overexpression (183). These data suggest GATA2 likely negatively regulates the early brown preadipocyte transition to a fully mature brown adipocyte.

The distinct origins of brown and white adipocytes may provide a foundation from which to understand their unique functions. However, the ability of these cell types to transdifferentiate (135, 184) in the presence of hormonal or environmental stimuli adds complexity to achieving an understanding of how they can be targeted pharmacologically to treat diabetes and obesity. Given the high respiratory capacity of BAT and skeletal muscle (particularly 'slow-twitch' or oxidative muscle), their shared developmental origins make sense. It is essential, nonetheless, to understand how BAT and WAT develop and function to identify important pharmacological targets. The acute ability of hormones to alter the physiology of these two cell types represents a unique opportunity for investigation. While studies investigating the role of selective agonists for the β_3-AR have largely shown poor efficacy in humans, the intracellular effectors of β-AR signaling in adipose tissue should be further evaluated for therapeutic potential.

β-AR signaling in BAT

A variety of signals regulate both BAT function and the expansion of BeAs, including NE, the cardiac natriuretic peptides, thyroid hormone (T3), and FGF21 among others (185-188). The molecular signals initiated by these hormones ultimately result in transcriptional responses that upregulate thermogenic gene expression in white adipocytes, altered adipocyte morphology of brown and beige adipocytes, and enhanced mitochondrial

respiration. While regulated by several hormones, BAT and BeA activity are primarily induced and regulated by NE (188).

During cold exposure, transient receptor potential melastinin 8 (TRPM8) ion channels in peripheral sensory neurons are activated (189); TRPM8 ion channels are calcium-sensitive cation channels. TRPM8-mediated activation of peripheral sensory neurons sends signals to the brain via dorsal root ganglia in the spinal cord, stimulating hypothalamic function (190, 191). Efferent neurons then activate sympathetic nerves innervating skeletal muscle, the vasculature, BAT, and other tissues (192). Brown fat is innervated by sympathetic nerves (193) resulting in activation of β-AR signaling as shown in Figure 5. This cold-stimulated NE release into skeletal muscle, the vasculature and BAT promotes both shivering and non-shivering thermogenesis (194). Other mechanisms that activate the SNS can also promote BAT activity (195).

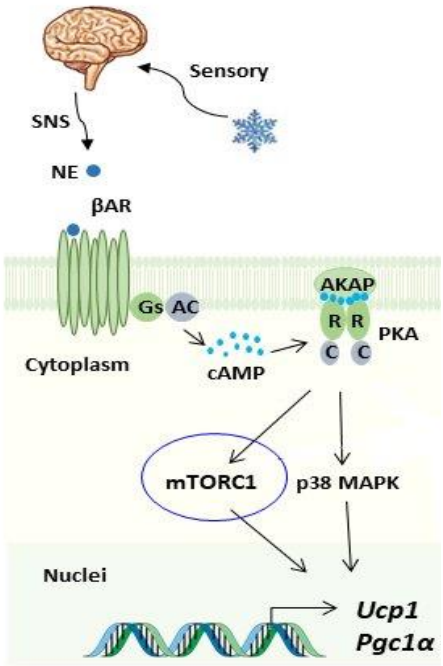

Figure 5: NE-activated signaling effectors in brown and beige adipocytes. Activation of the SNS by either cold or other stimuli enhances NE release from sympathetic nerve terminals. NE binds its cognate receptors, α- and β- adrenergic receptors in BAT with β-ARs primarily driving the thermogenic response. Activation of β-ARs activates the canonical $G_{\alpha s}$ signaling pathway leading to enhanced activity of protein kinase A (PKA) and phosphorylation of effector proteins including p38 MAPKs and mTORC1. These effectors ultimately enhance the activity of transcription factors that enhance the expression of thermogenic genes (i.e., *Ucp1* and *Pgc1α*). Increases in BAT activity or the stimulation of adipose tissue browning in WAT are the main outcomes. Adapted from Shi and Collins, Horm Mol Biol Clin Investig (2017).

All three β-ARs are G-protein coupled receptors (GPCRs) coupled to a canonical $G_{\alpha s}$ heterotrimeric G-protein signaling cascade. Each heterotrimeric G-protein, as the name implies, contains three subunits: G_{α}, G_{β}, and G_{γ}. Upon NE binding, β-ARs act as guanine nucleotide exchange factors (GEFs), activating the $G_{\alpha s}$ subunit (a weak GTP hydrolyzing protein or GTPase) by exchanging GDP for GTP; G_{α} bound to GTP is an active signaling effector. The exchange of GDP for GTP leads to dissociation of G_{α} from the $G_{\beta/\gamma}$ subunits. $G_{\alpha s}$ then

binds to membrane-bound adenylate cyclase, an enzyme that catalyzes the conversion of ATP to cyclic adenosine monophosphate (cAMP), the key second messenger of the G_s signaling cascade. Regulator of G protein signaling (RGS) proteins act as GTPase-activating proteins or GAPs which deactivate G_α by stimulating the hydrolysis of GTP into GDP. G_α bound to GDP is inactive as a signaling effector. cAMP advances G_s signaling by binding to the regulatory subunits (of which there are 2) of PKA in 2:1 stoichiometry. Importantly, the regulatory subunits of PKA are bound to the plasma membrane by A-kinase anchoring proteins (AKAPs). The two catalytic subunits of PKA dissociate from the regulatory subunits after cAMP binding to the latter and phosphorylate and activate intracellular substrates, such as iodothyronine deiodinase 2 (DIO2) and cAMP-response element binding protein (CREB). The $G_{\alpha s}$ signaling pathway described above is reviewed here (196). DIO2 catalyzes the production of T3 from T4, an inactive form of thyroid hormone (197). T3 potentiates the adrenergic induction of thermogenesis in BAT (198). CREB is a transcription factor that binds to genomic enhancer elements that stimulate the expression of *Ucp1* and *Pgc1*α (199, 200).

Given the primary role of β-ARs in regulating BAT thermogenesis and the positive metabolic benefits associated with BAT thermogenesis, these receptors have been pharmacologically targeted for their potential therapeutic efficacy. Notably, the β_3-AR is highly expressed in rodent and human AT relative to the other two subtypes (201-203). Early efforts to pharmacologically activate BAT in rodents used β_3-AR selective agonists such as CL316, 243 (204) and ICI D7114 (205). It is important to specify that these agonists are only representative of many others that were studied (206). In rodent studies, these agonists improved insulin action, fatty acid metabolism, and promoted energy expenditure and it was thought that similar effects would be observed in humans (207, 208). One clinical trial using CL316,243 in lean men proved that acute administration of a β_3-AR agonist enhanced insulin-mediated glucose disposal (209). However, after 8 weeks of administration, no changes were observed in body weight or composition nor plasma glucose or insulin levels, suggesting that CL316,243 did not have long-term efficacy in improving metabolic health. Interestingly, plasma free fatty acid levels remained high at the study endpoint, consistent with the role of β-ARs in stimulating lipolysis in AT. However, it was soon realized that the lack of long-term efficacy of CL316,243 in humans was due to differences in human and rodent β_3-AR pharmacology (210, 211). Thus, attempts were made to find agonists that were more

selective for the human β_3-AR and that could recapitulate the positive metabolic benefits observed in rodent studies.

An example of an agonist selective for the human β_3-AR is L-796568. In obese men, L-796568 did not alter energy expenditure nor glucose tolerance after 28 days of administration (212) despite its demonstrated selectivity for the human β_3-AR (213). Additional clinical studies using other human β_3-AR selective agonists produced similar results (206, 214), suggesting that the differences in rodent and human β_3-AR pharmacology were not the only reason β_3-AR agonists lacked therapeutic efficacy in humans. The relative specificity of β_3-AR expression in AT was hypothesized to allow selective activation of this receptor subtype without off-target effects in other tissues expressing β-ARs, primarily the heart, lungs, and the vasculature, an important consideration for human studies. Despite this assumption, off-target effects, such as increased heart rate (215) and tremor (216), were observed in some studies, highly undesirable outcomes. Due to their lack of long-term efficacy and off-target effects, β_3-AR selective agonists were abandoned as pharmacological tools to promote metabolic health (206, 214). Nonetheless, receptors only serve as the initiators of intracellular signaling pathways and activate a variety of downstream effector proteins that may themselves serve as viable pharmacological targets for harnessing the positive metabolic benefits of BAT.

The Collins laboratory has sought to identify the key intracellular effectors of β-adrenergic signaling in BAT. For example, pharmacological inhibition of p38α MAPK resulted in reduced isoproterenol (iso, a pan β-AR agonist) stimulated *Ucp1* expression in cultured brown adipocytes (217). Similar investigations in the Collins laboratory have identified mechanistic target of rapamycin complex 1 (mTORC1) as another central effector of β-adrenergic signaling in BAT. Both pharmacological inhibition and genetic deletion of Raptor, a defining component of mTORC1, resulted in a blunted browning response after both cold exposure and β_3-AR agonist administration (218). These studies have shown that while we understand that NE regulates BAT function and adipose tissue browning, much remains to be discovered about the molecules within brown and beige adipocytes that are responsible for its effects. A central aim of this thesis is to characterize a potential novel effector of β-adrenergic signaling in BAT.

Rationale for the research undertaken for this dissertation

Given the prevalence of obesity in the US and worldwide, it is imperative that the mechanisms underlying adipose tissue physiology are fully and completely understood, particularly in BAT and BeAs. Again, the ability of BeAs to be acutely regulated by drugs or cold exposure makes this cell type an attractive target for in-depth study to understand how adipocytes transition from an energy-storing function to an energy burning one given the potential broad clinical implications of these insights. In an obese state, adipocytes store too much lipid and lipids are ectopically deposited in other tissues such as skeletal muscle and liver. The key question is: can that excess energy (in the form of lipids) be expended in a controlled way? Can we refine our understanding of BAT activity and the adipose browning process to develop therapeutics to improve human health?

The discovery in the Collins laboratory that iso stimulation increased phosphorylation of ribosomal protein S6 kinase 1 (S6K1), an established mTORC1 substrate, and its target ribosomal protein S6, in adipocytes (219) led to a series of important discoveries in the Collins' laboratory. Before this discovery, it was considered dogma that S6K1 phosphorylation is increased after insulin and growth factor stimulation, but *not* after exposure to catecholamines. The prevailing thought in the field of adipose biology was that insulin and NE have opposing effects; insulin inhibits lipolysis, while NE stimulates it (220).

mTORC1 is canonically activated by growth factors (221-223), the most well-known being insulin (224). Insulin binding to its cognate receptor, the insulin receptor (IR), results in IR autophosphorylation and activation (225). Activated IR phosphorylates insulin receptor substrate 1 (IRS1) (226). IRS1 then binds and activates phosphatidylinositol 3-kinases (PI3Ks) (227) which convert phosphatidylinositol-4,5,-bisphosphate (PIP_2) in the plasma membrane into phosphatidylinositol-3,4,5-trisphosphate (PIP_3) (228, 229). PIP_3 then binds to and activates phosphoinositide-dependent kinase 1 (PDK1) (230), a kinase that phosphorylates and activates protein kinase B or Akt (PKB/Akt) at Thr308 (231), while mTORC2 phosphorylates Akt at Ser473 (232). Akt then phosphorylates tuberous sclerosis complex 2 (TSC2), a GAP (233). TSC2 exists in complex with tuberous sclerosis complex 1 (TSC1) (234). In the absence insulin (or other activators), the TSC1/2 complex inhibits Rheb (235), a small GTPase that ultimately promotes mTORC1 formation and activity (236). In the presence of insulin (and activated Akt), TSC1/2 is inactive and Rheb activates mTORC1 (233, 235). The mTORC1 complex consists of mTOR kinase, regulatory-associated protein of mTOR (Raptor), proline-rich AKT substrate of 40 kDa

(PRAS40), mammalian lethal with Sec13 protein 8 (mLST8), and DEP-domain containing mTOR-interacting protein (Deptor) (237). Notably, PRAS40 is an inhibitor of mTORC1 activity (238), but activated Akt phosphorylates and inhibits PRAS40, allowing full mTORC1 complex activation (239). mTORC1 via mTOR kinase activity then phosphorylates its intracellular substrates, namely S6K1 and eukaryotic translation initiation factor 4E (4E-BP1). mTORC1 phosphorylation of S6K1 and 4E-BP1 ultimately stimulate protein translation. S6K1 promotes translation and its phosphorylation by mTOR acts to positively regulate its endogenous function, while 4E-BP1 is a translation inhibitor and mTOR phosphorylation of 4E-BP1 inhibits this activity. Work from our laboratory has confirmed that other insulin-activated effectors such as Akt and extracellular regulated kinases (ERKS) are not activated by iso despite mTORC1 activation (240). These data suggest that iso uniquely activates mTORC1 without upstream signaling crosstalk. Thus, it is logical to conclude that upstream components of the insulin pathway do not affect β-AR stimulated mTORC1 activity via their own non-canonical activation by β-ARs.

It was particularly surprising that signals from these two hormones could lead to phosphorylation of S6K1, a convergence of two seemingly divergent signaling pathways. Our laboratory established that mTOR kinase and Raptor are directly phosphorylated and activated by PKA (218). Adipocyte-specific deletion of *Raptor* using AdipoQ-Cre (*Raptor* adKO) blocked cold-induced expression of *Ucp1* and mitochondrial genes in BAT, inguinal WAT, and gonadal WAT. Similarly, control mice administered CL316,243 in the presence of rapamycin (rapa, an mTORC1 inhibitor) exhibited reduced *Ucp1* expression and had fewer multilocular adipocytes in inguinal WAT relative to control mice treated with CL316,243 alone. Furthermore, the *Raptor* adKO mice had lower core body temperature relative to control mice during acute (10 hr) cold exposure (218), suggesting Raptor is essential for non-shivering thermogenesis.

Despite the critical finding that mTORC1 is an essential effector of the β-AR-stimulated browning response in adipose tissue, there remains a gap in our knowledge as to how PKA-activated mTORC1 communicates with downstream substrates and ultimately leads to increased adipose tissue browning. Stable Isotope Labeling in Cell culture (SILAC) coupled with mass spectrometry (MS) was used to identify substrates of PKA-activated mTORC1 in mouse adipocytes. The criteria for being considered a substrate of PKA-activated mTORC1 were 1) phosphorylation induced by iso and blocked by rapa and 2) the lack of phosphorylation in response to insulin stimulation. This strategy identified several potential substrates correlating with the β-AR-

stimulated browning response in adipose tissue, including phosphorylation of ***protein kinase D1*** (PRKD1) at serine 206.

The potential importance of PRKD1 in adipose browning

PRKD1 (formerly known as Protein kinase C μ) is a serine/threonine kinase whose activity is canonically activated downstream of $G_{\alpha q}$-coupled GPCRs, which activate phospholipase C (PLC), resulting in production of diacylglycerol (DAG) and inositol triphosphate (IP_3), the latter of which evokes release of calcium (Ca^{2+}) from intracellular stores (241, 242). $G_{\alpha q}$-stimulated PKCs then phosphorylate PRKD1 at two key serine residues in its activation loop: Ser744 and Ser748 (243). Phosphorylation of these residues in addition to DAG binding to PRKD1 results in full PRKD1 activation (244, 245).

Despite a great deal of experimental data characterizing how PRKD1 is regulated by upstream signals (241, 242), the substrates and physiological effects of PRKD1 have not been fully discovered. One phenotype attributed to PRKD1 is vesicle budding from the Golgi apparatus. Overexpression of kinase-dead PRKD1 in HeLa cells results in tubulation of the Golgi (246), a phenotype whereby secretory vesicles destined for the plasma membrane move away from the Golgi but fail to undergo scission. Other known roles of PRKD1 are apparent in a variety of important biological processes. Genetic deletion of *Prkd1* from pancreatic β-cells results in defective insulin secretion *in vivo* (247). Cardiomyocyte-specific deletion of *Prkd1* displayed improved cardiac function in response to pressure overload (248). In skeletal muscle, PRKD1 activity promotes muscle performance (249). Interestingly, PRKD1 regulates myocyte enhancer factor-2 (MEF2), a transcription factor that promotes myocyte differentiation, in both cardiac and skeletal muscle (248, 249). Other work has suggested a role for PRKD1 in cancer (250). While PRKD1 is involved in myriad physiological functions, little is known about its function in adipose tissue.

We found a potentially exciting link between our β-AR-mediated activation of mTORC1 and β-AR-mediated phosphorylation of PRKD1. Löffler and colleagues (251) reported that mice lacking *Prkd1* expression in adipocytes displayed improved insulin sensitivity and glucose tolerance after high-fat diet feeding. Additionally, they reported that differentiated inguinal adipose stromal vascular cells lacking *Prkd1* had basal increases in *Ucp1* gene expression that could be further potentiated by stimulation with iso. A second study (252) reported that deletion of *Prkd1* in mouse adipocytes had reduced expression of enzymes involved in *de novo* lipogenesis

using a *Prkd1* floxed mouse model crossed with aP2-Cre mice. Consequently, since this Cre-driver has been shown to be expressed in a number of cell types other than adipocyte (253-255), additional confirmatory studies would be valuable in confirming the interpretation that lowering PRKD1 expression, or activity, would necessarily improve insulin sensitivity and glucose tolerance for those consuming high fat diets, as in the experimental model of Löffler (251).

My studies directly test the hypothesis that *Prkd1* deletion in BAT and BeAs increases thermogenesis. To explore this question, I generated, using a Cre-loxP system, a *Prkd1* brown adipose-specific knockout mouse using a *Ucp1-Cre* mouse, which deletes *Prkd1* expression only in BAT and BeAs. I also explored novel PRKD1 phosphorylation sites and their ability to regulate PRKD1 function. Findings from these studies fill important gaps in knowledge in both the BAT and PRKD1 scientific fields. The goal of these studies is to characterize the role of *Prkd1* in β-AR-stimulated adipose tissue browning and BAT function, which will augment our knowledge of (and hopefully enhance the potential for therapeutics targeted to) the signaling pathways that regulate these important metabolic tissues.

Chapter II: Phosphorylation of Protein Kinase D1 (PRKD1) at Ser203 and Ser206 as a Potential Regulatory Mechanism for PRKD1 Function

INTRODUCTION

Studies from the Collins laboratory that have been aimed at identifying effectors of β-AR signaling in BAT demonstrated that PKA could directly phosphorylate and activate mechanistic target of rapamycin (mTOR) complex-1 (mTORC1). Furthermore, they showed that PKA-activated mTORC1 is required for β-AR-stimulated BAT activity and adipose tissue browning (218). This work is part of a major goal of the Collins laboratory to delineate the complete β-AR signaling pathway in BAT from receptor to response. While many components of this pathway are known, a review of the literature shows that additional molecules regulating BAT function are still being discovered, which tells us that there remains more to learn about β-AR signaling in BAT (256). We sought to identify effectors of this novel, non-canonically activated mTORC1 in BAT to enhance our understanding of BAT physiology, but also with the hope of discovering potential therapeutic targets. One of these was protein kinase D1 (PRKD1).

PRKD1 was identified in our initial phospho-proteomic screen for substrates of PKA-activated mTORC1 (described in Chapter 1). Two main criteria were used to classify potential substrates. The first criterion was that phosphorylation of a residue in the protein substrate was increased in the presence of iso and blocked by rapa; the second was the lack of phosphorylation in response to insulin. Phospho-Ser206 of PRKD1 met these criteria, suggesting that further study of PRKD1 as a potential effector of this novel signaling pathway was warranted. However, many phosphorylation events were induced by iso, *but unaltered by rapamycin*. Phospho-Ser203 of PRKD1, which is 3 amino acids from Ser206, was one such site. Since the sequence surrounding this site (RRRRL**S**^{203}) contains the canonical PKA phosphorylation site RRXS/T (257), we postulated that PKA activity results in PRKD1 Ser203 phosphorylation. This amino acid sequence also represents an Akt phosphorylation motif (RXRXXS/T) (258). The studies described in this chapter were designed to 1) demonstrate PRKD1 Ser203 phosphorylation occurs in response to β-AR agonists and 2) determine whether PRKD1 Ser203 phosphorylation altered PRKD1 kinase activity.

Given the close proximity of these two phospho-sites and that they are both induced by β-AR agonism, we sought to investigate whether these phosphorylation events (PRKD1 phospho-Ser203 and phospho-Ser206)

occurred co-operatively and whether either or both phosphorylation events altered PRKD1 activity. Canonically at least as far as is known from the literature, PRKD1 is activated by recruitment to the plasma membrane via diacylglycerol (DAG) binding and protein kinase C (PKC) phosphorylation of PRKD1 at Ser744 and Ser748 upon agonism of $G_{\alpha q}$-coupled GPCRs (241, 242). Both Ser203 and Ser206 are located between the C1a (CRD1) and C1b (CRD2) DAG-binding domains of PRKD1. The location of these sites lends credence to the hypothesis that they alter PRKD1-DAG interactions in some way as will be described later in the chapter. Despite many published studies on PRKD1 phosphorylation, only two papers discuss PRKD1 Ser203 phosphorylation and its effects on PRKD1 function, and only one of these discusses (and briefly at that) PRKD1 Ser206 phosphorylation (259, 260).

Work from Hausser et. al. (259) suggested that PRKD1 Ser203 and Ser206 together could form a 14-3-3 binding site and that 14-3-3 protein binding to PRKD1 is dependent on PRKD1 kinase activity. The authors speculated from these results that PRKD1 Ser203 and/or Ser206 could be autophosphorylation sites. Importantly, the authors showed that incubation of purified 14-3-3 with PRKD1 in an *in vitro* kinase assay reduced phosphorylation of aldolase, a PRKD1 substrate, which could indicate a negative regulatory effect on PRKD1 kinase activity by 14-3-3 proteins (259). These data *suggest* that PRKD1 kinase activity possesses an intrinsic negative feedback mechanism by potential autophosphorylation of Ser203 and Ser206, which promotes 14-3-3 protein binding to PRKD1 to reduce substrate phosphorylation.

Another study from the Rozengurt laboratory suggested that PRKD1 Ser203 is phosphorylated by class I p21-activated kinases (PAKs) in response to agonism of $G_{\alpha q}$-coupled GPCRs (260), which is of course distinct from $G_{\alpha s}$-coupled βARs. PAK phosphorylation of PRKD1 Ser203 facilitates PRKD1 dissociation from the plasma membrane and subsequent substrate phosphorylation. Pharmacological inhibition of PAKs did not alter PRKD1 recruitment to the plasma membrane, but rather inhibited its ability to dissociate from the plasma membrane and phosphorylate its nuclear targets, class II histone deacetylases (HDACs) (260). In a similar way, a PRKD1 phospho-null (Ser203Ala) mutant did not dissociate from the plasma membrane as rapidly as the wild-type enzyme (260). These data suggest that PRKD1 phosphorylation at Ser203 promotes its dissociation from the plasma membrane and thereby facilitates PRKD1-mediated phosphorylation events that can regulate gene transcription (i.e., via phosphorylation of class II HDACs). Adding to the complexity of how PRKD1 Ser203 is

phosphorylated and its potential impacts on PRKD1 function, our phospho-proteomic data suggest that a kinase effector of β-AR signaling, PKA, can also phosphorylate this residue.

While it has been reported that PRKD1 can modulate energy expenditure in mice by suppressing the expression of certain thermogenic genes (251), this study was based on adipose-specific gene deletion of PRKD1 and did not address how mechanisms of PRKD1 phosphorylation may contribute to the role of PRKD1 in regulating thermogenic gene expression. The studies presented here aim to address this gap in knowledge.

MATERIALS AND METHODS

Cell lines and purified PRKD1: HIB-1B cells (a gift from Spiegelman lab, Harvard) (261) and HEK293 cells (ATCC) were used to perform experiments investigating PRKD1 Ser203 phosphorylation. Recombinant PRKD1 (>99% purity, Invitrogen) was used for mass spectrometry applications.

Plasmids: Human PRKD1 cDNA was obtained from Addgene plasmid #10808 and subcloned into the p3X-FLAG-CMV10 mammalian expression plasmid. The p3x-FLAG-CMV10 plasmid contains three (3) FLAG epitope tags 5' of the multiple cloning site, resulting in expression of 3x N-terminally FLAG-tagged PRKD1 in mammalian cells. Ser203Ala PRKD1 was generated from the p3x-FLAG-CMV10 plasmid using site directed mutagenesis (QuikChange II site-directed mutagenesis kit, Agilent).

Iso stimulation of cell lines: HIB-1B cells were grown to near (80-90%) confluence in 6-well dishes followed by 3-days of differentiation using 1 μM rosiglitazone. HEK293 cells were plated in 6-well dishes and the next day were transfected with 1 μg of p3xFLAG-PRKD1 per well. Cells were then stimulated with 1 μM iso for 1 hour followed by lysis in 1X radioimmunoprecipitation assay (RIPA) buffer.

Immunoprecipitation of PRKD1: Five hundred μg of total protein containing-lysate from HEK293 cells overexpressing FLAG-PRKD1 was incubated with 25 μL FLAG mAb-agarose conjugated beads with gentle mixing overnight at 4 °C. Beads were washed 3x with 1X Tris-buffered saline (TBS-T) at 4 °C followed by elution in 4X Laemmli buffer for 5 minutes at 95 °C. The eluate was diluted such that the Laemmli buffer was at 1X dilution and resolved by 10 % SDS-PAGE and stained with Coomassie Brilliant Blue (for mass spectrometry applications).

Western Blot: HIB-1B and HEK293 cell lysates were generated using 1X RIPA buffer. Lysates were resolved by 8% SDS-PAGE (Tris-glycine, 6 V/cm^2) for 2 hours followed by transfer to nitrocellulose for 1.5 hours at 30 V.

Membranes were blocked in 5% non-fat milk in 1X TBS-T for 1 hour then incubated with primary antibodies: rabbit anti-PRKD1 (MyBioSource, MBS9404610, 1:1000) and rabbit anti-phosphoSer203 of PRKD1 (ThermoFisher, PA5-40259, 1:1000). Primary antibodies were diluted (according to manufacturer's protocol) in blocking buffer and incubated with membranes overnight at 4 °C. Membranes were washed 3x5 min in 1X TBS-T. Anti-rabbit IgG secondary antibody was diluted in blocking buffer (Anti-Rabbit IgG HRP conjugate, Cell Signaling, 7074S, 1:5000) and incubated with the membrane for 1 hour at room temperature. Membranes were washed 3x5 min in 1X TBS-T followed by chemiluminescent visualization.

RESULTS

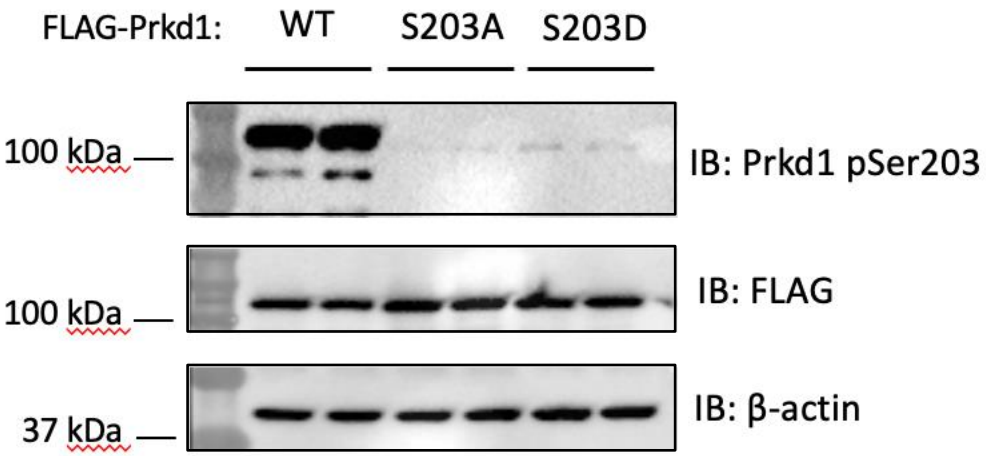

Figure 6: Validation of PRKD1 phospho-Ser203 antibody. HEK293 cells were transfected with WT PRKD1 or S203A or S203D mutants to confirm specific recognition of PRKD1 phospho-Ser203 by the antibody. The Western blots above show that the PRKD1 phospho-Ser203 antibody does not recognize the two S203 mutants, despite comparable expression of FLAG-tagged PRKD1 (FLAG blot) and equal amounts of protein loaded onto the gel (β-actin blot). These data confirm the specificity of the PRKD1 phospho-Ser203 antibody.

Since DAG binding to the C1a/C1b domains recruits PRKD1 to the plasma membrane and enhances its kinase activity, an initial hypothesis was that phosphorylation of Ser203 (theoretically by PKA) and Ser206 (by mTOR based on mass spectrometry in which the phosphorylation is blocked by rapa) alters DAG binding to PRKD1, and thereby its kinase activity. The goal of the initial experiments was to reproduce the increase in PRKD1 phospho-Ser203 by a β-AR agonist as observed in the phospho-proteomic screen. First, it was

necessary to identify a valid tool to detect PRKD1 Ser203 phosphorylation. A PRKD1 phospho-Ser203 antibody was validated (Fig. 6) using whole cell lysates transfected with WT, Ser203Ala, Ser203Asp PRKD1. The lower band in the WT lanes in Figure 6 likely indicates a small amount of cross reactivity with unphosphorylated PRKD1.

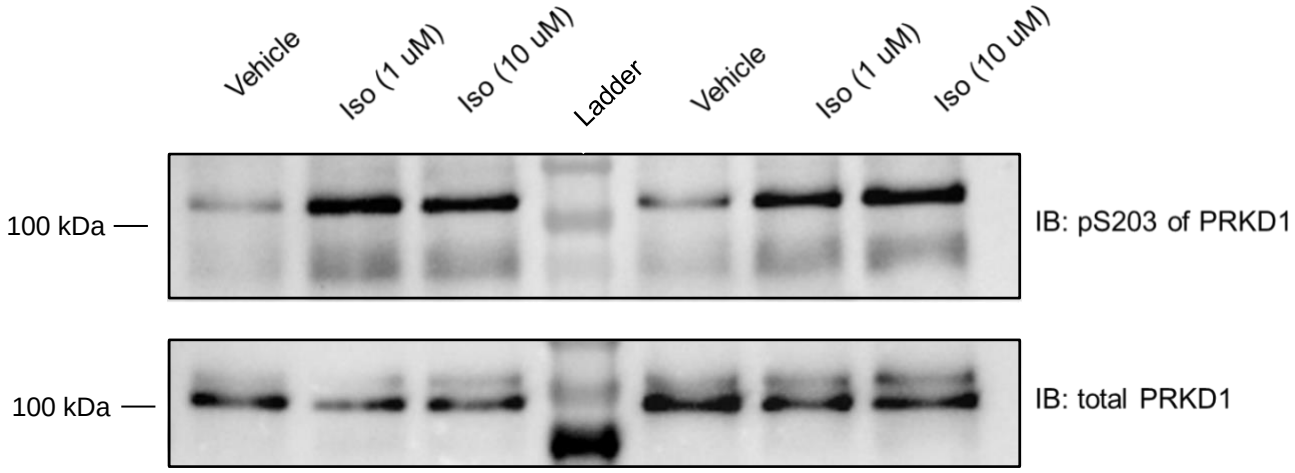

Figure 7: Iso stimulates PRKD1 Ser203 phosphorylation in HIB-1B cells. After 3 days of differentiation, HIB-1B cells were stimulated with either 1 or 10 μM iso for 1 hour. Vehicle was distilled H_2O. The Western blot shows that both 1 and 10 uM iso robustly increased the density of the PRKD1 phospho-Ser203 band over vehicle controls. Total PRKD1 is included to demonstrate that the increase in PRKD1 phospho-Ser203 levels is not the result of increased total PRKD1 protein levels due to iso stimulation. We conclude that β-AR activation results in PRKD1 Ser203 phosphorylation in a mouse brown adipocyte model.

HIB-1B brown adipocyte cells were stimulated with iso and levels of PRKD1 phospho-Ser203 were measured by Western blot (Fig. 7). Iso increased PRKD1 phospho-Ser203 levels relative to vehicle-treated control cells, demonstrating that iso could enhance PRKD1 Ser203 phosphorylation in cells similar to the SILAC studies. HEK293 cells overexpressing PRKD1 were stimulated with iso followed by Western blot to measure PRKD1 phospho-Ser203 levels (Fig. 8). Again, iso stimulation enhanced PRKD1 phospho-Ser203 levels relative to control cells. The conclusion from these studies is that iso can stimulate PRKD1 Ser203 phosphorylation, confirming the findings from the phospho-proteomics studies.

Mass spectrometry studies were performed to confirm both PRKD1 Ser203 and Ser206 phosphorylation in response to iso. Using FLAG-tagged PRKD1 immunoprecipitated from HEK293 cells (either with or without iso stimulation) and resolved by SDS-PAGE, mass spectrometry studies confirmed that levels of both PRKD1

Ser203 and 206 were detected in response to iso stimulation (Fig. 9). However, absolute quantitation was technically difficult (and expensive) due to varied cleavage patterns in the detected tryptic peptides containing PRKD1 phospho-Ser203 and phospho-Ser206.

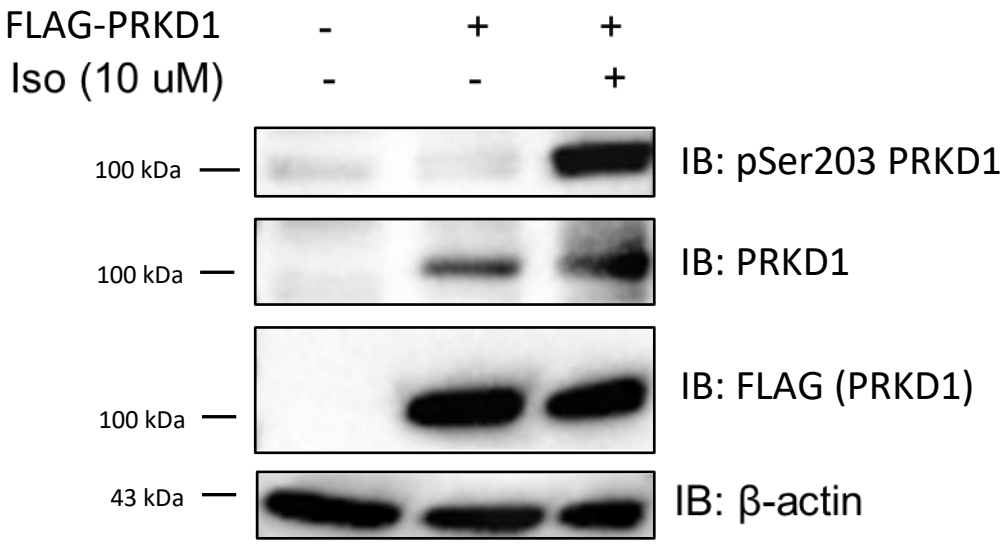

Figure 8: Iso stimulates PRKD1 Ser203 phosphorylation in HEK293 cells overexpressing PRKD1. HEK293 cells were transfected with p3x-FLAG-PRKD1. The following day, cells were stimulated with 10 μM iso for 1 hour. Control cells (-/-) were incubated with distilled H_2O. Here, expression of PRKD1 (second lane) was not sufficient to observe PRKD1 phospho-Ser203 signal. However, the addition of 10 μM iso in the presence of PRKD1 resulted in a robust increase in PRKD1 phospho-Ser203 signal. These data support our initial finding that activation of β-ARs stimulates PRKD1 Ser203 phosphorylation using a PRKD1 *in vitro* overexpression model.

The next goal was to identify which kinase(s) mediated PRKD1 Ser203 phosphorylation. The data indicated this kinase was most likely a kinase effector of the β-AR signaling pathway. However, the published studies discussed earlier suggested a complex regulation of PRKD1 Ser203 phosphorylation, including autophosphorylation or phosphorylation by PAKs. To test the hypothesis that PRKD1 Ser203 is an autophosphorylation site (as suggested by Hausser et. al. (259)), commercially available pure PRKD1 was used in an *in vitro* kinase assay in the presence or absence of ATP (data not shown). Without any experimental manipulation, MS confirmed that the commercially obtained pure PRKD1 (> 99%) was phosphorylated at Ser203.

MS confirmed that pure PRKD1 Ser206 was likewise constitutively phosphorylated (Fig. 10) – at present there are no available phospho-specific antibodies to PRKD1 phospho-Ser206.

Valid	A...	Sequence	SEQUE...	SEQUE...	Intensity	Prob	NTT	Modifications
✓	✓	(R)RLSNVSLTGVSTIR(T)	3.51	0.24		100%	2	Phospho (+80)
✓	✓	(R)RLSNVSLTGVSTIR(T)	2.99	0.33		100%	2	Phospho (+80)
✓	✓	(R)RLSNVSLTGVSTIR(T)	3.05	0.32		100%	2	Phospho (+80)
✓	✓	(R)RLSNVSLTGVSTIR(T)	2.80	0.28		100%	2	Phospho (+80)
✓	✓	(R)RLSNVSLTGVSTIR(T)	2.57	0.27		99%	2	Phospho (+80), Phospho (+80)
✓	✓	(R)RLSNVSLTGVSTIR(T)	2.51	0.23		98%	2	
✓	✓	(R)RLSNVSLTGVSTIR(T)	2.19	0.14		96%	2	Phospho (+80)
✓	✓	(R)LSNVSLTGVSTIR(T)	4.17	0.47		100%	2	

Figure 9: Mass spectrometry (MS) peptides showing PRKD1 Ser203 and Ser206 phosphorylation after iso stimulation in HEK293 cells. HEK203 cells were transfected with WT PRKD1 and stimulated with iso for 1 hour. Whole cell lysates were collected for PRKD1 IP. After resolution of PRKD1 IP eluate by SDS-PAGE, gels were stained with Coomasie Blue and bands corresponding to PRKD1 molecular weight were isolated for MS analysis. The "Sequence" column displays tryptic peptides identified in the MS analysis. Highlighted in green are the serine residues whose phosphorylation was detected. Notice that there are peptides with 1) Ser203 phosphorylation alone and 2) Ser203 and Ser206 phosphorylation (doubly phosphorylated).

Valid	A...	Sequence	Delta Da	Prob	SEQUE...	SEQUE..	NTT	Stop	Modifications
✓	✓	(R)LSNVSLTGVSTIR(T)	-0.00...	100%	2.76	0.37	2	216	Phospho (+80)
✓	✓	(R)LSNVSLTGVSTIR(T)	0.000...	100%	2.52	0.42	2	216	Phospho (+80...
✓	✓	(R)LSNVSLTGVSTIR(T)	-0.00...	100%	3.27	0.34	2	216	
✓	✓	(R)LSNVSLTGVSTIR(T)	-0.00...	100%	3.04	0.35	2	216	Phospho (+80)
✓	✓	(R)LSNVSLTGVSTIR(T)	-0.00...	100%	2.57	0.37	2	216	Phospho (+80)

Figure 10: Mass spectrometry (MS) peptides showing PRKD1 Ser203 and Ser206 phosphorylation from purified PRKD1. Purified PRKD1 was purchased and submitted for MS analysis. The "Sequence" column displays tryptic peptides identified in the MS analysis. Highlighted in green are the serine residues whose phosphorylation was detected. Notice that there are peptides with 1) Ser203 phosphorylation alone, 2) Ser206 phosphorylation alone, and 3) Ser203 and Ser206 phosphorylation (doubly phosphorylated).

DISCUSSION and CONCLUSIONS

The results of WBs using either endogenous or overexpressed PRKD1 from cells stimulated with iso showed that PRKD1 Ser203 phosphorylation can be induced by β-AR activation above the basal phosphorylation detected. MS studies using immunoprecipitated PRKD1 from HEK293 cells stimulated with iso also confirmed β-AR stimulation induces PRKD1 Ser203 phosphorylation. These studies reached an impasse during the effort to identify which kinase(s) phosphorylated PRKD1 Ser203 mainly due to technical limitations with MS, but also because it appeared that phosphorylation of Ser203 resulted from several different kinases. Although our studies

remain inconclusive, we were able to confirm our own key finding that activation of β-ARs stimulates PRKD1 Ser203 phosphorylation using two independent methodologies. Other than the published studies, which suggest that PRKD1 Ser203 phosphorylation can act as either a negative or positive regulator of PRKD1 function, the role of PRKD1 Ser203 in regulating PRKD1 function remains unclear. Our work opens a new avenue of discovery for this unique phosphorylation event and will hopefully lead to increased clarity about both how PRKD1 Ser203 is phosphorylated and its effects on PRKD1 function.

Chapter III: PRKD1 in brown adipose tissue thermogenesis

This chapter is adapted from "Protein Kinase D1 (*Prkd1)* deletion in brown adipose tissue leads to altered myogenic gene expression after cold exposure, while thermogenesis remains intact" published in *Physiological Reports* and has been reproduced with the permission of the publisher and my co-authors Shristi Shrestha, Jean-Phillipe Cartailler, and Sheila Collins

INTRODUCTION

The study of brown adipose tissue (BAT) has consistently revealed its beneficial metabolic effects both in rodents and humans. The high levels of respiration that occur in BAT provide a mechanism by which it carries out its principal function: thermogenesis or heat production. In fact, the improved insulin sensitivity and reduced percent body fat observed with increased BAT mass or activity are attributed to the high basal respiratory capacity of BAT (80, 97, 262). Research efforts focused on BAT physiology have led to many discoveries from the positive regulation of BAT activity by adrenaline and other hormones to the intracellular signaling effectors that ultimately drive enhanced BAT respiration (188, 263, 264). Work from our laboratory has shown that p38α MAPK and mechanistic target of rapamycin complex 1 (mTORC1) are key intracellular mediators of β-adrenergic receptor-stimulated BAT activity (217, 240, 265) However, the additional downstream effectors of these central signaling mediators in β-AR-stimulated BAT activity are unknown. We sought to identify these downstream effectors using phosphoproteomics in cultured brown adipocytes. Proteins with phosphorylation events that were enhanced after stimulation with isoproterenol (a pan β-AR agonist) and then reduced after rapamycin (an mTORC1 inhibitor) treatment were considered potential substrates of β-AR-stimulated mTORC1; insulin +/- rapamycin-stimulated cells were used to control for canonical mTORC1 activation. These studies showed that Protein Kinase D 1 (PRKD1) was a potential downstream mediator of β-AR-stimulated mTORC1 signaling in brown adipocytes.

Work from Löffler et al. (251) suggested a role for Protein Kinase D1 (PRKD1) in regulating energy expenditure in mouse adipose tissue. Using a *Prkd1* floxed mouse model crossed with AdipoQ-Cre mice, they reported that mice lacking *Prkd1* in adipocytes displayed improved insulin sensitivity and glucose tolerance after high-fat diet feeding. Additionally, they reported that differentiated inguinal adipose stromal vascular cells lacking *Prkd1* had basal increases in *Ucp1* expression that could be further potentiated by stimulation with the pan β-

AR agonist isoproterenol. A second study (252) reported that deletion of *Prkd1* in mouse adipocytes had reduced expression of enzymes in the *de novo* lipogenesis pathway. However, since they used Fabp4-Cre (aP2-Cre) to delete *Prkd1*, and this Cre-driver has been shown to be expressed in a number of cell types other than adipocytes (253-255), results using this model must be treated with caution.

PRKD1 is member of the Protein Kinase D subfamily of calcium/calmodulin-dependent protein kinase (CaMK) family of kinases (242). Originally named protein kinase Cμ, there are three members of the Protein Kinase D subfamily: PRKD1, 2, and 3. Regulation of catalytic activity and subcellular localization of PRKD1 has been widely studied in cell culture models and more recently, albeit to a lesser extent, in animal models that have demonstrated a role for PRKD1 in a variety of physiological processes including responses to cardiac remodeling after injury (248), skeletal muscle endurance (249), and insulin secretion (247) (see (266) for review). Many studies on PRKD1 have been focused on how the enzyme itself is regulated (phosphorylation, kinase activity, etc.) (241) but there is still much to be understood about the role of PRKD1 in a variety of physiological processes, including in brown/beige adipocytes. In the few papers examining a role for PRKD1 in adipocyte biology (251, 252), important standard maneuvers to study BAT thermogenesis and adipose 'browning', such as cold exposure or treatment with a selective β_3-AR agonist were not performed. This gap in knowledge, coupled with the relatively high expression of *Prkd1* in mouse iBAT (http://biogps.org/#goto=genereport&id=18760), led us to ask whether loss of *Prkd1* specifically in brown and beige adipocytes (i.e., UCP1-expressing cells) would modulate β-AR-stimulated brown adipose tissue thermogenesis.

Much of the published work in this unique tissue has thus been appropriately focused on efforts to modulate the function of mature brown adipocytes, the parenchymal cell of BAT. However, BAT is composed of numerous cell types including immune cells (macrophages, T cells, etc.), fibroblasts, adipocyte stem cells, and the cells composing its dense vascular and neural networks (endothelial, smooth muscle, and nerve cells among others) (267, 268). While most experiments performed in this study measured phenotypes classically attributed to mature brown adipocytes, RNA-sequencing studies in cold-exposed mice revealed *Prkd1*-dependent changes in myogenic gene expression in BAT. The only cell type in BAT known to possess a myogenic gene signature is the adipocyte precursor, a stem cell (142, 174, 269).

While the results of this study show that *Prkd1* deletion in BAT does not modulate phenotypes classically attributed to mature brown adipocytes, our data suggest that mature brown adipocytes lacking *Prkd1* may regulate brown adipocyte precursor cell function in a non cell-autonomous way.

MATERIALS AND METHODS

Animal experiments: *Prkd1*$^{fl/fl}$ mice were obtained from Eric Olson (UT Southwestern) and Jens Fielitz (MDC for Molecular Medicine in the Helmholtz Association, Berlin, Germany) and were crossed to mice expressing an uncoupling protein 1 (*Ucp1*)-driven Cre recombinase (JAX stock no. 024670), resulting in *Prkd1* deletion only in brown and beige adipocytes in these animals (*Prkd1*^{BKO}). All mice used for experiments were males between 12-14 weeks of age. See Fig S1 for validation of *Prkd1* deletion in whole iBAT.

Cold exposure: *Prkd1*$^{fl/fl}$ and *Prkd1*^{BKO} mice were housed at thermoneutrality (30 °C) in a temperature-controlled chamber (Powers Scientific) for 2 days, whereupon the temperature was lowered to 6 °C for 8 hours. This protocol was developed to reduce adrenergic signaling thus minimizing kinase activation prior to cold exposure (217).A control group for each genotype was acclimated at 30 °C for 2 days without cold exposure. At the end of the study, the iBAT was dissected and immediately placed in Trizol (ThermoFisher). For the 4-day cold exposure experiment, mice were housed at thermoneutrality for 2 days followed by 4 days of cold (6 °C) exposure. Controls were acclimated at 30 °C without cold exposure.

β_3-AR agonist (CL316, 243) administration: Prkd1$^{fl/fl}$ and *Prkd1*^{BKO} mice were administered 0.3 mg/kg BW CL316,243 (Tocris) intraperitoneally once daily for 4 days. On day 5, iBAT and iWAT were dissected and immediately placed in Trizol (ThermoFisher). Similar CL316.243 treatments in mice have been performed in the lab (218, 270).

Body temperature: *Prkd1*$^{fl/fl}$ and *Prkd1*^{BKO} mice were acclimated at thermoneutrality for 2 days followed by 4 days of cold (6 °C) exposure. Rectal temperatures were taken every day (including during thermoneutral acclimation) using the PhysiTemp® TH-5 Thermalert thermometer and RET-3 rectal probe for mice. Temperature measurements were made between 12-2 PM each day.

RNA isolation and quantitative PCR: Total RNA was extracted from adipose tissues using Trizol followed by purification on Qiagen RNA mini-columns. For qPCR, reverse transcription (High Capacity cDNA reverse

transcription kit, ThermoFisher) and cDNA amplification detected by SYBR Green (PowerUp SYBR Green Master Mix, Applied Biosystems) were performed according to manufacturer protocols. qPCR primer sequences are shown in Table 1. qPCR data were analyzed in consult with the Vanderbilt Biostatistics Clinic using a modified Livak method (271). C_t values for target genes were normalized to C_t values for 36B4 (reference gene) to obtain a ΔC_t value. ΔC_t values were plotted as relative fold change values. A two-way analysis of variance (ANOVA) + Tukey's honestly significant difference test were used for statistical analysis. The number of asterisks (*) shown in each graph indicates level of significance.

Table 1 qRT-PCR primers

	Forward (5' to 3')	Reverse (5' to 3')
mPrkd1	AAAATGTGGATATCAGCACAG	ACGATGTTTACCTCCATAAAC
mUcp1	GGCCTCTACGACTCAGTCCA	TAAGCCGGCTGAGATCTTGT
mPgc1α	GAAAGGGCCAAACAGAGAGA	GTAAATCACACGGCGCTCTT
mCidea	GTCTGCAAGCAACCAAAGAT	ATTGAGACAGCCGAGGAAGT
mElovl3	ACTTCGAGACGTTTCAGGACTTA	GACGACCACTATGAGAAATGAGC
mNdufa5 (C1)	GCGGAGCCAGATGTTAAAAA	CCATCCACCATCTGACACTG
mSdhb (CII)	CTGGTGGAACGGAGACAAGT	GTTAAGCCAATGCTCGCTTC
mUqcrb (CIII)	GGGGTGACCCTGAGTATTGA	ATGTAAGGCACCCAGTCCAG
mCox5b (CIV)	CAGAAGGGACTGGACCCATA	ATAACACAGGGGCTCAGTGG
mAtp5k (CV)	CGGTTCAGGTCTCTCCACTC	TGACGCCTCACTTGAGAATG

RNA-Seq: Another cohort of *Prkd1*$^{fl/fl}$ and *Prkd1*^{BKO} mice were housed at thermoneutrality (30 °C) for 2 days +/- 8 hours or 4 days cold (6 °C) exposure. iBAT RNA was isolated by Trizol (ThermoFisher) and Qiagen RNA extraction kit and sent to Vanderbilt Technologies for Advanced Genomics (VANTAGE) for RNA quality control assessment, library preparation, and next-generation sequencing. Only high integrity (RIN>7) poly-A selected RNA was used as input. Data analysis (including differential gene expression and pathway analyses) were performed by Creative Data Solutions, a Vanderbilt shared resource. An Illumina NovaSeq 6000 was used to produce paired-end, 150-bp reads yielding 35-45 million reads per sample. Three replicates for each genotype

in both thermoneutral and cold exposure states were included. Principal component and distance matrix analyses are shown Fig. S3 and S4, respectively.

Bioinformatics analysis of RNA-seq: Paired end raw fastq files were assessed for quality by FASTQC (https://www.bioinformatics.babraham.ac.uk/projects/fastqc/)
and TrimGalore (https://www.bioinformatics.babraham.ac.uk/projects/trim_galore/) respectively. Reads were aligned to the reference mouse genome mm10 (GRCm38) using The Spliced Transcripts Alignment to a Reference (STAR) version 2.6 (272). Approximately 70% of the raw reads were uniquely mapped to the reference genome. Raw read counts were obtained from STAR followed by pairwise differential gene expression analysis performed using DESeq2 (273). Genes with adjusted p-value <0.05 were considered significant. Gene Ontology analysis and visuals were performed using clusterProfiler R package (274). Metascape network visualizations of statistically enriched GO terms were performed as previously described (275).

Histology: Adipose tissues were fixed in 10% buffered formalin, embedded in paraffin, and sectioned (5-μm thickness). Slides were subjected to either UCP1 immunohistochemistry (IHC) or hematoxylin and eosin (H&E) staining. Images were captured using an Aperio AT2 digital slide scanner (20X magnification).

RESULTS

The primary goal of these studies was to determine whether loss of PRKD1 in UCP1-expressing adipocytes altered β-AR-stimulated BAT thermogenesis. Since mice are typically housed at 22-25 °C, which is a moderate thermal stress for a mouse, we chose to first acclimate *Prkd1*$^{fl/fl}$ and *Prkd1*^{BKO} mice at thermoneutrality (30 °C) for 2 days to minimize catecholaminergic tone. In the first study this was followed by 8 hours at 6 °C. A control group of both genotypes was housed at 30 °C only. As shown in Fig. 11A, RT-PCR analysis showed that cold exposure led to similar increases in the expression of *Ucp1* and *Pgc1α,* key genes involved in the thermogenic response in adipose tissue, in iBAT of both both *Prkd1*$^{fl/fl}$ and *Prkd1*^{BKO} mice. Also, the expression of mitochondrial complex genes was similar between genotypes after cold exposure (Fig. 11B), suggesting that the loss of PRKD1 in brown adipocytes does not affect the acute thermogenic response to cold. H&E staining of iBAT from mice either housed at thermoneutrality or after 8-hour cold exposure revealed no PRKD1-dependent

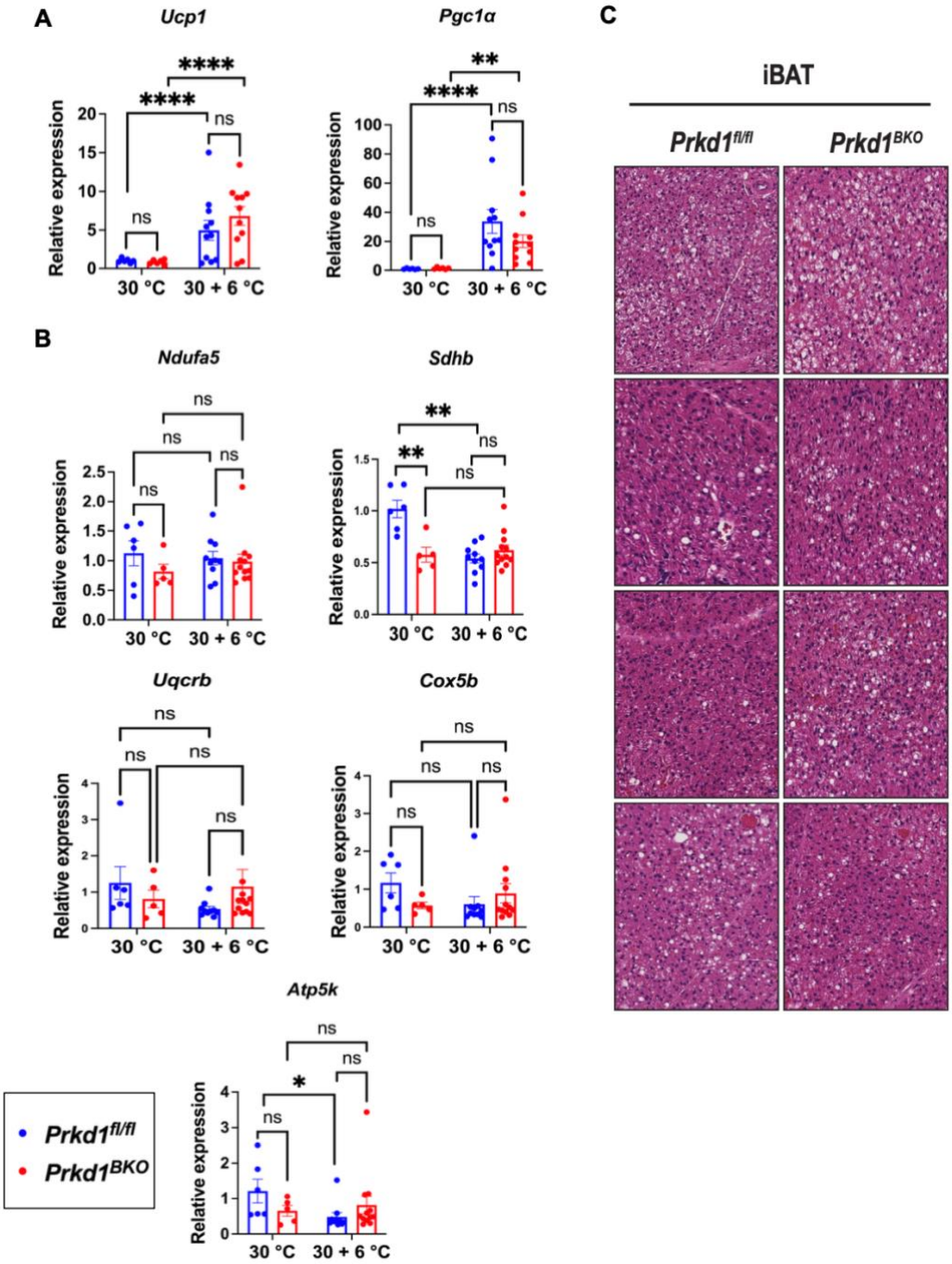

Figure 11: 8-hour cold exposure reveals similar thermogenic gene induction in iBAT between *Prkd1$^{fl/fl}$* and *Prkd1^{BKO}* mice. *Prkd1$^{fl/fl}$* and *Prkd1^{BKO}* mice were acclimated at 30 ℃ (thermoneutrality) for 2 days with or without an additional 8 hours at 6 ℃ (cold). A) *Ucp1* and *Pgc1α* expression in iBAT. B) Expression of subunits of mitochondrial complexes I-V in iBAT. n = 6-11 mice. Data are presented as mean ± s.e.m. (two-way ANOVA with Tukey's honestly significant difference test). C) *Prkd1$^{fl/fl}$* and *Prkd1^{BKO}* mice were housed at 30 °C for 2 days followed by 8 hours at 6 °C. iBAT was dissected for hematoxylin and eosin (H & E) staining. n = 5 mice per genotype.

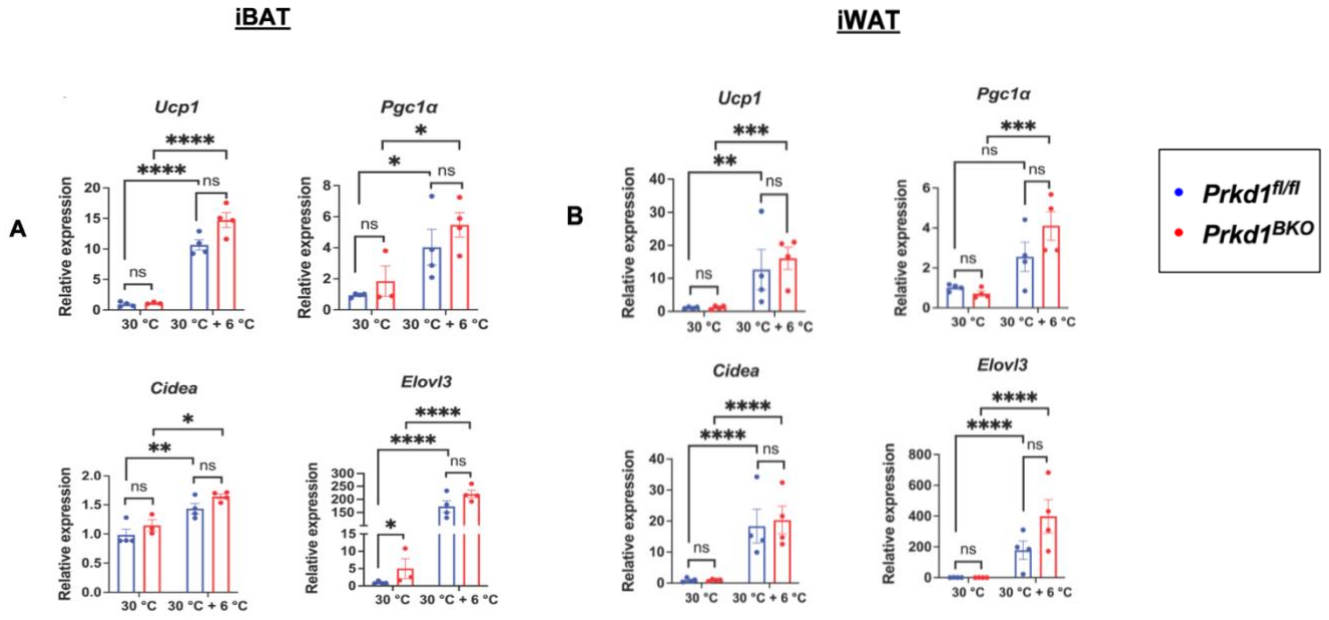

Figure 12: 4-day cold-exposed *Prkd1$^{fl/fl}$* and *Prkd1^{BKO}* mice have no significant differences in thermogenic gene induction in either iBAT or iWAT. *Prkd1$^{fl/fl}$* and *Prkd1^{BKO}* mice were acclimated at 30 ℃ (thermoneutrality) for 2 days with or without an additional 4 days at 6 ℃ (cold). A) *Ucp1, Pgc1α*, *Cidea* and *Elvol3* expression in iBAT. B) *Ucp1, Pgc1α*, *Cidea* and *Elvol3* expression in iWAT. n = 4 mice/group. Data are presented as mean ± s.e.m. (two-way ANOVA with Tukey's honestly significant difference test).

differences in adipocyte morphology (Fig. 11C). Taken together with the gene expression analysis, these data suggest that *PRKD1* is not a key regulator of the acute thermogenic response in iBAT.

We next performed a longer 4-day cold exposure in *Prkd1$^{fl/fl}$* and *Prkd1^{BKO}* mice, since more chronic stimulation will further promote brown and beige fat gene expression and thermogenesis. Similar to the results from the 8-hr cold exposure when comparing genotypes, we did not observe PRKD1-dependent changes in thermogenic gene induction after 4 days at 6°C in either iBAT (Fig. 12A) or iWAT (Fig. 12B), nor was there any difference in core body temperature between genotypes (Fig. 13). In addition, both H&E staining and UCP1 IHC for iBAT were similar between *Prkd1$^{fl/fl}$* and *Prkd1^{BKO}* mice (Fig. 14A and 14B). In the iWAT, while we observed for the most part the expected increases in gene expression in response to cold, *Pgc1α* expression in the *Prkd1$^{fl/fl}$* mice did not reach significance (Fig. 14B), perhaps due to the variation observed between mice.

As a companion experiment to the cold exposure, we took a pharmacological approach using the β_3-AR agonist, CL316,243 (CL) to assess effects of *Prkd1* loss on thermogenic gene induction in iBAT and iWAT. In iBAT, there was no significant increase in thermogenic gene expression (*Ucp1*, *Pgc1α*, *Cidea*, and *Elovl3*) (Fig.

15A), nor was mitochondrial gene expression altered in iBAT between genotypes (Fig. 15B). We attribute this result to the very high baseline expression of these genes in iBAT since BAT is densely innervated and tonically stimulated by endogenous NE. However, in iWAT, thermogenic gene expression (Fig. 15C), and some mitochondrial complex genes (Fig. 15D), were robustly induced by CL in both genotypes, but *Prkd1* deficiency did not alter the induction of these genes. These data are consistent with our observations from the acute and 4-day cold exposure studies, strongly suggesting that *Prkd1* is not a regulator of β-AR-stimulated thermogenic gene expression in UCP1-expressing adipocytes. Nevertheless, since in iWAT the expression of Cre recombinase endogenous *Ucp1* is induced, we did not observe deletion of *Prkd1* in iWAT in our experimental paradigm. It is possible that a longer period of cold or CL treatment may be needed to see changes in iWAT.

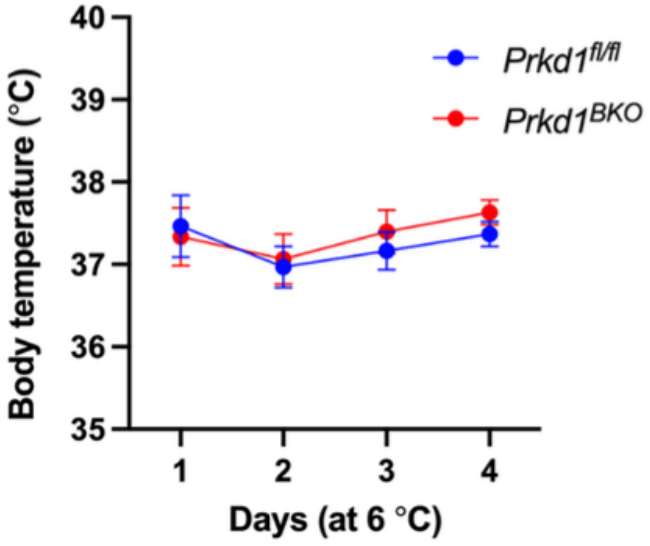

Figure 13: Core body temperature of *Prkd1*$^{fl/fl}$ and *Prkd1*^{BKO} mice during the 4-day cold exposure. *Prkd1*$^{fl/fl}$ and *Prkd1*^{BKO} mice were acclimated at 30 ℃ for 2 days followed by an additional 4 days at 6 ℃ (cold). Core body temperature was recorded each day as detailed in Methods. n = 4 mice/group.

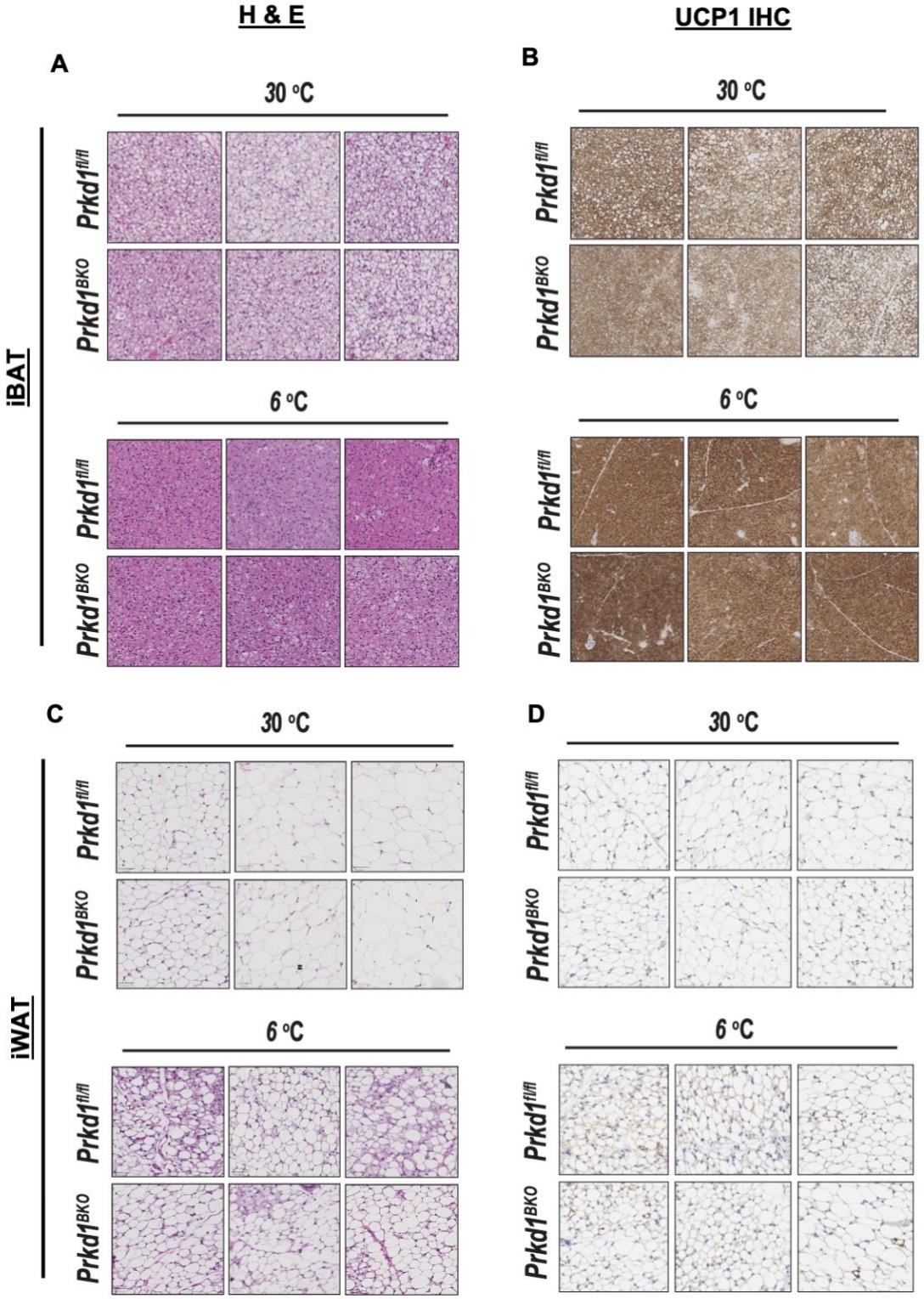

Figure 14: H & E staining and UCP1 immunohistochemistry of iBAT and iWAT after 4-day cold exposure. *Prkd1*$^{fl/fl}$ and *Prkd1*^{BKO} mice were housed at 30 °C for 2 days +/- 4 days at 6 °C. iBAT and iWAT were dissected for fixation and paraffin embedding followed by hematoxylin and eosin (H & E) staining and UCP1 IHC. A) iBAT H&E staining. B) iBAT UCP1 IHC. C) iWAT H & E. D) iWAT UCP1 IHC. n = 3 mice per group.

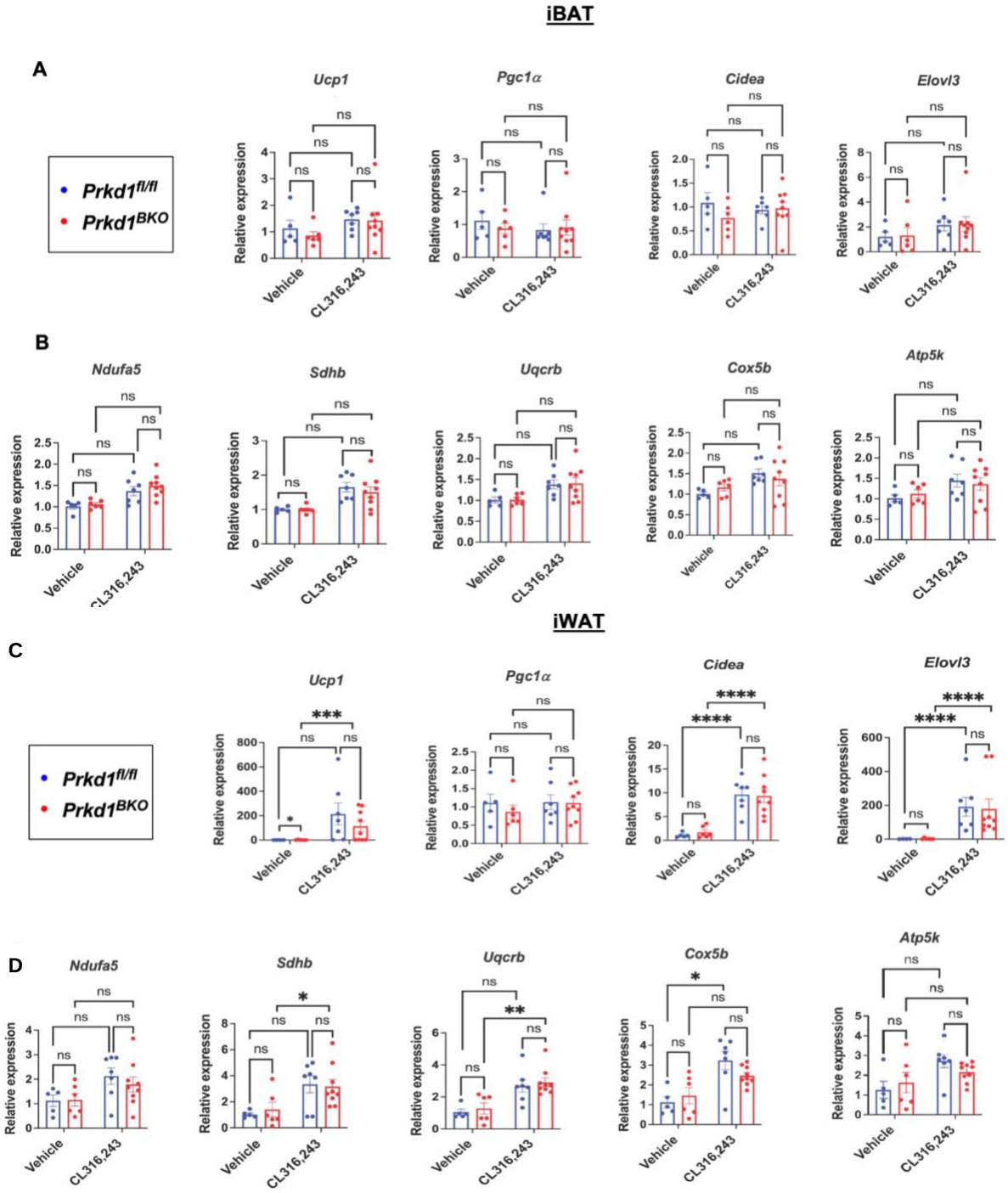

Figure 15: Loss of *Prkd1* in *Ucp1*-expressing adipocytes does not alter β3-AR agonist stimulated thermogenic gene expression in iBAT or iWAT. *Prkd1*$^{fl/fl}$ and *Prkd1*^{BKO} mice were intraperitoneally injected with 0.3 mg/kg CL316,243 (CL) once daily for 4 days before harvesting iBAT and iWAT for qRT-PCR. A) Expression of thermogenic genes in iBAT. B) Expression of subunits of mitochondrial complexes I-V in iBAT. C) Expression of thermogenic genes in iWAT. D) Expression of subunits of mitochondrial complexes I-V in iWAT. n = 5-9 mice. Data are presented as mean ± s.e.m. (two-way ANOVA with Tukey's honestly significant difference test).

Since based on prior literature (251) we provisionally expected to see heightened thermogenic gene expression in *Prkd1*^{BKO} mice, we next performed RNA-Seq to assess whether other transcriptional changes resulted from *Prkd1* deficiency in iBAT, first using the 8-hour cold exposure paradigm. For both genotypes, we observed comparable increases in expression of key thermogenic genes (e.g., *Ucp1*, *Pgc1α*, *Dio2*, *Cidea*) in response to the 8-hr cold relative to thermoneutrality (see Fig. S2). Thus, as in Fig. 11, there were no differences in cold-induced thermogenic gene induction between genotypes. Instead, what we did observe was a significantly increased myogenic gene signature in the *Prkd1*^{BKO} vs. *Prkd1*$^{fl/fl}$ mice after cold exposure (Fig. 16). However, there were no differences in this myogenic expression profile between genotypes at the thermoneutral temperature. For a more complete view of the genes and gene families that were changed in this experiment please see Fig. S5. This myogenic signature is interesting given that brown adipocytes and skeletal myocytes arise from a common progenitor that expresses *Myf5* (142, 174). The transcriptional regulator PRDM16 has been shown to drive the brown adipocyte differentiation pathway versus skeletal muscle (174, 276). In our dataset there were no differences in the levels of *Prdm16* between *Prkd1*$^{fl/fl}$ and *Prkd1*^{BKO} under any condition (see *data availability*). Moreover, since we used bulk RNA-Seq, these data cannot inform us about the cell type(s) in which these transcript changes are occurring.

Since the data from 8-hr cold exposure provides a snapshot of what may be occurring during this acute time frame, we next employed the longer 4-day cold exposure paradigm to determine whether other changes may be occurring during the sustained thermogenic stimulus when non-shivering thermogenesis is further established. In both genotypes we observed equally robust increases in expression of the canonical genes involved in non-shivering thermogenesis after cold exposure compared to their thermoneutral controls (see Fig. S2). These results again independently support the data in Fig. 12. Based on our 8-hr cold exposure data, we speculated that perhaps the myogenic gene signature in the iBAT of the *Prkd1*^{BKO} would persist and perhaps be amplified. However, as shown in Fig. 17, compared to *Prkd1*$^{fl/fl}$ mice, the *Prkd1*^{BKO} mice in fact displayed a suppressed myogenic gene signature after the 4-day cold exposure, suggesting that *Prkd1* loss in iBAT has different effects that are dependent on the length of cold exposure.

Another interesting finding from the RNA-Seq study (8-hour in particular) is that *Prkd1*-deficient iBAT has reduced lipogenic gene expression after 2-day acclimation at thermoneutrality. These findings are consistent

with other publications (45, 46) showing that adipose-specific deletion of *Prkd1* in mice reduces the expression of genes involved in *de novo* lipogenesis. The raw data for these studies is available here: https://figshare.com/projects/Bulk_RNAseq_of_Protein_Kinase_D1_Prkd1_knockout_in_thermoneutral_and_cold_exposure/148228.

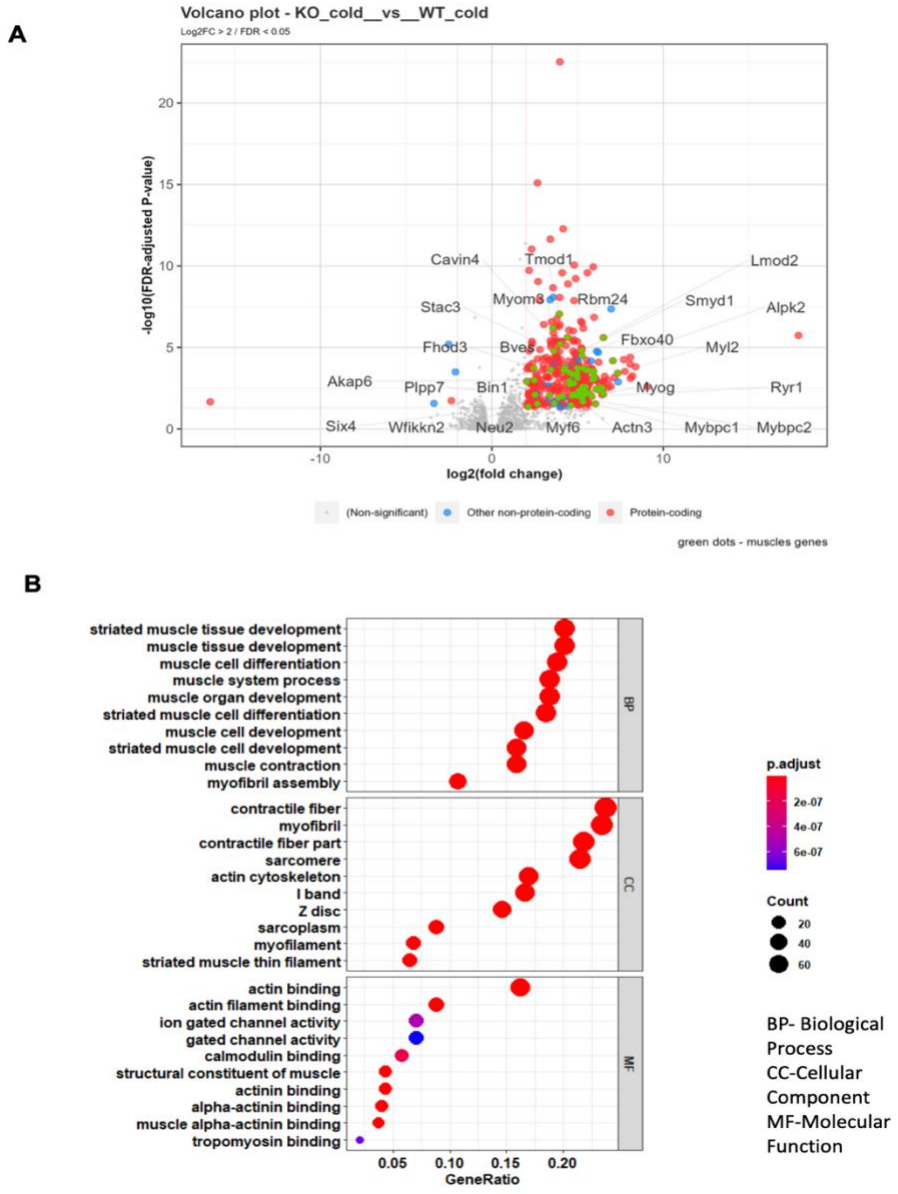

Figure 16: Gene ontology (GO) analysis of iBAT RNAs from *Prkd1*$^{fl/fl}$ and *Prkd1*^{BKO} mice after 8-hr cold exposure. GO plots show biological processes (BP), cellular components (CC), and molecular functions (MF) changed between the two groups being compared. The GeneRatio indicates the percentage of total differentially expressed genes (DEGs) in each GO term. A) Volcano plot of DEGs between both genotypes after cold exposure. B) GO terms for DEGs.

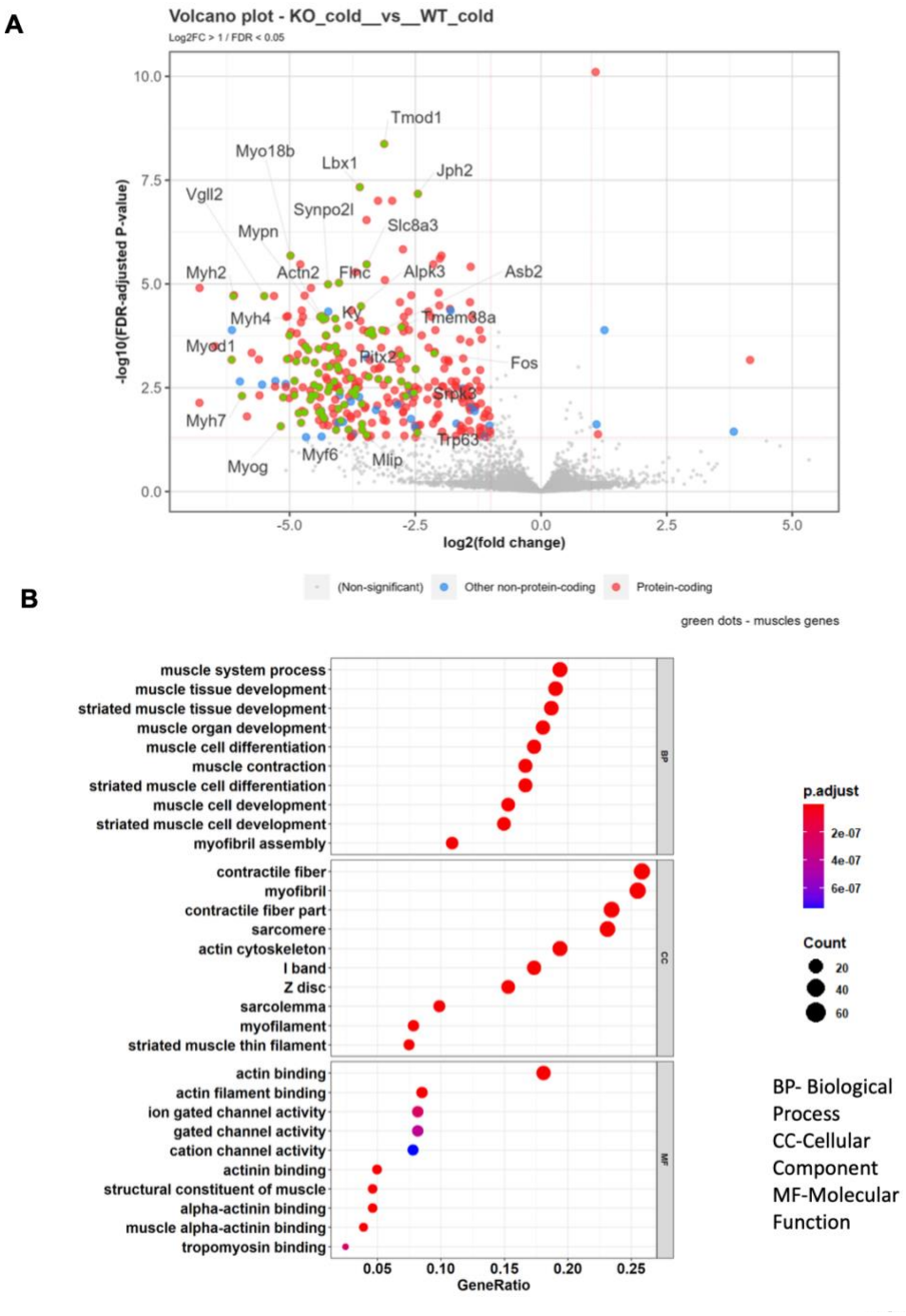

Figure 17: Gene ontology (GO) analysis of iBAT RNAs from *Prkd1$^{fl/fl}$* and *Prkd1^{BKO}* mice after 4-day cold exposure. GO plots show biological processes (BP), cellular components (CC), and molecular functions (MF) changed between the two groups being compared. The GeneRatio indicates the percentage of total differentially expressed genes (DEGs) in each GO term. A) Volcano plot of DEGs between both genotypes after cold exposure. B) GO terms for DEGs.

DISCUSSION and CONCLUSIONS

While many similarities exist between mouse and human BAT, there are distinctions. For example, in mice, the primary *bona fide* depot is located between the shoulders (i.e., interscapular BAT) and its cross-transplantation resulted in improved glucose metabolism (97). However, in humans, BAT exists in discretely distributed depots along the neck and spine (130) nor have studies been done testing the effects of BAT transplantation. Also, the lack of β_3-AR agonist efficacy in human clinical trials suggest that the β_3-AR is differentially expressed and/or regulated in humans versus mice (204, 211, 214). Thus, these data should be considered with these differences in mind. Our initial hypothesis in these studies, which was based upon prior literature showing that loss of *Prkd1* in adipose tissue enhanced energy expenditure (251), was that *Prkd1* loss in iBAT would similarly enhance thermogenesis. However, the data presented here show no difference in thermogenic gene expression, histological features or body temperature between *Prkd1*$^{fl/fl}$ and *Prkd1*^{BKO} mice after either cold exposure or β_3-AR agonist administration. Despite findings from Löffler et. al. that loss of *Prkd1* in adipose tissue (both white and brown) improved insulin sensitivity and glucose tolerance as well as potentiated isoproterenol stimulated *Ucp1* expression in cultured adipocytes, our data show that *Prkd1* is not a regulator of iBAT thermogenesis. One potential explanation for this discrepancy is that our animal model (*Prkd1*^{BKO}) only deleted *Prkd1* in *Ucp1*-expressing adipocytes, while the model used by Löffler et. al. (251) resulted in *Prkd1* deficiency in all adipose tissue depots. Importantly, Löffler et. al. did not examine BAT function in their study. Thus, the difference in model systems may explain why we failed to observe *Prkd1*-dependent differences in thermogenesis.

Loss of *Prkd1* in BAT did alter myogenic gene expression after both 8 hours and 4 days of cold exposure. The 8-hour cold-exposed *Prkd1*^{BKO} mice had elevated myogenic gene expression relative to 8-hour cold-exposed *Prkd1*$^{fl/fl}$ mice, while after 4 days of cold exposure, the trend tended to be reversed. Timmons and Seale showed that myogenic gene expression in BAT arises from early adipocyte progenitor cells before their commitment to the adipocyte lineage (142, 174). Additionally, Seale and colleagues demonstrated that this myogenic signature was inhibited by EBF2 (180) and PRDM16 (174), two transcription factors that promote brown and beige adipogenesis, allowing adipocyte progenitors to differentiate into mature brown and beige adipocytes. Other than this critical finding, there are no data to explain the expression of a myogenic signature in BAT.

Thus, we hypothesize that during acute (8-hour) cold exposure, loss of *Prkd1* promotes a transcriptional response in BAT that elevates myogenic gene expression, which could be generated by an increase in the number or transcriptional activity of early adipocyte progenitors. After 4 days in the cold, the cold-exposed *Prkd1*^{BKO} mice have reduced myogenic gene expression relative to *Prkd1*$^{fl/fl}$ cold-exposed mice. When comparing these changes in myogenic gene expression between the 8-hour and 4-day cold exposure studies, one reasonable hypothesis is that at the 4-day time point, a factor (i.e., enzyme, receptor, etc) compensating for the loss of *Prkd1* in mature brown adipocytes has suppressed the myogenic gene expression. Another possibility is that the differences in myogenic gene expression between 8-hrs and 4-days cold exposure could be related to enhanced differentiation of progenitors in the *Prkd1*$^{fl/fl}$ mice in chronic cold (Fig. 18) due to some factor released by the mature brown adipocyte. However, additional *in vivo* and *in vitro* experiments are needed to test these hypotheses to confirm both the cell type(s) of origin for the observed myogenic gene signature and its functional relevance in BAT.

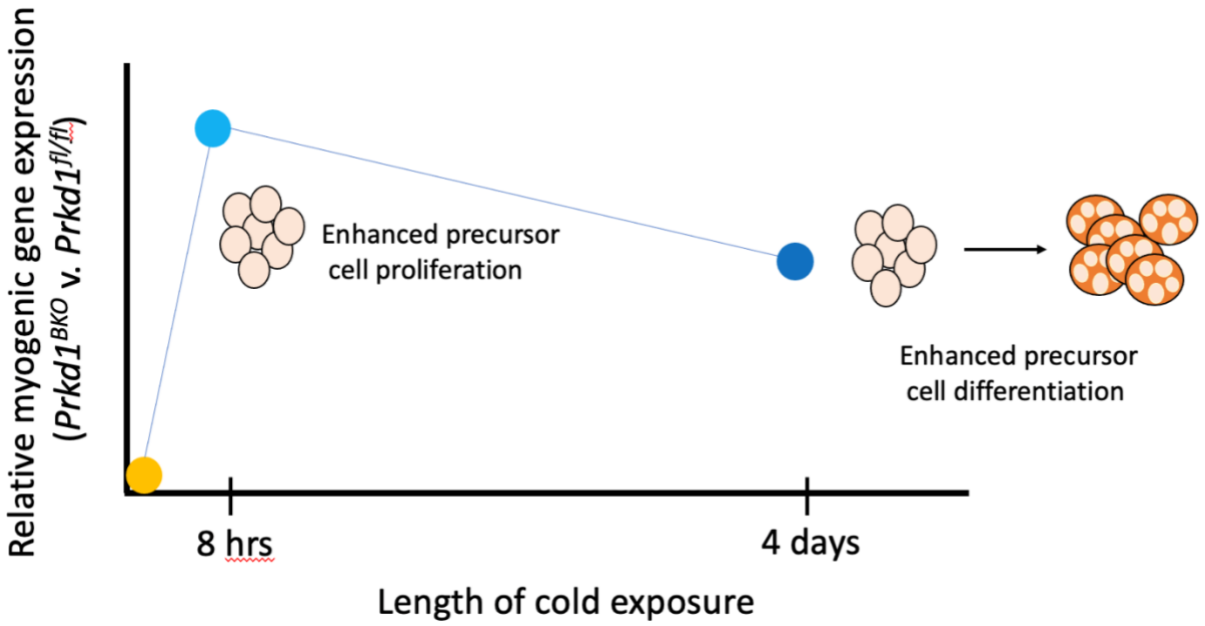

Figure 18: Hypothetical model of *Prkd1* effects on myogenic gene expression after cold exposure. After 8 hours of cold exposure, *Prkd1* loss in BAT enhances myogenic gene expression. Given that the only cell type in BAT known to express a myogenic gene signature is the brown adipocyte precursor, I hypothesize that loss of *Prkd1* results in enhanced brown adipocyte precursor cell proliferation after 8 hours of cold exposure. After 4 days of cold exposure, *Prkd1* loss resulted in reduced myogenic gene expression, though still higher than the thermoneutral baseline. Thus, I further hypothesize that *Prkd1* loss after 4 days of cold exposure promotes brown adipocyte precursor cell differentiation, reducing the number of brown adipocyte precursor cells that could contribute to a myogenic gene signature.

Chapter IV: Conclusions and Future Directions

Brown adipose tissue thermogenesis, as studied in this thesis, is not regulated by PRKD1. Given the compelling data from Löffler et. al. (251), the data presented here were surprising and a bit confusing. Nonetheless, using established methods for interrogating adaptive thermogenesis in adipose tissue, I found that deletion of PRKD1 in UCP1-expressing adipocytes did not alter 1) thermogenic gene expression, 2) adipocyte morphology, or 3) body temperature. There is not a significant body of literature examining the role of PRKD1 in adipose tissue biology. In fact, my publication is only one of three on this topic (277). What remains unresolved among the previously published reports is whether PRKD1 differentially regulates AT thermogenesis in BAT versus WAT, particularly the inguinal WAT. Additionally, an understanding of the functional role and mechanism of PRKD1 regulation of myogenic gene expression needs additional investigation.

Despite our unique findings, some of my data are consistent with published studies. First, in my studies, I observed that loss of *Prkd1* in BAT reduced the expression of lipogenic genes in the iBAT of mice acclimated at thermoneutrality for 2 days. Similarly, Löffler et. al. found that shRNA knockdown of Prkd1 in 3T3-L1 adipocytes – admittedly an immortalized cell line – reduced the rate of lipogenesis (incorporation of tritiated glucose to palmitate) (251). Both white and brown adipocytes increase the expression of lipogenic genes during differentiation to facilitate their function as energy reserves (278), whether to meet whole organism nutrient demand or thermogenic demand, respectively. Another similarity is the finding that SVF differentiated *in vitro* from the inguinal WAT of *Prkd1* adKO mice published by Löffler and colleagues (251) had higher expression of myogenic genes after 24 hours of iso stimulation than cells expressing *Prkd1*. This result is consistent with results presented in this thesis; *Prkd1* deletion in brown adipocytes enhances myogenic gene expression in BAT after acute (8 hour) exposure to cold (which can be mimicked by iso stimulation *in vitro*). Myf5+ progenitors constitute a small percentage (~11%) of adipocyte progenitors in the inguinal WAT and have the capacity to differentiate into both white and beige adipocytes (279). The presence of these “canonically BAT” progenitors may explain why changes in myogenic gene expression could be detected in cells from an established WAT depot. <u>Specifically, my data, taken together with those of Löffler and colleagues, are consistent with the interpretation that *PRKD1* acts to suppress myogenic gene expression during the initial phases (8-24 hours) of β-AR stimulation of both BAT and WAT.</u> The significance of this conclusion will be discussed later in this chapter. So,

it appears that regardless of the depot, *Prkd1* modulates transcriptional changes (i.e., lipogenic and myogenic) associated with adipocyte differentiation, albeit in opposite directions.

However, I observed no effect of *Prkd1* loss in UCP1-expressing brown adipocytes on thermogenesis (i.e., thermogenic gene expression, body temperature, and adipocyte morphology), while Löffler and colleagues (251) observed significant differences in thermogenesis in WAT depots expressing or lacking *Prkd1*. As this was discussed primarily in Chapter 3, it is sufficient to say that the differences in model systems used and AT depots examined likely accounts for these differences. Furthermore, comprehensive studies examining all AT depots using both the *Prkd1*$^{fl/fl}$; AdipoQ-Cre and *Ucp1*-Cre models would serve to clarify any differences observed between these two studies. Based on available data, it would be logical to conclude that *Prkd1* regulates energy expenditure in WAT, but not in BAT. Investigating how such a change in energy expenditure occurs – whether due to uncoupled respiration in mitochondria, or due to mitophagy, which is associated with mitochondrial fragmentation; a significant feature of the Löffler model, or other futile metabolic cycle such as simultaneous lipogenesis/lipolysis would be interesting to further explore.

My results indicate that *Prkd1* does regulate myogenic gene expression in BAT and WAT (data presented in this thesis [Chapter 3] and (251)). The primary source of myogenic gene expression in BAT is *Myf5*+ brown adipocyte progenitor cells (142, 175), which can, upon *in vitro* differentiation, become either brown adipocytes or skeletal myocytes (174, 180). This was discussed in Chapter 1, with the brown adipocyte differentiation pathway being driven by PRDM16. Though WAT has significantly fewer of these *Myf5*+ cells (279, 280), they seem to produce a detectable myogenic gene signature in cells derived from WAT also (251). In my experimental model, I used a *Prkd1*$^{fl/fl}$; *Ucp1*-Cre model, so *Prkd1* is only deleted in mature brown and beige adipocytes. From this, a central hypothesis arises: that *Prkd1* suppresses myogenic gene expression to promote the differentiation of brown and beige adipocytes. However, my data do not provide clarity as to whether this myogenic gene signature is derived from mature UCP1-expressing adipocytes or other cell types in BAT that may be non-cell autonomously regulated by mature brown adipocytes lacking *Prkd1*. So, a primary objective of any further investigation into the data presented in this thesis should include identifying the cell type of origin for the observed changes in myogenic gene expression.

First, single cell RNA-Seq would determine how the number and type of cells that constitute BAT and/or WAT changes after *Prkd1* loss; my studies used bulk RNA-Seq methods. Also, mature brown and white adipocytes should be harvested from *Prkd1*-expressing and deficient mice to examine their myogenic gene expression, particularly in the context of β-AR stimulation (i.e., iso) to discover whether the *Prkd1*-dependent changes in myogenic gene expression originate in mature brown or white adipocytes. Another way to test this hypothesis is to isolate adipocyte progenitors from *Prkd1*-expressing and knockout BAT and WAT using flow cytometry. Markers such as PREF1 and PDGFRα are validated markers for distinguishing adipocyte progenitor populations from other cell types in AT (134, 281). For this experiment, there should be 2 cell populations and 2 experimental ones. The control cells would be *Prkd1*-expressing progenitors from BAT or WAT (namely the inguinal depot), while the experimental cell populations are *Prkd1*-deficient/null progenitors from BAT or WAT and all would be differentiated *in vitro*. Myogenic gene expression would then be measured throughout the differentiation process to assess the effects of both *Prkd1* deficiency and differences between *Prkd1* effects in BAT and WAT. These studies would determine whether the myogenic gene expression changes I observed are produced by adipocyte progenitors and if yes, indicate at what stage of differentiation *Prkd1* begins to alter myogenic gene expression.

The hypothesis described in the previous paragraph is based on the assumption that altered myogenic gene *transcription* alone is responsible for the signature observed in the RNA-Seq data presented in this thesis. Another hypothesis is that adipocyte progenitor *number* is altered upon deletion of *Prkd1* from *mature* brown and beige adipocytes. The same flow cytometry strategy described above could be used to answer this question, except that cells would be counted rather than subjected to differentiation protocols. If loss of PRKD1 results in enhanced brown and beige adipocyte precursor number in these studies, such a result would be consistent with the findings of Löffler et. al. (251) as well as my 8-hour cold exposure data. Even when interpreting these data, caution must be taken due to the varied experimental conditions between my studies and those of Löffler and colleagues. A great deal more work must be performed at different temperature conditions to confirm how PRKD1 functions to modulate this unique, yet seemingly important gene signature in AT.

Several genome-wide association studies have identified *Prkd1* is an obesity risk allele in humans (282-285). Additionally, in rodents, *Prkd1* expression (mRNA) is highest in BAT and WAT relative to all other rodent

tissues (Novartis BioGPS). Taken together, these findings would lead an investigator to logically conclude that PRKD1 plays an important functional role in AT; however, our data demonstrate that such a conclusion does not include thermogenesis in BAT (i.e., adipocyte morphology, thermogenic gene expression, and body temperature). Examining other processes in BAT, including brown adipocyte development and differentiation, may provide a deeper understanding of how PRKD1 affects BAT physiology.

In most of the studies examining the physiology of BAT, the mature brown adipocyte has been the main focus. These studies are, thus, consistent with the prevailing evidence: that mature brown adipocyte number and activity are responsible for the beneficial effects of BAT on insulin sensitivity and fat mass in both rodents in humans. However, until the cell type of origin for the altered myogenic gene signature is confirmed, the adipocyte precursor is a viable target for investigation as it relates to the role of PRKD1 in BAT. In fact, the ability of these cells to acutely proliferate and differentiate in response to hormonal or environmental (namely cold) stimuli positions them as potential key modulators of BAT function and may help investigators to increase their understanding of this complex tissue.

Given the prior failure of agents such as selective β_3-AR agonists directly targeting the mature brown adipocytes in clinical trials, other avenues of experimentation are appropriate as scientists continue to understand both how BAT functions as a tissue and its contributions to whole body metabolism. These studies suggest that other cell types in BAT should be studied with greater intensity in order for society to harness the power of BAT for therapeutic benefit and work towards ending the obesity epidemic, once and for all.

REFERENCES

1. **Boutari C, and Mantzoros CS**. A 2022 update on the epidemiology of obesity and a call to action: as its twin COVID-19 pandemic appears to be receding, the obesity and dysmetabolism pandemic continues to rage on. *Metabolism* 133: 155217, 2022.
2. **Ahima RS, and Flier JS**. Adipose tissue as an endocrine organ. *Trends Endocrinol Metab* 11: 327-332, 2000.
3. **Berry R, and Rodeheffer MS**. Characterization of the adipocyte cellular lineage in vivo. *Nat Cell Biol* 15: 302-308, 2013.
4. **Garaulet M, Hernandez-Morante JJ, Lujan J, Tebar FJ, and Zamora S**. Relationship between fat cell size and number and fatty acid composition in adipose tissue from different fat depots in overweight/obese humans. *Int J Obes (Lond)* 30: 899-905, 2006.
5. **Lubetzki J, Mosse A, Roussel C, Duprey J, and Warnet A**. [Morphology of the adipose tissue in obesity. Relationship between the size and number of adipocytes and certain clinical and biological parameters of obesity]. *Ann Med Interne (Paris)* 128: 755-758, 1977.
6. **Lee JT, Pamir N, Liu NC, Kirk EA, Averill MM, Becker L, Larson I, Hagman DK, Foster-Schubert KE, van Yserloo B, Bornfeldt KE, LeBoeuf RC, Kratz M, and Heinecke JW**. Macrophage metalloelastase (MMP12) regulates adipose tissue expansion, insulin sensitivity, and expression of inducible nitric oxide synthase. *Endocrinology* 155: 3409-3420, 2014.
7. **Smith U**. Abdominal obesity: a marker of ectopic fat accumulation. *J Clin Invest* 125: 1790-1792, 2015.
8. **Snel M, Jonker JT, Schoones J, Lamb H, de Roos A, Pijl H, Smit JW, Meinders AE, and Jazet IM**. Ectopic fat and insulin resistance: pathophysiology and effect of diet and lifestyle interventions. *Int J Endocrinol* 2012: 983814, 2012.
9. **Adams JM, 2nd, Pratipanawatr T, Berria R, Wang E, DeFronzo RA, Sullards MC, and Mandarino LJ**. Ceramide content is increased in skeletal muscle from obese insulin-resistant humans. *Diabetes* 53: 25-31, 2004.
10. **Silverman JF, O'Brien KF, Long S, Leggett N, Khazanie PG, Pories WJ, Norris HT, and Caro JF**. Liver pathology in morbidly obese patients with and without diabetes. *Am J Gastroenterol* 85: 1349-1355, 1990.
11. **Nuttall FQ**. Body Mass Index: Obesity, BMI, and Health: A Critical Review. *Nutr Today* 50: 117-128, 2015.
12. **Alberti KGMM, and Zimmet PZ**. Definition, diagnosis and classification of diabetes mellitus and its complications. Part 1: diagnosis and classification of diabetes mellitus provisional report of a WHO consultation. *Diabet Med* 15: 539-553, 1998.
13. **Caballero B**. Humans against Obesity: Who Will Win? *Adv Nutr* 10: S4-S9, 2019.
14. **Tuck ML, Sowers J, Dornfeld L, Kledzik G, and Maxwell M**. The effect of weight reduction on blood pressure, plasma renin activity, and plasma aldosterone levels in obese patients. *N Engl J Med* 304: 930-933, 1981.
15. **Harp JB, Henry SA, and DiGirolamo M**. Dietary weight loss decreases serum angiotensin-converting enzyme activity in obese adults. *Obes Res* 10: 985-990, 2002.
16. **Norris SL, Zhang X, Avenell A, Gregg E, Bowman B, Serdula M, Brown TJ, Schmid CH, and Lau J**. Long-term effectiveness of lifestyle and behavioral weight loss interventions in adults with type 2 diabetes: a meta-analysis. *Am J Med* 117: 762-774, 2004.
17. **Passmore R, and Durnin JV**. Human energy expenditure. *Physiol Rev* 35: 801-840, 1955.
18. **Wisloff U, Nilsen TI, Droyvold WB, Morkved S, Slordahl SA, and Vatten LJ**. A single weekly bout of exercise may reduce cardiovascular mortality: how little pain for cardiac gain? 'The HUNT study, Norway'. *Eur J Cardiovasc Prev Rehabil* 13: 798-804, 2006.

19. **Stamatakis E, Ahmadi MN, Gill JMR, Thogersen-Ntoumani C, Gibala MJ, Doherty A, and Hamer M**. Association of wearable device-measured vigorous intermittent lifestyle physical activity with mortality. *Nat Med* 28: 2521-2529, 2022.
20. Vigorous intermittent lifestyle physical activity improves mortality risk. *Nat Med* 28: 2484-2485, 2022.
21. **Harris MB, and Kuo CH**. Scientific Challenges on Theory of Fat Burning by Exercise. *Front Physiol* 12: 685166, 2021.
22. **Jacob JJ, and Isaac R**. Behavioral therapy for management of obesity. *Indian J Endocrinol Metab* 16: 28-32, 2012.
23. **Grundlingh J, Dargan PI, El-Zanfaly M, and Wood DM**. 2,4-dinitrophenol (DNP): a weight loss agent with significant acute toxicity and risk of death. *J Med Toxicol* 7: 205-212, 2011.
24. **Laddu D, Dow C, Hingle M, Thomson C, and Going S**. A review of evidence-based strategies to treat obesity in adults. *Nutr Clin Pract* 26: 512-525, 2011.
25. **Goergen M, Arapis K, Limgba A, Schiltz M, Lens V, and Azagra JS**. Laparoscopic Roux-en-Y gastric bypass versus laparoscopic vertical banded gastroplasty: results of a 2-year follow-up study. *Surg Endosc* 21: 659-664, 2007.
26. **Khalaf KI, and Taegtmeyer H**. Clues from bariatric surgery: reversing insulin resistance to heal the heart. *Curr Diab Rep* 13: 245-251, 2013.
27. **Antonopulos C, Rebibo L, Calabrese D, Ribeiro-Parenti L, Arapis K, Dhahri A, Coupaye M, Hansel B, Marmuse JP, Regimbeau JM, and Msika S**. Comparison of Repeat Sleeve Gastrectomy and Roux-en-Y Gastric Bypass in Case of Weight Loss Failure After Sleeve Gastrectomy. *Obes Surg* 29: 3919-3927, 2019.
28. **Trujillo JM, Nuffer W, and Smith BA**. GLP-1 receptor agonists: an updated review of head-to-head clinical studies. *Ther Adv Endocrinol Metab* 12: 2042018821997320, 2021.
29. **Pass A, Bialonczyk D, Chiquette E, and Goldman JD**. Oral Superabsorbent Hydrogel (Plenity) for Weight Management. *Ann Pharmacother* 55: 1146-1152, 2021.
30. **Chavda VP, Ajabiya J, Teli D, Bojarska J, and Apostolopoulos V**. Tirzepatide, a New Era of Dual-Targeted Treatment for Diabetes and Obesity: A Mini-Review. *Molecules* 27: 2022.
31. **Stepien M, Stepien A, Wlazel RN, Paradowski M, Banach M, and Rysz J**. Obesity indices and inflammatory markers in obese non-diabetic normo- and hypertensive patients: a comparative pilot study. *Lipids Health Dis* 13: 29, 2014.
32. **Stenlof K, Wernstedt I, Fjallman T, Wallenius V, Wallenius K, and Jansson JO**. Interleukin-6 levels in the central nervous system are negatively correlated with fat mass in overweight/obese subjects. *J Clin Endocrinol Metab* 88: 4379-4383, 2003.
33. **Cinti S, Mitchell G, Barbatelli G, Murano I, Ceresi E, Faloia E, Wang S, Fortier M, Greenberg AS, and Obin MS**. Adipocyte death defines macrophage localization and function in adipose tissue of obese mice and humans. *J Lipid Res* 46: 2347-2355, 2005.
34. **Cinti S**. The adipose organ. Milano: Kurtis, 1999.
35. **Barzilai N, Wang J, Massilon D, Vuguin P, Hawkins M, and Rossetti L**. Leptin selectively decreases visceral adiposity and enhances insullin action. *J Clin Invest* 100, no. 12: 3105-3110, 1997.
36. **Harris R, Zhou J, Redmann S, Smagin G, Smith S, Rodgers E, and Zachwieja J**. A leptin dose-response study in obese (ob/ob) and lean (+/?) mice. *Endocrinology* 139, no. 1: 8-19, 1998.
37. **Elmquist JK, Elias CF, and Saper CB**. From lesions to leptin: hypothalamic control of food intake and body weight. *Neuron* 22: 221-232, 1999.
38. **Gavrila A, Chan JL, Yiannakouris N, Kontogianni M, Miller LC, Orlova C, and Mantzoros CS**. Serum adiponectin levels are inversely associated with overall and central fat distribution but are not directly regulated by acute fasting or leptin administration in humans: cross-sectional and interventional studies. *J Clin Endocrinol Metab* 88: 4823-4831, 2003.

39. **Antuna-Puente B, Feve B, Fellahi S, and Bastard JP**. Adipokines: the missing link between insulin resistance and obesity. *Diabetes Metab* 34: 2-11, 2008.
40. **Cinti S**. The adipose organ at a glance. *Dis Model Mech* 5: 588-594, 2012.
41. **Trayhurn P**. The biology of obesity. *Proc Nutr Soc* 64: 31-38, 2005.
42. **Cinti S**. Adipocyte differentiation and transdifferentiation: plasticity of the adipose organ. *J Endocrinol Invest* 25: 823-835, 2002.
43. **Cinti S, Zingaretti MC, Cancello R, Ceresi E, and Ferrara P**. Morphologic techniques for the study of brown adipose tissue and white adipose tissue. In: *Methods Mol Biol*, edited by Ailhaud G. Totowa, NJ: Humana Press, 2001, p. 21-51.
44. **Rosen ED, and Spiegelman BM**. What we talk about when we talk about fat. *Cell* 156: S28-33, 2014.
45. **Berg AH, and Scherer PE**. Adipose tissue, inflammation, and cardiovascular disease. *Circ Res* 96: 939-949, 2005.
46. **Wang P, Mariman E, Renes J, and Keijer J**. The secretory function of adipocytes in the physiology of white adipose tissue. *J Cell Physiol* 216: 3-13, 2008.
47. **Rotondo F, Ho-Palma AC, Remesar X, Fernandez-Lopez JA, Romero MDM, and Alemany M**. Glycerol is synthesized and secreted by adipocytes to dispose of excess glucose, via glycerogenesis and increased acyl-glycerol turnover. *Sci Rep* 7: 8983, 2017.
48. **Silva Figueiredo P, Carla Inada A, Marcelino G, Maiara Lopes Cardozo C, de Cassia Freitas K, de Cassia Avellaneda Guimaraes R, Pereira de Castro A, Aragao do Nascimento V, and Aiko Hiane P**. Fatty Acids Consumption: The Role Metabolic Aspects Involved in Obesity and Its Associated Disorders. *Nutrients* 9: 2017.
49. **Ameer F, Scandiuzzi L, Hasnain S, Kalbacher H, and Zaidi N**. *De novo* lipogenesis in health and disease. *Metabolism* 63: 895-902, 2014.
50. **Funai K, Song H, Yin L, Lodhi IJ, Wei X, Yoshino J, Coleman T, and Semenkovich CF**. Muscle lipogenesis balances insulin sensitivity and strength through calcium signaling. *J Clin Invest* 123: 1229-1240, 2013.
51. **Solinas G, Boren J, and Dulloo AG**. De novo lipogenesis in metabolic homeostasis: More friend than foe? *Mol Metab* 4: 367-377, 2015.
52. **Ferramosca A, and Zara V**. Dietary fat and hepatic lipogenesis: mitochondrial citrate carrier as a sensor of metabolic changes. *Adv Nutr* 5: 217-225, 2014.
53. **Foster DW**. Malonyl-CoA: the regulator of fatty acid synthesis and oxidation. *J Clin Invest* 122: 1958-1959, 2012.
54. **Chakravarty B, Gu Z, Chirala SS, Wakil SJ, and Quiocho FA**. Human fatty acid synthase: structure and substrate selectivity of the thioesterase domain. *Proc Natl Acad Sci U S A* 101: 15567-15572, 2004.
55. **Jensen-Urstad AP, and Semenkovich CF**. Fatty acid synthase and liver triglyceride metabolism: housekeeper or messenger? *Biochim Biophys Acta* 1821: 747-753, 2012.
56. **Ahmadian M, Wang Y, and Sul HS**. Lipolysis in adipocytes. *Int J Biochem Cell Biol* 42: 555-559, 2010.
57. **Recinella L, Orlando G, Ferrante C, Chiavaroli A, Brunetti L, and Leone S**. Adipokines: New Potential Therapeutic Target for Obesity and Metabolic, Rheumatic, and Cardiovascular Diseases. *Front Physiol* 11: 578966, 2020.
58. **Ouchi N, Parker JL, Lugus JJ, and Walsh K**. Adipokines in inflammation and metabolic disease. *Nat Rev Immunol* 11: 85-97, 2011.
59. **Cinti S, Frederich RC, Zingaretti MC, de Matteis R, Flier JS, and Lowell BB**. Immunohistochemical localization of leptin and uncoupling protein in white and brown adipose tissue. *Endocrinology* 138: 797-804, 1997.
60. **Friedman JM, and Halaas JL**. Leptin and the regulation of body weight in mammals. *Nature* 395: 763-770, 1998.

61. **Friedman JM, Leibel RL, Siegel DS, Walsh J, and Bahary N**. Molecular mapping of the mouse ob mutation. *Genomics* 11: 1054-1062, 1991.
62. **Ingalls AM, Dickie MM, and Snell GD**. Obese, a new mutation in the house mouse. *Obes Res* 4: 101, 1996.
63. **MacDougald OA, Hwang CS, Fan H, and Lane MD**. Regulated expression of the obese gene product (leptin) in white adipose tissue and 3T3-L1 adipocytes. *Proc Natl Acad Sci U S A* 92: 9034-9037, 1995.
64. **Oliver P, Pico C, and Palou A**. Ontogenesis of leptin expression in different adipose tissue depots in the rat. *Pflugers Arch* 442: 383-390, 2001.
65. **Mason MM, He Y, Chen H, Quon MJ, and Reitman M**. Regulation of leptin promoter function by Sp1, C/EBP, and a novel factor. *Endocrinology* 139: 1013-1022, 1998.
66. **Caron A, Dungan Lemko HM, Castorena CM, Fujikawa T, Lee S, Lord CC, Ahmed N, Lee CE, Holland WL, Liu C, and Elmquist JK**. POMC neurons expressing leptin receptors coordinate metabolic responses to fasting via suppression of leptin levels. *Elife* 7: 2018.
67. **Ahima RS, Saper CB, Flier JS, and Elmquist JK**. Leptin regulation of neuroendocrine systems. *Front Neuroendocrinol* 21: 263-307, 2000.
68. **Coleman DL**. Effects of parabiosis of obese with diabetes and normal mice. *Diabetologia* 9: 294-298, 1973.
69. **Liu M, and Liu F**. Transcriptional and post-translational regulation of adiponectin. *Biochem J* 425: 41-52, 2009.
70. **Turer AT, and Scherer PE**. Adiponectin: mechanistic insights and clinical implications. *Diabetologia* 55: 2319-2326, 2012.
71. **Esteve Rafols M**. Adipose tissue: cell heterogeneity and functional diversity. *Endocrinol Nutr* 61: 100-112, 2014.
72. **Strissel KJ, Stancheva Z, Miyoshi H, Perfield JW, DeFuria J, Jick Z, Greenberg AS, and Obin MS**. Adipocyte death, adipose tissue remodeling, and obesity complications. *Diabetes* 56: 2910-2918, 2007.
73. **Apovian CM, Bigornia S, Mott M, Meyers MR, Ulloor J, Gagua M, McDonnell M, Hess D, Joseph L, and Gokce N**. Adipose macrophage infiltration is associated with insulin resistance and vascular endothelial dysfunction in obese subjects. *Arterioscler Thromb Vasc Biol* 28: 1654-1659, 2008.
74. **Bastard J-P, Maachi M, Lagathu C, Kim MJ, Caron M, Vidal H, Capeau J, and Feve B**. Recent advances in the relationship between obesity, inflammation, and insulin resistance. *Eur Cytokine Netw* 17: 4-12, 2006.
75. **Cannon B, and Nedergaard J**. Brown adipose tissue: function and physiological significance. *Physiol Rev* 84: 277-359, 2004.
76. **Blondin DP, Labbe SM, Christian Tingelstad H, Noll C, Kunach M, Phoenix S, Guerin B, Turcotte EE, Carpentier AC, Richard D, and Haman F**. Increased brown adipose tissue oxidative capacity in cold-acclimated humans. *J Clin Endocrinol Metab* 99: E438-E446, 2014.
77. **Argyropoulos G, and Harper ME**. Uncoupling proteins and thermoregulation. *J Appl Physiol* 92: 2187-2198, 2002.
78. **Blondin DP, Daoud A, Taylor T, Tingelstad HC, Bezaire V, Richard D, Carpentier AC, Taylor AW, Harper ME, Aguer C, and Haman F**. Four-week cold acclimation in adult humans shifts uncoupling thermogenesis from skeletal muscles to brown adipose tissue. *J Physiol* 595: 2099-2113, 2017.
79. **Gordon K, Blondin DP, Friesen BJ, Tingelstad HC, Kenny GP, and Haman F**. Seven days of cold acclimation substantially reduces shivering intensity and increases nonshivering thermogenesis in adult humans. *J Appl Physiol (1985)* 126: 1598-1606, 2019.
80. **Chondronikola M, Volpi E, Borsheim E, Porter C, Annamalai P, Enerback S, Lidell ME, Saraf MK, Labbe SM, Hurren NM, Yfanti C, Chao T, Andersen CR, Cesani F, Hawkins H,**

and Sidossis LS. Brown adipose tissue improves whole-body glucose homeostasis and insulin sensitivity in humans. *Diabetes* 63: 4089-4099, 2014.

81. **Bartelt A, and Heeren J**. Adipose tissue browning and metabolic health. *Nat Rev Endocrinol* 10: 24-36, 2014.
82. **Becher T, Palanisamy S, Kramer DJ, Eljalby M, Marx SJ, Wibmer AG, Butler SD, Jiang CS, Vaughan R, Schoder H, Mark A, and Cohen P**. Brown adipose tissue is associated with cardiometabolic health. *Nat Med* 27: 58-65, 2021.
83. **Bartelt A, Bruns OT, Reimer R, Hohenberg H, Ittrich H, Peldschus K, Kaul MG, Tromsdorf UI, Weller H, Waurisch C, Eychmuller A, Gordts PL, Rinninger F, Bruegelmann K, Freund B, Nielsen P, Merkel M, and Heeren J**. Brown adipose tissue activity controls triglyceride clearance. *Nat Med* 17: 200-205, 2011.
84. **Liu X, Zheng Z, Zhu X, Meng M, Li L, Shen Y, Chi Q, Wang D, Zhang Z, Li C, Li Y, Xue Y, Speakman JR, and Jin W**. Brown adipose tissue transplantation improves whole-body energy metabolism. *Cell Res* 23: 851-854, 2013.
85. **Cypess AM, Lehman S, Williams G, Tal I, Rodman D, Goldfine AB, Kuo FC, Palmer EL, Tseng YH, Doria A, Kolodny GM, and Kahn CR**. Identification and importance of brown adipose tissue in adult humans. *N Engl J Med* 360: 1509-1517, 2009.
86. **Graja A, and Schulz TJ**. Mechanisms of aging-related impairment of brown adipocyte development and function. *Gerontology* 61: 211-217, 2015.
87. **Mancini C, Gohlke S, Garcia-Carrizo F, Zagoriy V, Stephanowitz H, and Schulz TJ**. Identification of biomarkers of brown adipose tissue aging highlights the role of dysfunctional energy and nucleotide metabolism pathways. *Sci Rep* 11: 19928, 2021.
88. **In Het Panhuis W, Schonke M, Siebeler R, Afkir S, Baelde R, Pronk ACM, Streefland TCM, Sips HCM, Lalai RA, Rensen PCN, and Kooijman S**. Aging attenuates diurnal lipid uptake by brown adipose tissue. *Aging (Albany NY)* 14: 7734-7751, 2022.
89. **Nedergaard J, Bengtsson T, and Cannon B**. Unexpected evidence for active brown adipose tissue in adult humans. *Am J Physiol Endocrinol Metab* 293: E444-452, 2007.
90. **van Rooijen BD, van der Lans AA, Brans B, Wildberger JE, Mottaghy FM, Schrauwen P, Backes WH, and van Marken Lichtenbelt WD**. Imaging Cold-Activated Brown Adipose Tissue Using Dynamic T2*-Weighted Magnetic Resonance Imaging and 2-Deoxy-2-[18F]fluoro-D-glucose Positron Emission Tomography. *Invest Radiol* 2013.
91. **Halpern B, Mancini MC, and Halpern A**. Brown adipose tissue: what have we learned since its recent identification in human adults. *Arq Bras Endocrinol Metabol* 58: 889-899, 2014.
92. **Mo Q, Salley J, Roshan T, Baer LA, May FJ, Jaehnig EJ, Lehnig AC, Guo X, Tong Q, Nuotio-Antar AM, Shamsi F, Tseng YH, Stanford KI, and Chen MH**. Identification and characterization of a supraclavicular brown adipose tissue in mice. *JCI Insight* 2: 2017.
93. **de Jong JMA, Sun W, Pires ND, Frontini A, Balaz M, Jespersen NZ, Feizi A, Petrovic K, Fischer AW, Bokhari MH, Niemi T, Nuutila P, Cinti S, Nielsen S, Scheele C, Virtanen K, Cannon B, Nedergaard J, Wolfrum C, and Petrovic N**. Human brown adipose tissue is phenocopied by classical brown adipose tissue in physiologically humanized mice. *Nat Metab* 1: 830-843, 2019.
94. **Afzelius BJ**. Brown adipose tissue: its gross anatomy, histology, and cytology. In: *Brown Adipose Tissue*, edited by Lindberg O. New York: American Elsevier Publishing Co., 1970, p. 1-31.
95. **Cinti S, Zingaretti MC, Cancello R, Ceresi E, and Ferrara P**. Morphologic techniques for the study of brown adipose tissue and white adipose tissue. *Methods Mol Biol* 155: 21-51, 2001.
96. **Arch JRS, Cawthorne MA, Coney KA, Gusterson BA, Piercy V, Sennitt MV, Smith SA, Wallace J, and Wilson S**. ®-Adrenoceptor-mediated control of thermogenesis, body

composition and glucose homeostasis. In: *Obesity and Cachexia*, edited by Rothwell NJ, and Stock MJ. New York: John Wiley & Sons Ltd., 1991, p. 241-268.
97. **Stanford KI, Middelbeek RJ, Townsend KL, An D, Nygaard EB, Hitchcox KM, Markan KR, Nakano K, Hirshman MF, Tseng YH, and Goodyear LJ**. Brown adipose tissue regulates glucose homeostasis and insulin sensitivity. *J Clin Invest* 123: 215-223, 2013.
98. **van Marken Lichtenbelt WD, and Schrauwen P**. Implications of non-shivering thermogenesis for energy balance regulation in humans. *Am J Physiol Regul Integr Comp Physiol* 2011.
99. **Uldry M, Yang W, St-Pierre J, Lin J, Seale P, and Spiegelman BM**. Complementary action of the PGC-1 coactivators in mitochondrial biogenesis and brown fat differentiation. *Cell Metab* 3: 333-341, 2006.
100. **Ricquier D**. Uncoupling protein 1 of brown adipocytes, the only uncoupler: a historical perspective. *Front Endocrinol (Lausanne)* 2: 85, 2011.
101. **Zhao RZ, Jiang S, Zhang L, and Yu ZB**. Mitochondrial electron transport chain, ROS generation and uncoupling (Review). *Int J Mol Med* 44: 3-15, 2019.
102. **Mitchell P**. Vectorial chemistry and the molecular mechanics of chemiosmotic coupling: power transmission by proticity. *Biochem Soc Trans* 4: 399-430, 1976.
103. **Chouchani ET, Kazak L, and Spiegelman BM**. New Advances in Adaptive Thermogenesis: UCP1 and Beyond. *Cell Metab* 29: 27-37, 2019.
104. **Arechaga I, Ledesma A, and Rial E**. The mitochondrial uncoupling protein UCP1: a gated pore. *IUBMB Life* 52: 165-173, 2001.
105. **Brand MD, Brindle KM, Buckingham JA, Harper JA, Rolfe DF, and Stuart JA**. The significance and mechanism of mitochondrial proton conductance. *Int J Obes Relat Metab Disord* 23 Suppl 6: S4-11, 1999.
106. **Mitchell P**. Coupling of phosphorylation to electron and hydrogen transfer by a chemi-osmotic type of mechanism. *Nature* 191: 144-148, 1961.
107. **Wang Z, Ning T, Song A, Rutter J, Wang QA, and Jiang L**. Chronic cold exposure enhances glucose oxidation in brown adipose tissue. *EMBO Rep* 21: e50085, 2020.
108. **Townsend KL, and Tseng YH**. Brown fat fuel utilization and thermogenesis. *Trends Endocrinol Metab* 25: 168-177, 2014.
109. **Bamshad M, Song CK, and Bartness TJ**. CNS origins of the sympathetic nervous system outflow to brown adipose tissue. *Am J Physiol* 276: R1569-1578, 1999.
110. **Bengtsson T, Cannon B, and Nedergaard J**. Differential adrenergic regulation of the gene expression of the beta-adrenoceptor subtypes beta1, beta2 and beta3 in brown adipocytes. *Biochem J* 347 Pt 3: 643-651, 2000.
111. **Lafontan M, and Berlan M**. Fat cell adrenergic receptors and the control of white and brown fat cell function. *J Lipid Res* 34: 1057-1091, 1993.
112. **Atgie C, D'Allaire F, and Bukowiecki LJ**. Role of beta1- and beta3-adrenoceptors in the regulation of lipolysis and thermogenesis in rat brown adipocytes. *Am J Physiol* 273: C1136-1142, 1997.
113. **Bukowiecki L, Collet AJ, Follea N, Guay G, and Jahjah L**. Brown adipose tissue hyperplasia: a fundamental mechanism of adaptation to cold and hyperphagia. *Am J Physiol* 242: E353-359, 1982.
114. **Cannon B, Jacobsson A, Rehnmark s, and Nedergaard J**. Signal transduction in brown adipose tissue recruitment: noradrenaline and beyond. *Int J Obesity* 20: S36-S42, 1996.
115. **Bronnikov G, Houstek J, and Nedergaard J**. ®-Adrenergic, cAMP-mediated stimulation of proliferation of brown fat cells in primary culture. *J Biol Chem* 267: 2006-2013, 1992.
116. **Gantner ML, Hazen BC, Eury E, Brown EL, and Kralli A**. Complementary Roles of Estrogen-Related Receptors in Brown Adipocyte Thermogenic Function. *Endocrinology* 157: 4770-4781, 2016.

117. **Fedorenko A, Lishko PV, and Kirichok Y**. Mechanism of fatty-acid-dependent UCP1 uncoupling in brown fat mitochondria. *Cell* 151: 400-413, 2012.
118. **Robinson LJ, Law JM, Symonds ME, and Budge H**. Brown adipose tissue activation as measured by infrared thermography by mild anticipatory psychological stress in lean healthy females. *Exp Physiol* 101: 549-557, 2016.
119. **Ramage LE, Akyol M, Fletcher AM, Forsythe J, Nixon M, Carter RN, van Beek EJ, Morton NM, Walker BR, and Stimson RH**. Glucocorticoids Acutely Increase Brown Adipose Tissue Activity in Humans, Revealing Species-Specific Differences in UCP-1 Regulation. *Cell Metab* 24: 130-141, 2016.
120. **Hasan N, Nagata N, Morishige JI, Islam MT, Jing Z, Harada KI, Mieda M, Ono M, Fujiwara H, Daikoku T, Fujiwara T, Maida Y, Ota T, Shimba S, Kaneko S, Fujimura A, and Ando H**. Brown adipocyte-specific knockout of Bmal1 causes mild but significant thermogenesis impairment in mice. *Mol Metab* 49: 101202, 2021.
121. **Woon PY, Kaisaki PJ, Braganca J, Bihoreau MT, Levy JC, Farrall M, and Gauguier D**. Aryl hydrocarbon receptor nuclear translocator-like (BMAL1) is associated with susceptibility to hypertension and type 2 diabetes. *Proc Natl Acad Sci U S A* 104: 14412-14417, 2007.
122. **Sookoian S, Gemma C, Gianotti TF, Burgueno A, Castano G, and Pirola CJ**. Genetic variants of Clock transcription factor are associated with individual susceptibility to obesity. *Am J Clin Nutr* 87: 1606-1615, 2008.
123. **Finlin BS, Memetimin H, Confides AL, Kasza I, Zhu B, Vekaria HJ, Harfmann B, Jones KA, Johnson ZR, Westgate PM, Alexander CM, Sullivan PG, Dupont-Versteegden EE, and Kern PA**. Human adipose beiging in response to cold and mirabegron. *JCI Insight* 3: e121510, 2018.
124. **Wu J, Bostrom P, Sparks LM, Ye L, Choi JH, Giang AH, Khandekar M, Virtanen KA, Nuutila P, Schaart G, Huang K, Tu H, van Marken Lichtenbelt WD, Hoeks J, Enerback S, Schrauwen P, and Spiegelman BM**. Beige adipocytes are a distinct type of thermogenic fat cell in mouse and human. *Cell* 150: 366-376, 2012.
125. **Bartness TJ, Vaughan CH, and Song CK**. Sympathetic and sensory innervation of brown adipose tissue. *Int J Obes (Lond)* 34 Suppl 1: S36-42, 2010.
126. **Feldmann HM, Golozoubova V, Cannon B, and Nedergaard J**. UCP1 ablation induces obesity and abolishes diet-induced thermogenesis in mice exempt from thermal stress by living at thermoneutrality. *Cell Metab* 9: 203-209, 2009.
127. **Garcia RA, Roemmich JN, and Claycombe KJ**. Evaluation of markers of beige adipocytes in white adipose tissue of the mouse. *Nutr Metab (Lond)* 13: 24, 2016.
128. **Kiefer FW**. The significance of beige and brown fat in humans. *Endocr Connect* 6: R70-R79, 2017.
129. **Cypess AM, White AP, Vernochet C, Schulz TJ, Xue R, Sass CA, Huang TL, Roberts-Toler C, Weiner LS, Sze C, Chacko AT, Deschamps LN, Herder LM, Truchan N, Glasgow AL, Holman AR, Gavrila A, Hasselgren PO, Mori MA, Molla M, and Tseng YH**. Anatomical localization, gene expression profiling and functional characterization of adult human neck brown fat. *Nat Med* 19: 635-639, 2013.
130. **Leitner BP, Huang S, Brychta RJ, Duckworth CJ, Baskin AS, McGehee S, Tal I, Dieckmann W, Gupta G, Kolodny GM, Pacak K, Herscovitch P, Cypess AM, and Chen KY**. Mapping of human brown adipose tissue in lean and obese young men. *Proc Natl Acad Sci U S A* 114: 8649-8654, 2017.
131. **van Marken Lichtenbelt WD, Vanhommerig JW, Smulders NM, Drossaerts JM, Kemerink GJ, Bouvy ND, Schrauwen P, and Teule GJ**. Cold-activated brown adipose tissue in healthy men. *N Engl J Med* 360: 1500-1508, 2009.

132. **Hepler C, Shao M, Xia JY, Ghaben AL, Pearson MJ, Vishvanath L, Sharma AX, Morley TS, Holland WL, and Gupta RK**. Directing visceral white adipocyte precursors to a thermogenic adipocyte fate improves insulin sensitivity in obese mice. *Elife* 6: 2017.
133. **Shao M, Wang QA, Song A, Vishvanath L, Busbuso NC, Scherer PE, and Gupta RK**. Cellular Origins of Beige Fat Cells Revisited. *Diabetes* 68: 1874-1885, 2019.
134. **Lee YH, Petkova AP, Konkar AA, and Granneman JG**. Cellular origins of cold-induced brown adipocytes in adult mice. *Faseb J* 29: 286-299, 2015.
135. **Rosenwald M, Perdikari A, Rulicke T, and Wolfrum C**. Bi-directional interconversion of brite and white adipocytes. *Nat Cell Biol* 15: 659-657, 2013.
136. **Wang QA, Tao C, Gupta RK, and Scherer PE**. Tracking adipogenesis during white adipose tissue development, expansion and regeneration. *Nat Med* 19: 1338-1344, 2013.
137. **Vishvanath L, MacPherson KA, Hepler C, Wang QA, Shao M, Spurgin SB, Wang MY, Kusminski CM, Morley TS, and Gupta RK**. Pdgfrbeta+ Mural Preadipocytes Contribute to Adipocyte Hyperplasia Induced by High-Fat-Diet Feeding and Prolonged Cold Exposure in Adult Mice. *Cell Metab* 23: 350-359, 2016.
138. **Gupta RK, Arany Z, Seale P, Mepani RJ, Ye L, Conroe HM, Roby YA, Kulaga H, Reed RR, and Spiegelman BM**. Transcriptional control of preadipocyte determination by Zfp423. *Nature* 464: 619-623, 2010.
139. **Shao M, Ishibashi J, Kusminski CM, Wang QA, Hepler C, Vishvanath L, MacPherson KA, Spurgin SB, Sun K, Holland WL, Seale P, and Gupta RK**. Zfp423 Maintains White Adipocyte Identity through Suppression of the Beige Cell Thermogenic Gene Program. *Cell Metab* 23: 1167-1184, 2016.
140. **Simon G**. Histogenesis. In: *Handbook of Physiology Adipose Tissue*, edited by A. E. Renold GFC, Jr. Washington, D.C.: American Physiological Society, 1965, p. 101-107.
141. **Wassermann F**. The development of adipose tissue. In: *Handbook of Physiology Adipose Tissue*, edited by A. E. Renold GFC, Jr. Washington, D.C.: American Physiological Society, 1965, p. 87-100.
142. **Timmons JA, Wennmalm K, Larsson O, Walden TB, Lassmann T, Petrovic N, Hamilton DL, Gimeno RE, Wahlestedt C, Baar K, Nedergaard J, and Cannon B**. Myogenic gene expression signature establishes that brown and white adipocytes originate from distinct cell lineages. *Proc Natl Acad Sci U S A* 104: 4401-4406, 2007.
143. **Rosenwald M, and Wolfrum C**. The origin and definition of brite versus white and classical brown adipocytes. *Adipocyte* 3: 4-9, 2014.
144. **Brun RP, Kim JB, Hu E, Altiok S, and Spiegelman BM**. Adipocyte differentiation: a transcriptional regulatory cascade. *Curr Opin Cell Biol* 8: 826-832, 1996.
145. **Brun R, Kim J, Hu E, and Spiegelman B**. Peroxisome proliferator-activated receptor gamma and the control of adipogenesis. *Curr Opin Lipidology* 8: 212-218, 1997.
146. **Hollenberg CH, and Vost A**. Regulation of DNA synthesis in fat cells and stromal elements from rat adipose tissue. *J Clin Invest* 47: 2485-2498, 1969.
147. **Gregoire F, Todoroff G, Hauser N, and Remacle C**. The stroma-vascular fraction of rat inguinal and epididymal adipose tissue and the adipoconversion of fat cell precursors in primary culture. *Biol Cell* 69: 215-222, 1990.
148. **Poznanski WJ, Waheed I, and Van R**. Human fat cell precursors. Morphologic and metabolic differentiation in culture. *Lab Invest* 29: 570-576, 1973.
149. **Van RL, and Roncari DA**. Isolation of fat cell precursors from adult rat adipose tissue. *Cell Tissue Res* 181: 197-203, 1977.
150. **Negrel R, Grimaldi P, Forest C, and Ailhaud G**. Establishment and characterization of fibroblast-like cell Lines derived from adipocytes with the capacity to redifferentiate into adipocyte-like cells. *Meth Enzymol* 109: 377-385, 1985.

151. **Negrel R, Grimaldi P, and Ailhaud G**. Establishment of preadipocyte clonal line from epididymal fat pad of ob/ob mouse that responds to insulin and to lipolytic hormones. *Proc Natl Acad Sci U S A* 75: 6054-6058, 1978.
152. **Chapman AB, Knight DM, Dieckmann BS, and Ringold GM**. Analysis of gene expression during differentiation of adipogenic cells in culture and hormonal control of the developmental program. *J Biol Chem* 259: 1-8, 1984.
153. **Green H, and Kehinde O**. Sublines of mouse 3T3 cells that accumulate lipid. *Cell* 1: 113-116, 1974.
154. **Tontonoz P, Hu E, and Spiegelman BM**. Stimulation of adipogenesis in fibroblasts by PPAR©2, a lipid-activated transcription factor. *Cell* 79: 1147-1156, 1994.
155. **Tontonoz P, Hu E, and Spiegelman BM**. Regulation of adipocyte gene expression and differentiation by peroxisome proliferator activated receptor gamma. *Curr Opin Genet Dev* 5: 571-576, 1995.
156. **Rosen ED, Sarraf P, Troy AE, Bradwin G, Moore K, Milstone DS, Spiegelman BM, and Mortensen RM**. PPAR gamma is required for the differentiation of adipose tissue in vivo and in vitro. *Mol Cell* 4: 611-617, 1999.
157. **Rosen ED, Hsu CH, Wang X, Sakai S, Freeman MW, Gonzalez FJ, and Spiegelman BM**. C/EBPalpha induces adipogenesis through PPARgamma: a unified pathway. *Genes Dev* 16: 22-26, 2002.
158. **Chawla A, and Lazar MA**. Peroxisome proliferator and retinoid signaling pathways co-regulate preadipocyte phenotype and survival. *Biochemistry* 91: 1786-1790, 1994.
159. **Cao Z, Umek RM, and McKnight SL**. Regulated expression of three C/EBP isoforms during adipose conversion of 3T3-L1 cells. *Genes & Dev* 5: 1538-1552, 1991.
160. **Yeh WC, Cao Z, Classon M, and McKnight SL**. Cascade regulation of terminal adipocyte differentiation by three members of the C/EBP family of leucine zipper proteins. *Genes & Dev* 9: 168-181, 1995.
161. **Xue J, Schwartz E, Chawla A, and Lazar M**. Distinct stages in adipogenesis revealed by retinoid inhibition of differentiation after induction of PPAR©. *Mol Cell Biol* 16, no. 4: 1567-1575, 1996.
162. **Lin FT, and Lane MD**. CCAAT/enhancer binding protein alpha is sufficient to initiate the 3T3-L1 adipocyte differentiation program. *Proc Natl Acad Sci U S A* 91: 8757-8761, 1994.
163. **Rosen ED, Walkey CJ, Puigserver P, and Spiegelman BM**. Transcriptional regulation of adipogenesis. *Genes Dev* 14: 1293-1307, 2000.
164. **Wu Z, Rosen ED, Brun R, Hauser S, Adelmant G, Troy AE, MeKeon C, Darlington GJ, and Spiegelman BM**. Cross-Regulation of C/EBP〈 and PPAR© controls the transcriptional pathway of adipogenesis and insulin sensitivity. *Molecular Cell* 3: 151-158, 1999.
165. **Spiegelman BM, Choy L, Hotamisligil GS, Graves RA, and Tontonoz P**. Regulation of adipocyte gene expression in differentiation and syndromes of obesity/diabetes. *Journal of Biological Chemistry* 268,: 6823-6826, 1993.
166. **Rodeheffer MS, Birsoy K, and Friedman JM**. Identification of white adipocyte progenitor cells in vivo. *Cell* 135: 240-249, 2008.
167. **Farahani RM, and Xaymardan M**. Platelet-Derived Growth Factor Receptor Alpha as a Marker of Mesenchymal Stem Cells in Development and Stem Cell Biology. *Stem Cells Int* 2015: 362753, 2015.
168. **Hepler C, Vishvanath L, and Gupta RK**. Sorting out adipocyte precursors and their role in physiology and disease. *Genes Dev* 31: 127-140, 2017.
169. **Lee YH, Petkova AP, Mottillo EP, and Granneman JG**. In vivo identification of bipotential adipocyte progenitors recruited by beta3-adrenoceptor activation and high-fat feeding. *Cell Metab* 15: 480-491, 2012.

170. **Hong KY, Bae H, Park I, Park DY, Kim KH, Kubota Y, Cho ES, Kim H, Adams RH, Yoo OJ, and Koh GY**. Perilipin+ embryonic preadipocytes actively proliferate along growing vasculatures for adipose expansion. *Development* 142: 2623-2632, 2015.
171. **Greenberg AS, Egan JJ, Wek SA, Garty NB, Blanchette-Mackie EJ, and Londos C**. Perilipin, a major hormonally regulated adipocyte-specific phosphoprotein associated with the periphery of lipid storage droplets. *J Biol Chem* 266: 11341-11346, 1991.
172. **Ailhaud G, Grimaldi P, and Negrel R**. Cellular and molecular aspects of adipose tissue development. *Annual review of nutrition* 12: 207-233, 1992.
173. **Blanchette-Mackie EJ, Dwyer NK, Barber T, Coxey RA, Takeda T, Rondinone CM, Theodorakis JL, Greenberg AS, and Londos C**. Perilipin is located on the surface layer of intracellular lipid droplets in adipocytes. *J Lipid Res* 36: 1211-1226, 1995.
174. **Seale P, Bjork B, Yang W, Kajimura S, Chin S, Kuang S, Scime A, Devarakonda S, Conroe HM, Erdjument-Bromage H, Tempst P, Rudnicki MA, Beier DR, and Spiegelman BM**. PRDM16 controls a brown fat/skeletal muscle switch. *Nature* 454: 961-967, 2008.
175. **Kajimura S, Seale P, Kubota K, Lunsford E, Frangioni JV, Gygi SP, and Spiegelman BM**. Initiation of myoblast to brown fat switch by a PRDM16-C/EBP-beta transcriptional complex. *Nature* 460: 1154-1158, 2009.
176. **Atit R, Sgaier SK, Mohamed OA, Taketo MM, Dufort D, Joyner AL, Niswander L, and Conlon RA**. Beta-catenin activation is necessary and sufficient to specify the dorsal dermal fate in the mouse. *Dev Biol* 296: 164-176, 2006.
177. **Lepper C, and Fan CM**. Inducible lineage tracing of Pax7-descendant cells reveals embryonic origin of adult satellite cells. *Genesis* 48: 424-436, 2010.
178. **Di Rocco G, Iachininoto MG, Tritarelli A, Straino S, Zacheo A, Germani A, Crea F, and Capogrossi MC**. Myogenic potential of adipose-tissue-derived cells. *J Cell Sci* 119: 2945-2952, 2006.
179. **Wang W, Kissig M, Rajakumari S, Huang L, Lim HW, Won KJ, and Seale P**. Ebf2 is a selective marker of brown and beige adipogenic precursor cells. *Proc Natl Acad Sci U S A* 111: 14466-14471, 2014.
180. **Rajakumari S, Wu J, Ishibashi J, Lim HW, Giang AH, Won KJ, Reed RR, and Seale P**. EBF2 determines and maintains brown adipocyte identity. *Cell Metab* 17: 562-574, 2013.
181. **Schupp M, Cristancho AG, Lefterova MI, Hanniman EA, Briggs ER, Steger DJ, Qatanani M, Curtin JC, Schug J, Ochsner SA, McKenna NJ, and Lazar MA**. Re-expression of GATA2 cooperates with peroxisome proliferator-activated receptor-gamma depletion to revert the adipocyte phenotype. *J Biol Chem* 284: 9458-9464, 2009.
182. **Tong Q, Dalgin G, Xu H, Ting CN, Leiden JM, and Hotamisligil GS**. Function of GATA transcription factors in preadipocyte-adipocyte transition. *Science* 290: 134-138, 2000.
183. **Tsai J, Tong Q, Tan G, Chang AN, Orkin SH, and Hotamisligil GS**. The transcription factor GATA2 regulates differentiation of brown adipocytes. *EMBO Rep* 6: 879-884, 2005.
184. **Harms M, and Seale P**. Brown and beige fat: development, function and therapeutic potential. *Nat Med* 19: 1252-1263, 2013.
185. **Cao W, Medvedev AV, Daniel KW, and Collins S**. ®-Adrenergic activation of p38 MAP kinase in adipocytes: cAMP induction of the uncoupling protein-1 (UCP1) gene requires p38 MAP kinase. *J Biol Chem* 276: 27077-27082, 2001.
186. **Chartoumpekis DV, Habeos IG, Ziros PG, Psyrogiannis AI, Kyriazopoulou VE, and Papavassiliou AG**. Brown adipose tissue responds to cold and adrenergic stimulation by induction of FGF21. *Mol Med* 17: 736-740, 2011.
187. **Weiner J, Kranz M, Kloting N, Kunath A, Steinhoff K, Rijntjes E, Kohrle J, Zeisig V, Hankir M, Gebhardt C, Deuther-Conrad W, Heiker JT, Kralisch S, Stumvoll M, Bluher M, Sabri O,**

Hesse S, Brust P, Tonjes A, and Krause K. Thyroid hormone status defines brown adipose tissue activity and browning of white adipose tissues in mice. *Sci Rep* 6: 38124, 2016.
188. **Shi F, and Collins S**. Second messenger signaling mechanisms of the brown adipocyte thermogenic program: an integrative perspective. *Horm Mol Biol Clin Investig* 31: 2017.
189. **Bautista DM, Siemens J, Glazer JM, Tsuruda PR, Basbaum AI, Stucky CL, Jordt SE, and Julius D**. The menthol receptor TRPM8 is the principal detector of environmental cold. *Nature* 448: 204-208, 2007.
190. **Reimundez A, Fernandez-Pena C, Ordas P, Hernandez-Ortego P, Gallego R, Morenilla-Palao C, Navarro J, Martin-Cora F, Pardo-Vazquez JL, Schwarz LA, Arce V, Viana F, and Senaris R**. The cold-sensing ion channel TRPM8 regulates central and peripheral clockwork and the circadian oscillations of body temperature. *Acta Physiol (Oxf)* 237: e13896, 2023.
191. **Voronova IP, Khramova GM, Evtushenko AA, and Kozyreva TV**. Effect of Skin Ion Channel TRPM8 Activation by Cold and Menthol on Thermoregulation and the Expression of Genes of Thermosensitive TRP Ion Channels in the Hypothalamus of Hypertensive Rats. *Int J Mol Sci* 23: 2022.
192. **Dulloo AG, and Jacquet J**. An adipose-specific control of thermogenesis in body weight regulation. *Int J Obes Relat Metab Disord* 25 Suppl 5: S22-29, 2001.
193. **Wirsen C**. Adrenergic Innervation of Adipose Tissue Examined by Fluorescence Microscopy. *Nature* 202: 913, 1964.
194. **Cannon B, and Nedergaard J**. Nonshivering thermogenesis and brown adipose tissue. In: *Physiology and Pathophysiology of Temperature Regulation*, edited by Blatteis CM. Singapore, New Jersey, London, Hong Kong: World Scientific, 1998, p. 63-77.
195. **Morrison SF, Nakamura K, and Madden CJ**. Central control of thermogenesis in mammals. *Exp Physiol* 93: 773-797, 2008.
196. **Syrovatkina V, Alegre KO, Dey R, and Huang XY**. Regulation, Signaling, and Physiological Functions of G-Proteins. *J Mol Biol* 428: 3850-3868, 2016.
197. **Arrojo EDR, Fonseca TL, Werneck-de-Castro JP, and Bianco AC**. Role of the type 2 iodothyronine deiodinase (D2) in the control of thyroid hormone signaling. *Biochim Biophys Acta* 1830: 3956-3964, 2013.
198. **Yau WW, Singh BK, Lesmana R, Zhou J, Sinha RA, Wong KA, Wu Y, Bay BH, Sugii S, Sun L, and Yen PM**. Thyroid hormone (T(3)) stimulates brown adipose tissue activation via mitochondrial biogenesis and MTOR-mediated mitophagy. *Autophagy* 15: 131-150, 2019.
199. **Rim JS, and Kozak LP**. Regulatory Motifs for CREB-binding Protein and Nfe2l2 Transcription Factors in the Upstream Enhancer of the Mitochondrial Uncoupling Protein 1 Gene. *J Biol Chem* 277: 34589-34600, 2002.
200. **Fernandez-Marcos PJ, and Auwerx J**. Regulation of PGC-1alpha, a nodal regulator of mitochondrial biogenesis. *Am J Clin Nutr* 93: 884S-890, 2011.
201. **Granneman JG, and Lahners KN**. Analysis of human and rodent beta 3-adrenergic receptor messenger ribonucleic acids. *Endocrinology* 135: 1025-1031, 1994.
202. **Krief S, Lonnqvist F, Raimbault S, Baude B, Van Spronsen A, Arner P, Strosberg AD, Ricquier D, and Emorine LJ**. Tissue distribution of beta 3-adrenergic receptor mRNA in man. *J Clin Invest* 91: 344-349, 1993.
203. **Nahmias C, Blin N, Elalouf JM, Mattei MG, Strosberg AD, and Emorine LJ**. Molecular characterization of the mouse beta 3-adrenergic receptor: relationship with the atypical receptor of adipocytes. *EMBO J* 10: 3721-3727, 1991.
204. **Bloom JD, Dutia MD, Johnson BD, Wissner A, Burns MG, Largis EE, Dolan JA, and Claus TH**. Disodium (R,R)-5-[2-[[2-(3-chlorophenyl)-2-hydroxyethyl]-amino] propyl]-1,3-benzodioxole-2,2-dicarboxylate (CL 316,243). A potent beta-adrenergic agonist virtually specific for beta 3 receptors. A promising antidiabetic and antiobesity agent. *J Med Chem* 35: 3081-3084, 1992.

205. **Howe R, Rao BS, Holloway BR, and Stribling D**. Selective beta 3-adrenergic agonists of brown adipose tissue and thermogenesis. 2. [4-[2-[(2-Hydroxy-3-phenoxypropyl)amino]ethoxy]phenoxy]acetamides. *J Med Chem* 35: 1759-1764, 1992.
206. **Arch JR, and Wilson S**. Prospects for beta 3-adrenoceptor agonists in the treatment of obesity and diabetes. *Int J Obes Relat Metab Disord* 20: 191-199, 1996.
207. **Arch JR, Ainsworth AT, Ellis RD, Piercy V, Thody VE, Thurlby PL, Wilson C, Wilson S, and Young P**. Treatment of obesity with thermogenic beta-adrenoceptor agonists: studies on BRL 26830A in rodents. *Int J Obes* 8 Suppl 1: 1-11, 1984.
208. **de Souza CJ, Hirshman MF, and Horton ES**. CL-316,243, a beta3-specific adrenoceptor agonist, enhances insulin- stimulated glucose disposal in nonobese rats. *Diabetes* 46: 1257-1263., 1997.
209. **Weyer C, Tataranni PA, Snitker S, Danforth E, Jr., and Ravussin E**. Increase in insulin action and fat oxidation after treatment with CL 316,243, a highly selective beta3-adrenoceptor agonist in humans. *Diabetes* 47: 1555-1561, 1998.
210. **Liggett SB**. Functional properties of the rat and human beta 3-adrenergic receptors: differential agonist activation of recombinant receptors in Chinese hamster ovary cells. *Mol Pharmacol* 42: 634-637, 1992.
211. **Pietri-Rouxel F, and Strosberg AD**. Pharmacological characteristics and species-related variations of beta 3-adrenergic receptors. *Fundam Clin Pharmacol* 9: 211-218, 1995.
212. **Larsen TM, Toubro S, van Baak MA, Gottesdiener KM, Larson P, Saris WH, and Astrup A**. Effect of a 28-d treatment with L-796568, a novel beta(3)-adrenergic receptor agonist, on energy expenditure and body composition in obese men. *Am J Clin Nutr* 76: 780-788, 2002.
213. **Dow RL, Paight ES, Schneider SR, Hadcock JR, Hargrove DM, Martin KA, Maurer TS, Nardone NA, Tess DA, and DaSilva-Jardine P**. Potent and selective, sulfamide-based human beta 3-adrenergic receptor agonists. *Bioorg Med Chem Lett* 14: 3235-3240, 2004.
214. **Weyer C, Gautier JF, and Danforth E, Jr.** Development of beta 3-adrenoceptor agonists for the treatment of obesity and diabetes--an update. *Diabetes Metab* 25: 11-21, 1999.
215. **Wheeldon NM, McDevitt DG, and Lipworth BJ**. Cardiac effects of the beta 3-adrenoceptor agonist BRL35135 in man. *Br J Clin Pharmacol* 37: 363-369, 1994.
216. **Connacher AA, Lakie M, Powers N, Elton RA, Walsh EG, and Jung RT**. Tremor and the anti-obesity drug BRL 26830A. *Br J Clin Pharmacol* 30: 613-615, 1990.
217. **Cao W, Daniel KW, Robidoux J, Puigserver P, Medvedev AV, Bai X, Floering LM, Spiegelman BM, and Collins S**. p38 mitogen-activated protein kinase is the central regulator of cyclic AMP-dependent transcription of the brown fat uncoupling protein 1 gene. *Mol Cell Biol* 24: 3057-3067, 2004.
218. **Liu D, Bordicchia M, Zhang C, Fang H, Wei W, Li JL, Guilherme A, Guntur K, Czech MP, and Collins S**. Activation of mTORC1 is essential for ®-adrenergic stimulation of adipose browning. *J Clin Invest* 126: 1704-1716, 2016.
219. **Moule SK, Welsh GI, Edgell NJ, Foulstone EJ, Proud CG, and Denton RM**. Regulation of protein kinase B and glycogen synthase kinase-3 by insulin and beta-adrenergic agonists in rat epididymal fat cells. Activation of protein kinase B by wortmannin-sensitive and -insensitive mechanisms. *J Biol Chem* 272: 7713-7719, 1997.
220. **Jonsson C, Castor Batista AP, Kjolhede P, and Stralfors P**. Insulin and beta-adrenergic receptors mediate lipolytic and anti-lipolytic signalling that is not altered by type 2 diabetes in human adipocytes. *Biochem J* 476: 2883-2908, 2019.
221. **Sekulic A, Hudson CC, Homme JL, Yin P, Otterness DM, Karnitz LM, and Abraham RT**. A direct linkage between the phosphoinositide 3-kinase-AKT signaling pathway and the mammalian target of rapamycin in mitogen-stimulated and transformed cells. *Cancer Res* 60: 3504-3513, 2000.

222. **Nomura M, He Z, Koyama I, Ma WY, Miyamoto K, and Dong Z**. Involvement of the Akt/mTOR pathway on EGF-induced cell transformation. *Mol Carcinog* 38: 25-32, 2003.
223. **Fan QW, Cheng C, Knight ZA, Haas-Kogan D, Stokoe D, James CD, McCormick F, Shokat KM, and Weiss WA**. EGFR signals to mTOR through PKC and independently of Akt in glioma. *Sci Signal* 2: ra4, 2009.
224. **Bond P**. Regulation of mTORC1 by growth factors, energy status, amino acids and mechanical stimuli at a glance. *J Int Soc Sports Nutr* 13: 8, 2016.
225. **Kasuga M, Karlsson FA, and Kahn CR**. Insulin stimulates the phosphorylation of the 95,000-dalton subunit of its own receptor. *Science* 215: 185-187, 1982.
226. **Sun XJ, Miralpeix M, Myers MG, Jr., Glasheen EM, Backer JM, Kahn CR, and White MF**. Expression and function of IRS-1 in insulin signal transmission. *J Biol Chem* 267: 22662-22672, 1992.
227. **Terauchi Y, Tsuji Y, Satoh S, Minoura H, Murakami K, Okuno A, Inukai K, Asano T, Kaburagi Y, Ueki K, Nakajima H, Hanafusa T, Matsuzawa Y, Sekihara H, Yin Y, Barrett JC, Oda H, Ishikawa T, Akanuma Y, Komuro I, Suzuki M, Yamamura K, Kodama T, Suzuki H, Yamamura K, Kodama T, Suzuki H, Koyasu S, Aizawa S, Tobe K, Fukui Y, Yazaki Y, and Kadowaki T**. Increased insulin sensitivity and hypoglycaemia in mice lacking the p85 alpha subunit of phosphoinositide 3-kinase. *Nat Genet* 21: 230-235, 1999.
228. **Auger KR, Serunian LA, Soltoff SP, Libby P, and Cantley LC**. PDGF-dependent tyrosine phosphorylation stimulates production of novel polyphosphoinositides in intact cells. *Cell* 57: 167-175, 1989.
229. **Carpenter CL, Duckworth BC, Auger KR, Cohen B, Schaffhausen BS, and Cantley LC**. Purification and characterization of phosphoinositide 3-kinase from rat liver. *J Biol Chem* 265: 19704-19711, 1990.
230. **Currie RA, Walker KS, Gray A, Deak M, Casamayor A, Downes CP, Cohen P, Alessi DR, and Lucocq J**. Role of phosphatidylinositol 3,4,5-trisphosphate in regulating the activity and localization of 3-phosphoinositide-dependent protein kinase-1. *Biochem J* 337 (Pt 3): 575-583, 1999.
231. **Alessi DR, James SR, Downes CP, Holmes AB, Gaffney PR, Reese CB, and Cohen P**. Characterization of a 3-phosphoinositide-dependent protein kinase which phosphorylates and activates protein kinase Balpha. *Curr Biol* 7: 261-269, 1997.
232. **Sarbassov DD, Guertin DA, Ali SM, and Sabatini DM**. Phosphorylation and regulation of Akt/PKB by the rictor-mTOR complex. *Science* 307: 1098-1101, 2005.
233. **Inoki K, Li Y, Zhu T, Wu J, and Guan KL**. TSC2 is phosphorylated and inhibited by Akt and suppresses mTOR signalling. *Nat Cell Biol* 4: 648-657, 2002.
234. **Nellist M, van Slegtenhorst MA, Goedbloed M, van den Ouweland AM, Halley DJ, and van der Sluijs P**. Characterization of the cytosolic tuberin-hamartin complex. Tuberin is a cytosolic chaperone for hamartin. *J Biol Chem* 274: 35647-35652, 1999.
235. **Inoki K, Li Y, Xu T, and Guan KL**. Rheb GTPase is a direct target of TSC2 GAP activity and regulates mTOR signaling. *Genes Dev* 17: 1829-1834, 2003.
236. **Huang J, Dibble CC, Matsuzaki M, and Manning BD**. The TSC1-TSC2 complex is required for proper activation of mTOR complex 2. *Mol Cell Biol* 28: 4104-4115, 2008.
237. **Laplante M, and Sabatini DM**. mTOR Signaling. *Cold Spring Harb Perspect Biol* 4: 2012.
238. **Wang L, Harris TE, Roth RA, and Lawrence JC, Jr.** PRAS40 regulates mTORC1 kinase activity by functioning as a direct inhibitor of substrate binding. *J Biol Chem* 282: 20036-20044, 2007.
239. **Vander Haar E, Lee SI, Bandhakavi S, Griffin TJ, and Kim DH**. Insulin signalling to mTOR mediated by the Akt/PKB substrate PRAS40. *Nat Cell Biol* 9: 316-323, 2007.

240. **Liu D, Bordicchia M, Zhang C, Fang H, Wei W, Li JL, Guilherme A, Guntur K, Czech MP, and Collins S**. Activation of mTORC1 is essential for beta-adrenergic stimulation of adipose browning. *J Clin Invest* 126: 1704-1716, 2016.
241. **Steinberg SF**. Regulation of protein kinase D1 activity. *Mol Pharmacol* 81: 284-291, 2012.
242. **Rozengurt E, Rey O, and Waldron RT**. Protein kinase D signaling. *J Biol Chem* 280: 13205-13208, 2005.
243. **Waldron RT, Rey O, Iglesias T, Tugal T, Cantrell D, and Rozengurt E**. Activation loop Ser744 and Ser748 in protein kinase D are transphosphorylated in vivo. *J Biol Chem* 276: 32606-32615, 2001.
244. **Jacamo R, Sinnett-Smith J, Rey O, Waldron RT, and Rozengurt E**. Sequential protein kinase C (PKC)-dependent and PKC-independent protein kinase D catalytic activation via Gq-coupled receptors: differential regulation of activation loop Ser(744) and Ser(748) phosphorylation. *J Biol Chem* 283: 12877-12887, 2008.
245. **Chen J, Deng F, Li J, and Wang QJ**. Selective binding of phorbol esters and diacylglycerol by individual C1 domains of the PKD family. *Biochem J* 411: 333-342, 2008.
246. **Liljedahl M, Maeda Y, Colanzi A, Ayala I, Van Lint J, and Malhotra V**. Protein kinase D regulates the fission of cell surface destined transport carriers from the trans-Golgi network. *Cell* 104: 409-420, 2001.
247. **Bergeron V, Ghislain J, Vivot K, Tamarina N, Philipson LH, Fielitz J, and Poitout V**. Deletion of Protein Kinase D1 in Pancreatic beta-Cells Impairs Insulin Secretion in High-Fat Diet-Fed Mice. *Diabetes* 67: 71-77, 2018.
248. **Fielitz J, Kim MS, Shelton JM, Qi X, Hill JA, Richardson JA, Bassel-Duby R, and Olson EN**. Requirement of protein kinase D1 for pathological cardiac remodeling. *Proc Natl Acad Sci U S A* 105: 3059-3063, 2008.
249. **Kim MS, Fielitz J, McAnally J, Shelton JM, Lemon DD, McKinsey TA, Richardson JA, Bassel-Duby R, and Olson EN**. Protein kinase D1 stimulates MEF2 activity in skeletal muscle and enhances muscle performance. *Mol Cell Biol* 28: 3600-3609, 2008.
250. **Sundram V, Chauhan SC, and Jaggi M**. Emerging roles of protein kinase D1 in cancer. *Mol Cancer Res* 9: 985-996, 2011.
251. **Loffler MC, Mayer AE, Trujillo Viera J, Loza Valdes A, El-Merahbi R, Ade CP, Karwen T, Schmitz W, Slotta A, Erk M, Janaki-Raman S, Matesanz N, Torres JL, Marcos M, Sabio G, Eilers M, Schulze A, and Sumara G**. Protein kinase D1 deletion in adipocytes enhances energy dissipation and protects against adiposity. *EMBO J* 37: 2018.
252. **Li G, Xing Z, Wang W, Luo W, Ma Z, Wu Z, Chen H, Li Y, Wang C, Zeng F, and Deng F**. Adipose-specific knockout of Protein Kinase D1 suppresses de novo lipogenesis in mice via SREBP1c-dependent signaling. *Exp Cell Res* 401: 112548, 2021.
253. **Jeffery E, Berry R, Church CD, Yu S, Shook BA, Horsley V, Rosen ED, and Rodeheffer MS**. Characterization of Cre recombinase models for the study of adipose tissue. *Adipocyte* 3: 206-211, 2014.
254. **Lee KY, Russell SJ, Ussar S, Boucher J, Vernochet C, Mori MA, Smyth G, Rourk M, Cederquist C, Rosen ED, Kahn BB, and Kahn CR**. Lessons on conditional gene targeting in mouse adipose tissue. *Diabetes* 62: 864-874, 2013.
255. **Mullican SE, Tomaru T, Gaddis CA, Peed LC, Sundaram A, and Lazar MA**. A novel adipose-specific gene deletion model demonstrates potential pitfalls of existing methods. *Mol Endocrinol* 27: 127-134, 2013.
256. **Tabuchi C, and Sul HS**. Signaling Pathways Regulating Thermogenesis. *Front Endocrinol (Lausanne)* 12: 595020, 2021.
257. **Zetterqvist O, and Ragnarsson U**. The structural requirements of substrates of cyclic AMP-dependent protein kinase. *FEBS Lett* 139: 287-290, 1982.

258. **Manning BD, and Cantley LC**. AKT/PKB signaling: navigating downstream. *Cell* 129: 1261-1274, 2007.
259. **Hausser A, Storz P, Link G, Stoll H, Liu YC, Altman A, Pfizenmaier K, and Johannes FJ**. Protein kinase C mu is negatively regulated by 14-3-3 signal transduction proteins. *J Biol Chem* 274: 9258-9264, 1999.
260. **Chang JK, Ni Y, Han L, Sinnett-Smith J, Jacamo R, Rey O, Young SH, and Rozengurt E**. Protein kinase D1 (PKD1) phosphorylation on Ser(203) by type I p21-activated kinase (PAK) regulates PKD1 localization. *J Biol Chem* 292: 9523-9539, 2017.
261. **Ross SR, Choy L, Graves RA, Fox N, Solevjeva V, Klaus S, Ricquier D, and Spiegelman BM**. Hibernoma formation in transgenic mice and isolation of a brown adipocyte cell line expressing the uncoupling protein gene. *Proc Natl Acad Sci* 89: 7561-7565, 1992.
262. **Hamann A, Glier HS, and Lowell BB**. Decreased brown fat markedly enhances susceptibility to diet-Induced obesity, diabetes, and hyperlipidemia. *Endocrinology* 137: 21-29, 1996.
263. **Collins S**. beta-Adrenergic Receptors and Adipose Tissue Metabolism: Evolution of an Old Story. *Annu Rev Physiol* 84: 1-16, 2022.
264. **Collins S, and Surwit RS**. The beta-adrenergic receptors and the control of adipose tissue metabolism and thermogenesis. *Recent progress in hormone research* 56: 309-328, 2001.
265. **Cao W, Medvedev AV, Daniel KW, and Collins S**. β-Adrenergic activation of p38 MAP kinase in adipocytes: cAMP induction of the uncoupling protein-1 (UCP1) gene requires p38 MAP kinase. *J Biol Chem* 276: 27077-27082, 2001.
266. **Renton MC, McGee SL, and Howlett KF**. The role of protein kinase D (PKD) in intracellular nutrient sensing and regulation of adaptive responses to the obese environment. *Obes Rev* 22: e13145, 2021.
267. **Oguri Y, and Kajimura S**. Cellular heterogeneity in brown adipose tissue. *J Clin Invest* 130: 65-67, 2020.
268. **Shinde AB, Song A, and Wang QA**. Brown Adipose Tissue Heterogeneity, Energy Metabolism, and Beyond. *Front Endocrinol (Lausanne)* 12: 651763, 2021.
269. **Schulz TJ, Huang TL, Tran TT, Zhang H, Townsend KL, Shadrach JL, Cerletti M, McDougall LE, Giorgadze N, Tchkonia T, Schrier D, Falb D, Kirkland JL, Wagers AJ, and Tseng YH**. Identification of inducible brown adipocyte progenitors residing in skeletal muscle and white fat. *Proc Natl Acad Sci U S A* 108: 143-148, 2011.
270. **Ceddia RP, Liu D, Shi F, Crowder MK, Mishra S, Kass DA, and Collins S**. Increased Energy Expenditure and Protection From Diet-Induced Obesity in Mice Lacking the cGMP-Specific Phosphodiesterase PDE9. *Diabetes* 70: 2823-2836, 2021.
271. **Livak KJ, and Schmittgen TD**. Analysis of relative gene expression data using real-time quantitative PCR and the 2(-Delta Delta C(T)) Method. *Methods* 25: 402-408, 2001.
272. **Dobin A, Davis CA, Schlesinger F, Drenkow J, Zaleski C, Jha S, Batut P, Chaisson M, and Gingeras TR**. STAR: ultrafast universal RNA-seq aligner. *Bioinformatics* 29: 15-21, 2013.
273. **Love MI, Huber W, and Anders S**. Moderated estimation of fold change and dispersion for RNA-seq data with DESeq2. *Genome Biol* 15: 550, 2014.
274. **Yu G, Wang LG, Han Y, and He QY**. clusterProfiler: an R package for comparing biological themes among gene clusters. *OMICS* 16: 284-287, 2012.
275. **Zhou Y, Zhou B, Pache L, Chang M, Khodabakhshi AH, Tanaseichuk O, Benner C, and Chanda SK**. Metascape provides a biologist-oriented resource for the analysis of systems-level datasets. *Nat Commun* 10: 1523, 2019.
276. **Harms MJ, Ishibashi J, Wang W, Lim HW, Goyama S, Sato T, Kurokawa M, Won KJ, and Seale P**. Prdm16 is required for the maintenance of brown adipocyte identity and function in adult mice. *Cell Metab* 19: 593-604, 2014.

277. **Crowder MK, Shrestha S, Cartailler JP, and Collins S**. Protein kinase D1 (Prkd1) deletion in brown adipose tissue leads to altered myogenic gene expression after cold exposure, while thermogenesis remains intact. *Physiol Rep* 11: e15576, 2023.
278. **Kersten S**. Mechanisms of nutritional and hormonal regulation of lipogenesis. *EMBO Rep* 2: 282-286, 2001.
279. **Shan T, Liang X, Bi P, Zhang P, Liu W, and Kuang S**. Distinct populations of adipogenic and myogenic Myf5-lineage progenitors in white adipose tissues. *J Lipid Res* 54: 2214-2224, 2013.
280. **Sanchez-Gurmaches J, and Guertin DA**. Adipocytes arise from multiple lineages that are heterogeneously and dynamically distributed. *Nat Commun* 5: 4099, 2014.
281. **Wang Y, Kim KA, Kim JH, and Sul HS**. Pref-1, a preadipocyte secreted factor that inhibits adipogenesis. *J Nutr* 136: 2953-2956, 2006.
282. **Speliotes EK, Willer CJ, Berndt SI, Monda KL, Thorleifsson G, Jackson AU, Lango Allen H, Lindgren CM, Luan J, Magi R, Randall JC, Vedantam S, Winkler TW, Qi L, Workalemahu T, Heid IM, Steinthorsdottir V, Stringham HM, Weedon MN, Wheeler E, Wood AR, Ferreira T, Weyant RJ, Segre AV, Estrada K, Liang L, Nemesh J, Park JH, Gustafsson S, Kilpelainen TO, Yang J, Bouatia-Naji N, Esko T, Feitosa MF, Kutalik Z, Mangino M, Raychaudhuri S, Scherag A, Smith AV, Welch R, Zhao JH, Aben KK, Absher DM, Amin N, Dixon AL, Fisher E, Glazer NL, Goddard ME, Heard-Costa NL, Hoesel V, Hottenga JJ, Johansson A, Johnson T, Ketkar S, Lamina C, Li S, Moffatt MF, Myers RH, Narisu N, Perry JR, Peters MJ, Preuss M, Ripatti S, Rivadeneira F, Sandholt C, Scott LJ, Timpson NJ, Tyrer JP, van Wingerden S, Watanabe RM, White CC, Wiklund F, Barlassina C, Chasman DI, Cooper MN, Jansson JO, Lawrence RW, Pellikka N, Prokopenko I, Shi J, Thiering E, Alavere H, Alibrandi MT, Almgren P, Arnold AM, Aspelund T, Atwood LD, Balkau B, Balmforth AJ, Bennett AJ, Ben-Shlomo Y, Bergman RN, Bergmann S, Biebermann H, Blakemore AI, Boes T, Bonnycastle LL, Bornstein SR, Brown MJ, Buchanan TA, Busonero F, Campbell H, Cappuccio FP, Cavalcanti-Proenca C, Chen YD, Chen CM, Chines PS, Clarke R, Coin L, Connell J, Day IN, den Heijer M, Duan J, Ebrahim S, Elliott P, Elosua R, Eiriksdottir G, Erdos MR, Eriksson JG, Facheris MF, Felix SB, Fischer-Posovszky P, Folsom AR, Friedrich N, Freimer NB, Fu M, Gaget S, Gejman PV, Geus EJ, Gieger C, Gjesing AP, Goel A, Goyette P, Grallert H, Grassler J, Greenawalt DM, Groves CJ, Gudnason V, Guiducci C, Hartikainen AL, Hassanali N, Hall AS, Havulinna AS, Hayward C, Heath AC, Hengstenberg C, Hicks AA, Hinney A, Hofman A, Homuth G, Hui J, Igl W, Iribarren C, Isomaa B, Jacobs KB, Jarick I, Jewell E, John U, Jorgensen T, Jousilahti P, Jula A, Kaakinen M, Kajantie E, Kaplan LM, Kathiresan S, Kettunen J, Kinnunen L, Knowles JW, Kolcic I, Konig IR, Koskinen S, Kovacs P, Kuusisto J, Kraft P, Kvaloy K, Laitinen J, Lantieri O, Lanzani C, Launer LJ, Lecoeur C, Lehtimaki T, Lettre G, Liu J, Lokki ML, Lorentzon M, Luben RN, Ludwig B, Magic, Manunta P, Marek D, Marre M, Martin NG, McArdle WL, McCarthy A, McKnight B, Meitinger T, Melander O, Meyre D, Midthjell K, Montgomery GW, Morken MA, Morris AP, Mulic R, Ngwa JS, Nelis M, Neville MJ, Nyholt DR, O'Donnell CJ, O'Rahilly S, Ong KK, Oostra B, Pare G, Parker AN, Perola M, Pichler I, Pietilainen KH, Platou CG, Polasek O, Pouta A, Rafelt S, Raitakari O, Rayner NW, Ridderstrale M, Rief W, Ruokonen A, Robertson NR, Rzehak P, Salomaa V, Sanders AR, Sandhu MS, Sanna S, Saramies J, Savolainen MJ, Scherag S, Schipf S, Schreiber S, Schunkert H, Silander K, Sinisalo J, Siscovick DS, Smit JH, Soranzo N, Sovio U, Stephens J, Surakka I, Swift AJ, Tammesoo ML, Tardif JC, Teder-Laving M, Teslovich TM, Thompson JR, Thomson B, Tonjes A, Tuomi T, van Meurs JB, van Ommen GJ, Vatin V, Viikari J, Visvikis-Siest S, Vitart V, Vogel CI, Voight BF, Waite LL, Wallaschofski H, Walters GB, Widen E, Wiegand S, Wild SH, Willemsen G, Witte DR, Witteman JC, Xu J, Zhang Q, Zgaga L, Ziegler A, Zitting P, Beilby JP, Farooqi IS, Hebebrand J, Huikuri HV, James AL, Kahonen M, Levinson DF, Macciardi F, Nieminen MS, Ohlsson C, Palmer LJ, Ridker PM,**

Stumvoll M, Beckmann JS, Boeing H, Boerwinkle E, Boomsma DI, Caulfield MJ, Chanock SJ, Collins FS, Cupples LA, Smith GD, Erdmann J, Froguel P, Gronberg H, Gyllensten U, Hall P, Hansen T, Harris TB, Hattersley AT, Hayes RB, Heinrich J, Hu FB, Hveem K, Illig T, Jarvelin MR, Kaprio J, Karpe F, Khaw KT, Kiemeney LA, Krude H, Laakso M, Lawlor DA, Metspalu A, Munroe PB, Ouwehand WH, Pedersen O, Penninx BW, Peters A, Pramstaller PP, Quertermous T, Reinehr T, Rissanen A, Rudan I, Samani NJ, Schwarz PE, Shuldiner AR, Spector TD, Tuomilehto J, Uda M, Uitterlinden A, Valle TT, Wabitsch M, Waeber G, Wareham NJ, Watkins H, Procardis C, Wilson JF, Wright AF, Zillikens MC, Chatterjee N, McCarroll SA, Purcell S, Schadt EE, Visscher PM, Assimes TL, Borecki IB, Deloukas P, Fox CS, Groop LC, Haritunians T, Hunter DJ, Kaplan RC, Mohlke KL, O'Connell JR, Peltonen L, Schlessinger D, Strachan DP, van Duijn CM, Wichmann HE, Frayling TM, Thorsteinsdottir U, Abecasis GR, Barroso I, Boehnke M, Stefansson K, North KE, McCarthy MI, Hirschhorn JN, Ingelsson E, and Loos RJ. Association analyses of 249,796 individuals reveal 18 new loci associated with body mass index. *Nat Genet* 42: 937-948, 2010.

283. **Magi R, Manning S, Yousseif A, Pucci A, Santini F, Karra E, Querci G, Pelosini C, McCarthy MI, Lindgren CM, and Batterham RL**. Contribution of 32 GWAS-identified common variants to severe obesity in European adults referred for bariatric surgery. *PLoS One* 8: e70735, 2013.

284. **Seyednasrollah F, Makela J, Pitkanen N, Juonala M, Hutri-Kahonen N, Lehtimaki T, Viikari J, Kelly T, Li C, Bazzano L, Elo LL, and Raitakari OT**. Prediction of adulthood obesity using genetic and childhood clinical risk factors in the Cardiovascular Risk in Young Finns Study. *Circ Cardiovasc Genet* 10: 2017.

285. **Llewellyn CH, Trzaskowski M, van Jaarsveld CHM, Plomin R, and Wardle J**. Satiety mechanisms in genetic risk of obesity. *JAMA Pediatr* 168: 338-344, 2014.

Appendix A: Supplemental Figures for Chapter 3

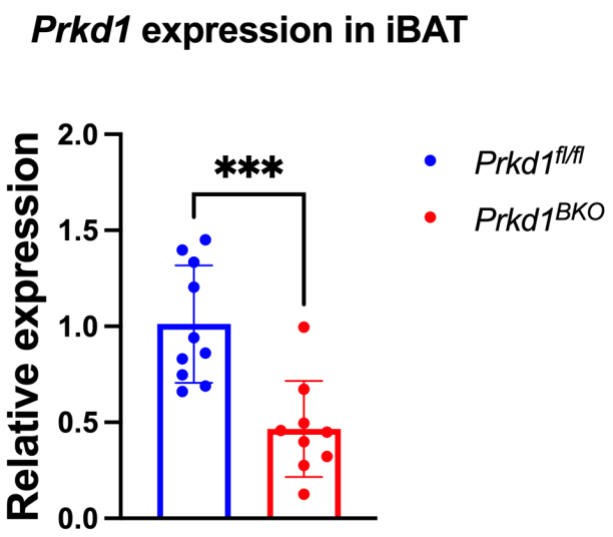

Figure S1: *Prkd1* mRNA expression in iBAT of *Prkd1*$^{fl/fl}$ and *Prkd1*^{BKO} mice. Prkd1 mRNA was measured using q-RT-PCR from total iBAT RNAs. N = 9-10. Statistics are paired t-test (p= 0.006).

8 hour cold RNA-Seq

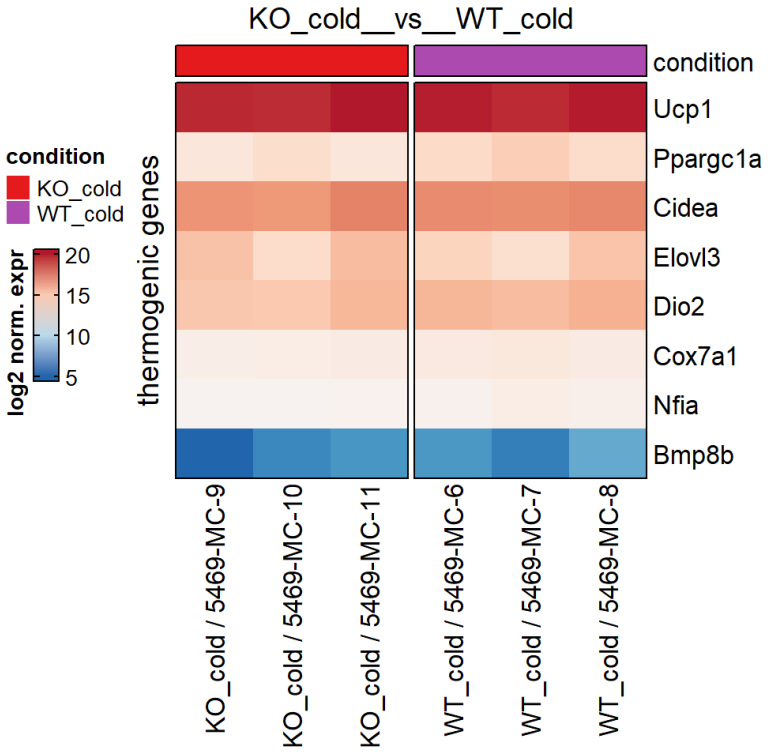

4-day cold RNA-Seq

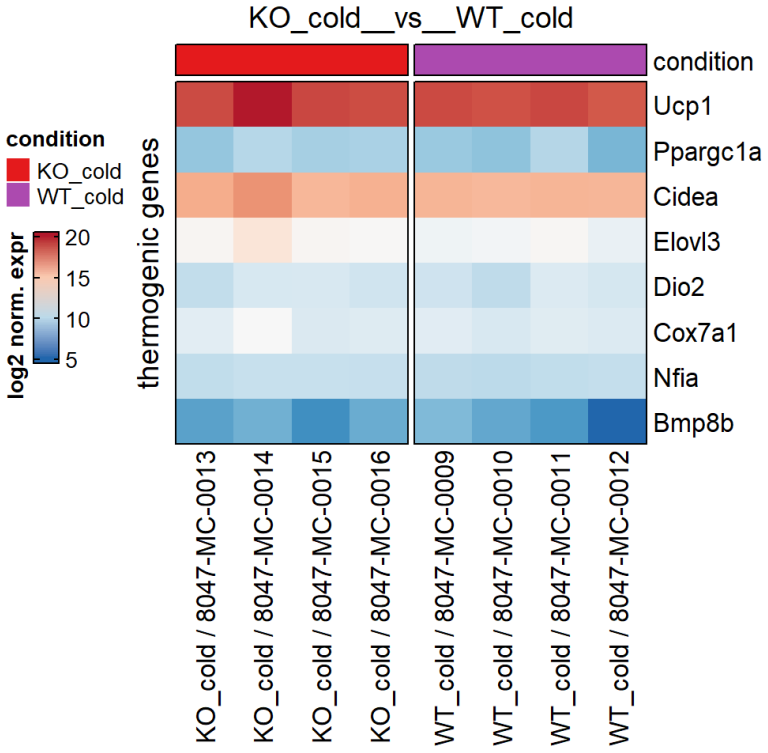

Figure S2: Heatmaps showing log_2 normalized counts of selected thermogenic genes in *Prkd1*^{BKO}(KO) and *Prkd1*$^{fl/fl}$ (WT) samples in cold exposure. Selected thermogenic gene expression in 8-hour and 4-day cold exposed iBAT from WT and KO mice. Names listed on X-axis represent individual mouse iBAT RNAs after cold exposure. As show to the left of each heatmap, the color of each box indicates the relative change in normalized gene expression on a log_2 scale. Genotype is denoted by colored bands above each heatmap.

8 hour cold RNA-Seq

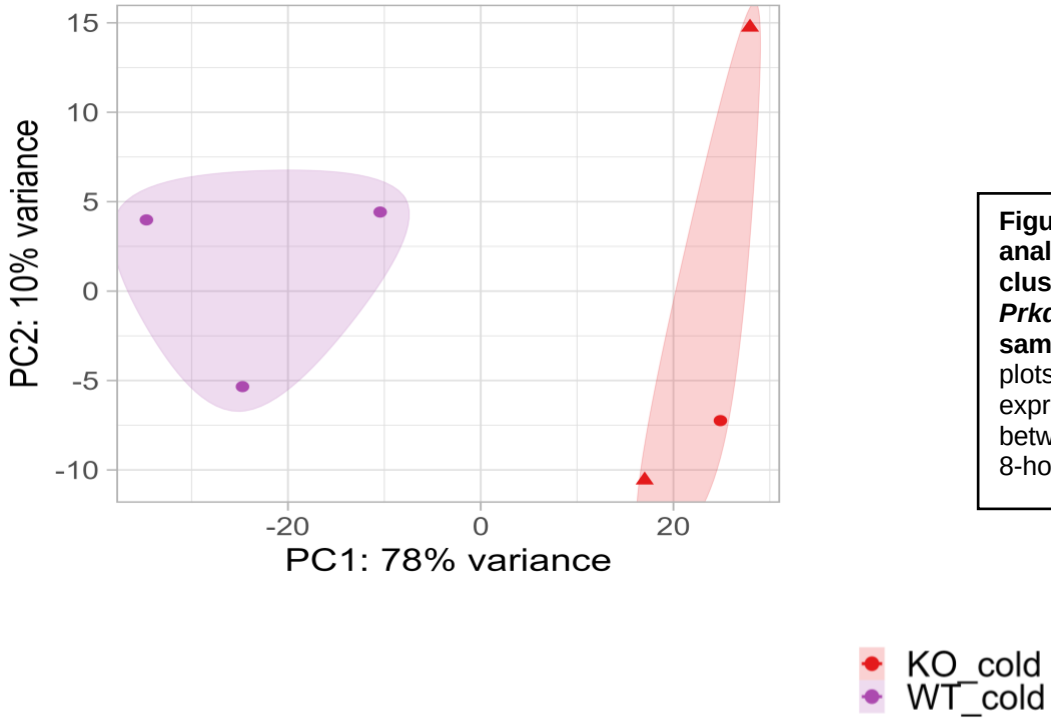

Figure S3: Principal-component analyses (PCA) plot shows clustering of samples from *Prkd1*^{BKO}(KO) and *Prkd1*$^{fl/fl}$ (WT) samples in cold exposure. PCA plots showing the similarity in gene expression changes within and between each genotype after either 8-hour or 4-day cold exposure.

4-day cold RNA-Seq

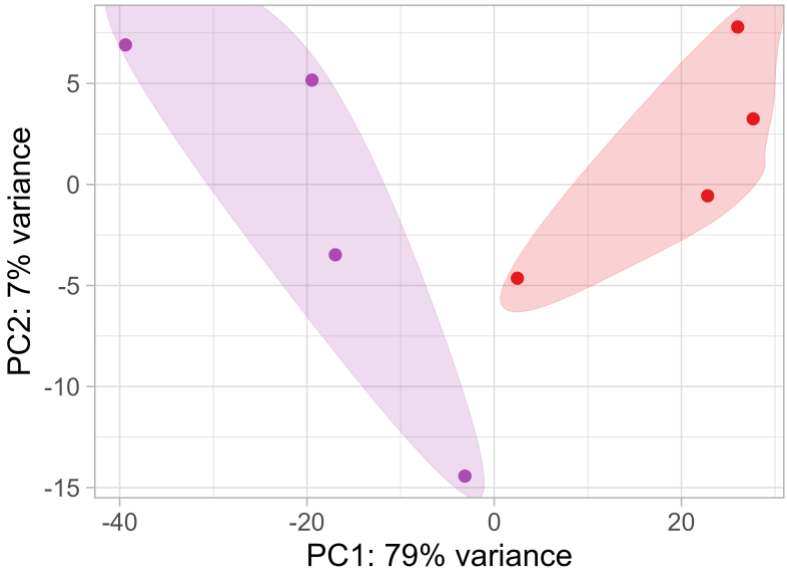

8 hour cold RNA-Seq

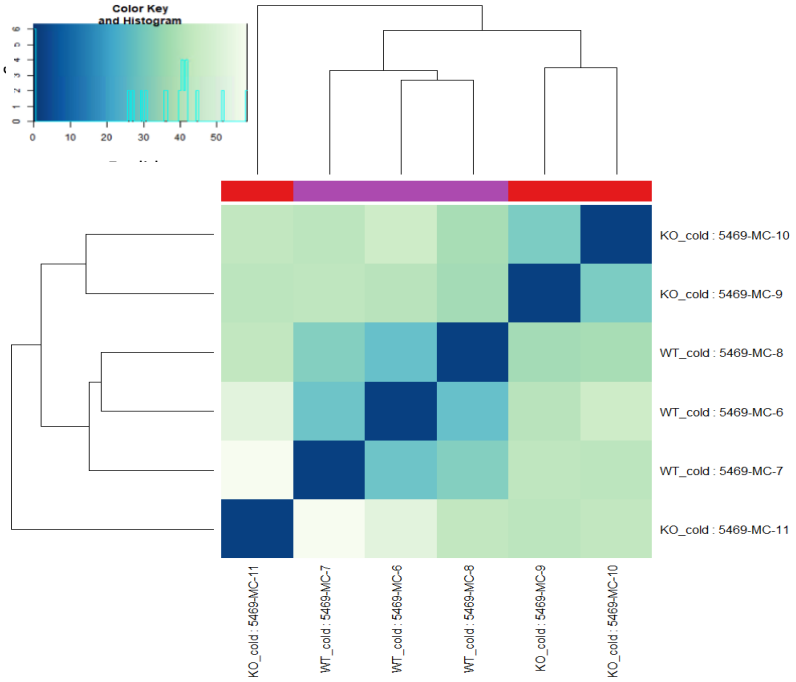

Figure S4: Heatmaps of sample-to-sample distance matrix showing overview of clustering between samples.
Similar to PCA analysis in Fig. S3, these heatmaps are used to show the sample-to-sample variability. The branch-like structures show associations between samples similar to an evolutionary tree. The color of each box represents the degree of hierarchical clustering between samples in arbitrary units.

4-day cold RNA-Seq

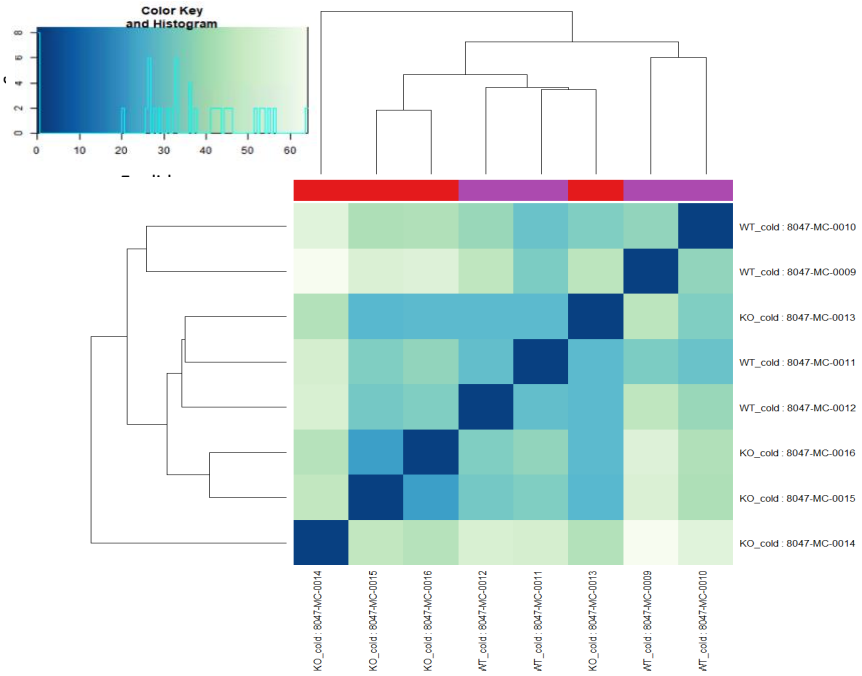

Metascape analysis – 8 hour cold RNA-Seq

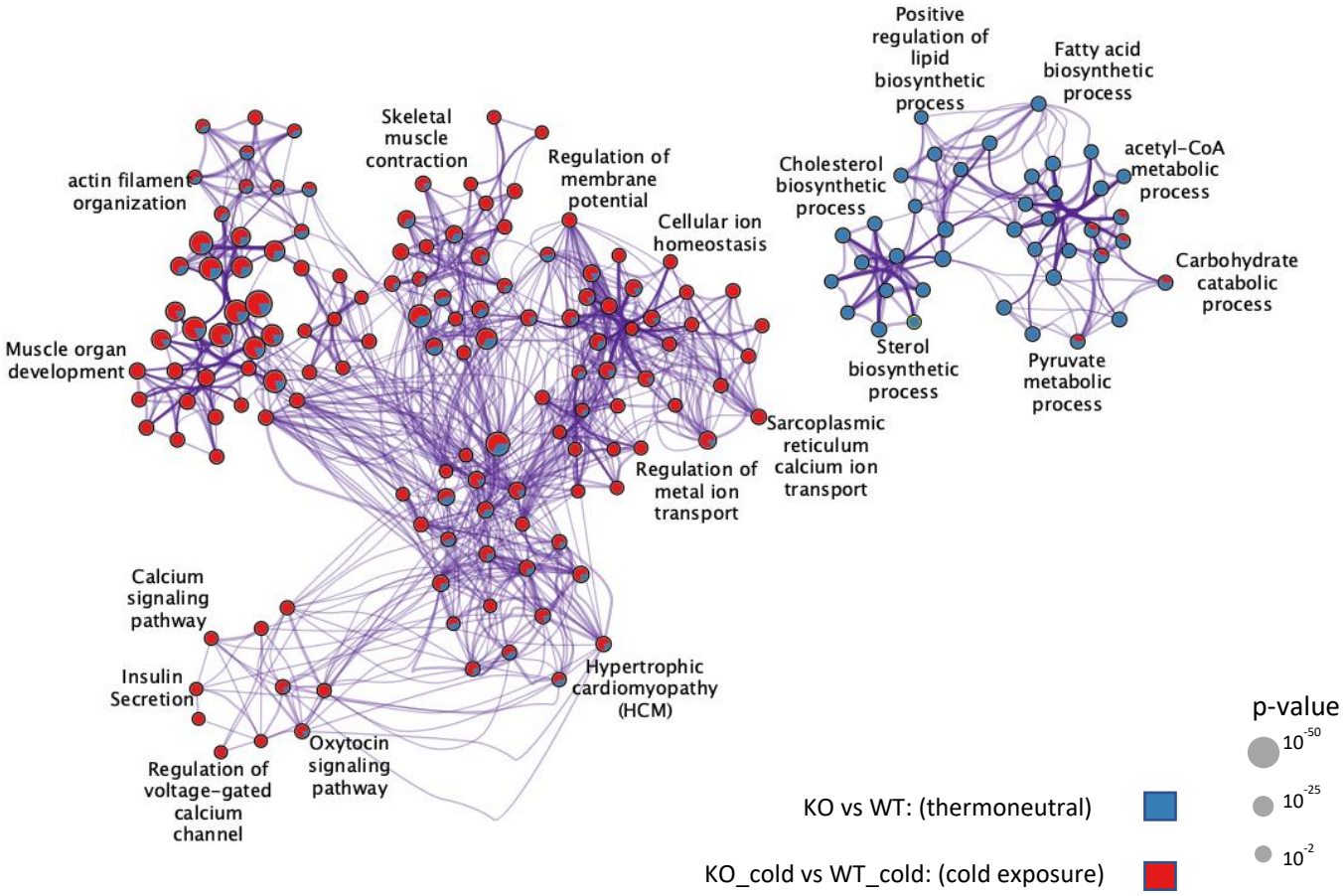

Figure S5: Metascape network visualizations of statistically enriched gene ontology terms between thermoneutral and cold-exposure condition of *Prkd1*^{BKO} (KO) vs *Prkd1*$^{fl/fl}$ (WT) for 8 hour cold exposure RNA-Seq experiment. The network has its nodes displayed as pies. Each pie sector is proportional to the number of differentially expressed genes originated from PRKD1-KO vs wild type in cold exposure (red) or thermoneutral condition (blue). p-values are calculated based on the accumulative hypergeometric distribution. Kappa-statistical similarities among their gene memberships are used as the similarity metric when performing hierarchical clustering on the enriched terms.

Metascape analysis – 4 day cold RNA-Seq

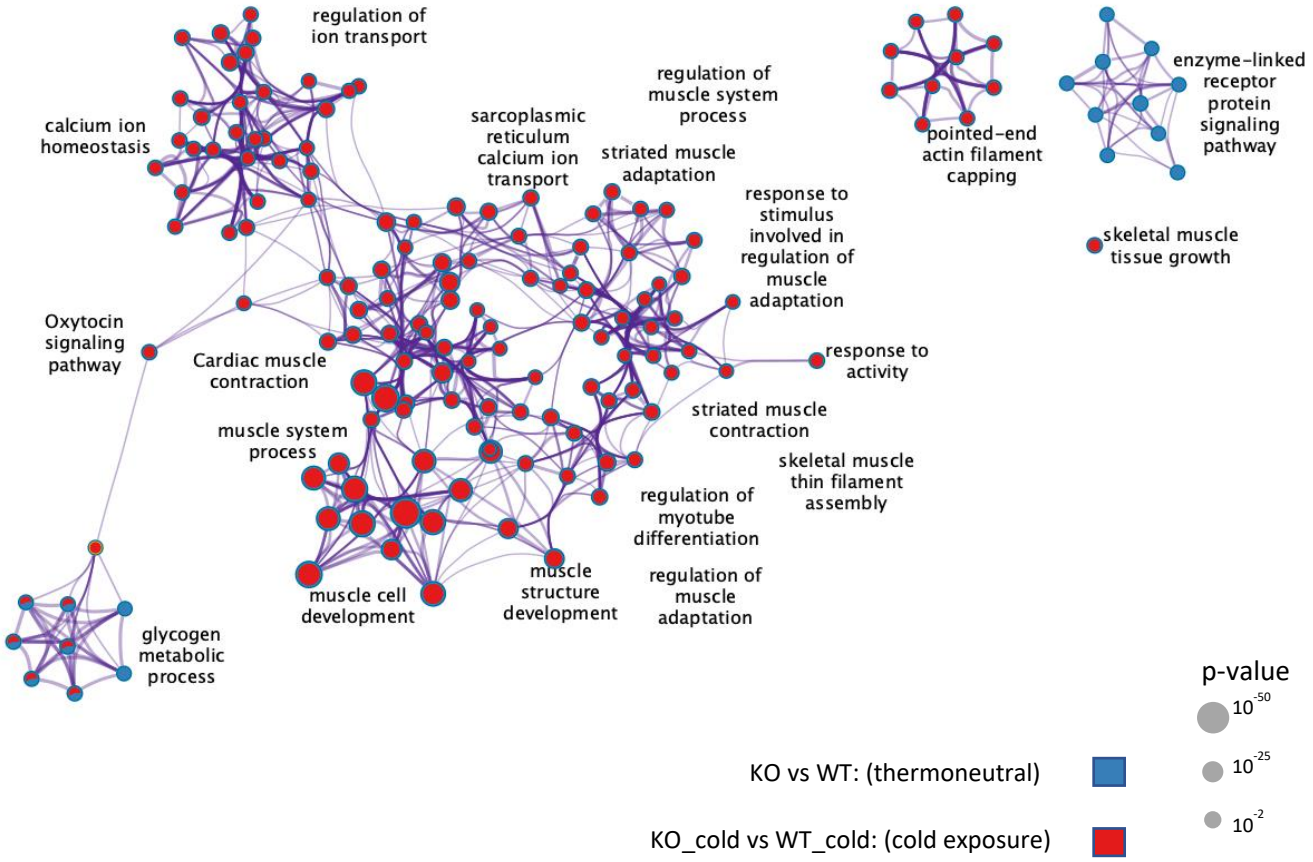

Figure S6: Metascape network visualizations of statistically enriched gene ontology terms between thermoneutral and cold-exposure condition of *Prkd1*^{BKO} (KO) vs *Prkd1*$^{fl/fl}$ (WT) for 4-day cold exposure RNA-Seq experiment. The network has its nodes displayed as pies. Each pie sector is proportional to the number of differentially expressed genes originated from PRKD1-KO vs wild type in cold exposure(red) or thermoneutral condition(blue). p-values are calculated based on the accumulative hypergeometric distribution. Kappa-statistical similarities among their gene memberships are used as the similarity metric when performing hierarchical clustering on the enriched terms.

Appendix B. RNA-Seq normalized counts for 8-hour cold exposure (*Prkd1*^{BKO} cold v. *Prkd1*$^{fl/fl}$ cold) (significantly changed genes only: p_{adj}<0.05)

KO_cold__vs__WT_cold-DESeq2-results-all-data											
ensemblid	Row.names	gene_ symbol	Log 2-Fold Change	p-value	padj	KO_cold / 5469-MC-9	KO_cold / 5469-MC-10	KO_cold / 5469-MC-11	WT_cold / 5469-MC-6	WT_cold / 5469-MC-7	WT_cold / 5469-MC-8
ENSMUSG00000022270	ENSMUSG00000022270.16	Retreg1	3.965731101	2.05E-27	2.97E-23	1538	2192	1588	137	104	281
ENSMUSG00000057897	ENSMUSG00000057897.14	Camk2b	2.668087575	1.1E-19	8E-16	205	323	274	54	29	75
ENSMUSG00000030433	ENSMUSG00000030433.15	Sbk2	4.161089641	1.1E-16	5.32E-13	368	792	939	53	31	93
ENSMUSG00000022358	ENSMUSG00000022358.7	Fbxo32	3.411858549	6.3E-16	2.28E-12	1847	2254	1325	219	169	445
ENSMUSG00000019194	ENSMUSG00000019194.15	Scn1b	1.965790324	1.43E-15	4.13E-12	1452	1904	2397	454	363	665
ENSMUSG00000039496	ENSMUSG00000039496.8	Cdnf	2.322783666	3.85E-15	9.29E-12	109	163	177	40	27	43
ENSMUSG00000073700	ENSMUSG00000073700.3	Klhl21	1.643805174	1.87E-14	3.87E-11	578	771	872	225	236	372
ENSMUSG00000039891	ENSMUSG00000039891.6	Txlnb	4.803276177	4.84E-14	8.77E-11	978	1673	2705	78	64	190
ENSMUSG00000038201	ENSMUSG00000038201.10	Kcna7	5.912435554	7.11E-14	1.14E-10	102	281	373	2	6	10
ENSMUSG00000047205	ENSMUSG00000047205.12	Dusp18	2.174848228	1.3E-13	1.88E-10	764	1087	1000	234	177	464
ENSMUSG00000029862	ENSMUSG00000029862.15	Clcn1	5.576054925	2.07E-13	2.64E-10	108	281	303	2	6	16
ENSMUSG00000090799	ENSMUSG00000090799.2	Klhl33	4.106413344	2.19E-13	2.64E-10	328	628	427	28	35	62
ENSMUSG00000028927	ENSMUSG00000028927.6	Padi2	4.890396163	5.44E-13	6.06E-10	363	878	685	25	23	70

ENSMUSG00000047875	ENSMUSG00000047875.6	Gpr157	2.696863077	8.78E-13	9.09E-10	322	539	232	54	65	91
ENSMUSG00000031791	ENSMUSG00000031791.8	Tmem38a	4.441175794	1.3E-12	1.26E-09	1484	2800	2585	108	82	333
ENSMUSG00000061816	ENSMUSG00000061816.15	Myl1	3.570194185	2.42E-12	2.19E-09	4965	9277	6718	526	792	1418
ENSMUSG00000101655	ENSMUSG00000101655.1	2310040G24Rik	3.577758121	9.81E-12	8.36E-09	53	122	102	11	3	15
ENSMUSG00000020882	ENSMUSG00000020882.17	Cacnb1	3.960022649	1.07E-11	8.61E-09	176	433	418	18	21	59
ENSMUSG00000001403	ENSMUSG00000001403.13	Ube2c	2.75103664	1.61E-11	1.18E-08	133	256	245	25	33	36
ENSMUSG00000113178	ENSMUSG00000113178.1	Mylf-ps	3.404276813	1.64E-11	1.18E-08	1463	3065	2185	200	260	486
ENSMUSG00000022357	ENSMUSG00000022357.2	Klhl38	4.794609121	1.95E-11	1.35E-08	150	156	95	7	8	13
ENSMUSG00000010492	ENSMUSG00000010492.10	Uckl1os	6.957341118	6.61E-11	4.36E-08	45	114	166	0	1	3
ENSMUSG00000028328	ENSMUSG00000028328.13	Tmod1	3.934113539	1.41E-10	8.92E-08	511	1059	942	53	60	156
ENSMUSG00000058975	ENSMUSG00000058975.7	Kcnc1	5.968889158	2.35E-10	1.42E-07	68	168	122	1	0	7
ENSMUSG00000001420	ENSMUSG00000001420.13	Tmem79	-0.974369465	2.53E-10	1.47E-07	999	654	1251	1155	853	1488
ENSMUSG00000042686	ENSMUSG00000042686.5	Jph1	3.781153775	3.21E-10	1.79E-07	450	766	867	52	39	136
ENSMUSG00000046345	ENSMUSG00000046345.4	Smco1	5.193257886	4.61E-10	2.48E-07	40	95	82	0	4	5
ENSMUSG00000029361	ENSMUSG00000029361.18	Nos1	3.484305148	5.19E-10	2.69E-07	130	283	372	37	31	52
ENSMUSG00000079055	ENSMUSG00000079055.10	Slc8a3	5.261921324	6.26E-10	3.13E-07	58	187	209	3	4	14

ENSMUSG00000036854	ENSMUSG00000036854.14	Hspb6	3.961300012	7.98E-10	3.86E-07	1434	2879	2920	190	196	526
ENSMUSG00000033065	ENSMUSG00000033065.14	Pfkm	3.030650936	8.34E-10	3.9E-07	2205	4402	5360	379	352	1187
ENSMUSG00000022519	ENSMUSG00000022519.14	Srl	3.756428384	1.04E-09	4.72E-07	2432	4237	4934	442	285	788
ENSMUSG00000027499	ENSMUSG00000027499.12	Pkia	3.898377798	1.24E-09	5.44E-07	713	1354	1471	73	66	221
ENSMUSG00000055493	ENSMUSG00000055493.4	Epm2a	1.772095783	1.43E-09	6.11E-07	204	309	378	69	83	143
ENSMUSG00000037139	ENSMUSG00000037139.15	Myom3	3.575371998	1.58E-09	6.53E-07	251	374	644	40	33	76
ENSMUSG00000038204	ENSMUSG00000038204.13	Asb10	5.338199817	1.67E-09	6.72E-07	75	199	177	2	0	16
ENSMUSG00000042895	ENSMUSG00000042895.6	Abra	4.495954002	2.19E-09	8.6E-07	220	315	509	18	10	55
ENSMUSG00000028838	ENSMUSG00000028838.11	Extl1	4.741467811	2.56E-09	9.77E-07	60	170	116	4	1	14
ENSMUSG00000028278	ENSMUSG00000028278.14	Rragd	3.595929227	3.52E-09	1.31E-06	490	910	1119	78	74	170
ENSMUSG00000069049	ENSMUSG00000069049.11	Eif2s3y	17.90769718	5.03E-09	1.82E-06	1279	0	1833	0	0	0
ENSMUSG00000038132	ENSMUSG00000038132.6	Rbm24	4.42412828	6.91E-09	2.44E-06	336	629	526	17	19	102
ENSMUSG00000001333	ENSMUSG00000001333.9	Sync	4.418543542	7.37E-09	2.48E-06	40	104	144	8	6	5
ENSMUSG00000029683	ENSMUSG00000029683.7	Lmod2	6.507739862	7.21E-09	2.48E-06	668	1040	1253	10	14	62
ENSMUSG00000001604	ENSMUSG00000001604.14	Tcea3	3.671747117	8.08E-09	2.66E-06	205	301	411	22	20	67
ENSMUSG00000063142	ENSMUSG00000063142.15	Kcnma1	4.77868026	1.03E-08	3.31E-06	49	122	142	8	3	15
ENSMUSG00000043639	ENSMUSG00000043639.14	Rbm20	3.412081396	1.24E-08	3.89E-06	88	132	103	13	12	34

ENSMUSG00000052852	ENSMUSG00000052852.8	Reep1	3.663043221	1.37E-08	4.24E-06	81	150	162	15	9	26
ENSMUSG00000027868	ENSMUSG00000027868.11	Tbx15	2.339970448	1.46E-08	4.24E-06	520	812	863	156	116	250
ENSMUSG00000032355	ENSMUSG00000032355.16	Mlip	4.016444195	1.49E-08	4.24E-06	103	184	152	13	11	28
ENSMUSG00000010461	ENSMUSG00000010461.15	Eya4	4.7535851	1.44E-08	4.24E-06	58	80	66	3	2	5
ENSMUSG00000020722	ENSMUSG00000020722.5	Cacng1	4.085851911	1.47E-08	4.24E-06	143	276	266	6	10	47
ENSMUSG00000026778	ENSMUSG00000026778.13	Prkcq	3.827252392	1.6E-08	4.37E-06	171	235	349	17	17	52
ENSMUSG00000032523	ENSMUSG00000032523.11	Hhatl	4.995345518	1.59E-08	4.37E-06	90	119	117	1	3	15
ENSMUSG00000042529	ENSMUSG00000042529.14	Kcnj12	3.78433037	1.66E-08	4.45E-06	98	192	224	18	15	22
ENSMUSG00000030401	ENSMUSG00000030401.16	Rtn2	3.457222667	2.23E-08	5.87E-06	509	1094	1184	63	114	208
ENSMUSG00000042476	ENSMUSG00000042476.12	Abcb4	2.339087296	2.42E-08	6.26E-06	277	477	501	92	103	145
ENSMUSG00000028348	ENSMUSG00000028348.7	Cavin4	3.978859383	2.48E-08	6.31E-06	239	378	497	38	39	57
ENSMUSG00000112384	ENSMUSG00000112384.1	Gm34921	-2.520781611	2.58E-08	6.46E-06	507	212	695	1134	1458	1063
ENSMUSG00000029189	ENSMUSG00000029189.10	Sel1l3	4.319272852	3.17E-08	7.79E-06	56	186	80	7	8	18
ENSMUSG00000038663	ENSMUSG00000038663.7	Fsd2	3.446343871	3.64E-08	8.79E-06	439	766	838	50	85	127
ENSMUSG00000041889	ENSMUSG00000041889.7	Shisa4	3.73202772	4.51E-08	1.05E-05	157	273	172	7	12	56
ENSMUSG00000049173	ENSMUSG00000049173.7	Myoz3	5.221952135	4.47E-08	1.05E-05	18	56	44	0	1	4

ENSMUSG00000028841	ENSMUSG00000028841.14	Cnksr1	5.238018218	5.04E-08	1.16E-05	94	149	130	0	2	17
ENSMUSG00000032366	ENSMUSG00000032366.15	Tpm1	2.802673375	5.99E-08	1.36E-05	9657	15525	13249	2106	2330	3969
ENSMUSG00000055027	ENSMUSG00000055027.17	Smyd1	5.238558312	6.75E-08	1.5E-05	428	1188	1175	21	19	106
ENSMUSG00000040287	ENSMUSG00000040287.9	Stac3	3.62666087	7.35E-08	1.62E-05	114	250	284	14	10	51
ENSMUSG00000032643	ENSMUSG00000032643.12	Fhl3	2.181376528	7.64E-08	1.65E-05	584	783	986	204	203	271
ENSMUSG00000001508	ENSMUSG00000001508.15	Sgca	4.733753334	7.9E-08	1.68E-05	128	211	251	4	5	35
ENSMUSG00000000031	ENSMUSG00000000031.16	H19	6.121234612	8.28E-08	1.74E-05	1657	5267	6725	50	71	436
ENSMUSG00000006435	ENSMUSG00000006435.15	Neurl1a	3.944895364	8.63E-08	1.79E-05	213	407	640	11	28	77
ENSMUSG00000081194	ENSMUSG00000081194.1	Gm8424	6.20440601	9.86E-08	2.01E-05	17	51	44	0	2	1
ENSMUSG00000042451	ENSMUSG00000042451.12	Mybph	4.921628076	1.02E-07	2.06E-05	78	228	13	0	8	19
ENSMUSG00000030319	ENSMUSG00000030319.8	Cand2	3.743755794	1.13E-07	2.25E-05	90	216	266	18	18	38
ENSMUSG00000025425	ENSMUSG00000025425.17	St8sia5	4.835567876	1.28E-07	2.5E-05	49	112	160	2	3	13
ENSMUSG00000047746	ENSMUSG00000047746.14	Fbxo40	5.24391695	1.64E-07	3.16E-05	448	791	1059	17	10	89
ENSMUSG00000022464	ENSMUSG00000022464.14	Slc38a4	3.81492386	2.05E-07	3.91E-05	82	134	138	12	7	26
ENSMUSG00000089718	ENSMUSG00000089718.1	2310075C17Rik	5.02246298	2.1E-07	3.95E-05	39	64	34	0	0	6
ENSMUSG00000021536	ENSMUSG00000021536.7	Adcy2	4.911037729	2.13E-07	3.95E-05	66	117	222	5	3	16
ENSMUSG00000027107	ENSMUSG00000027107.3	Chrna1	8.077520373	2.27E-07	4.06E-05	21	64	32	0	0	1

ENSMUSG00000027510	ENSMUSG00000027510.17	Rbm38	1.916477336	2.26E-07	4.06E-05	326	711	870	250	101	232
ENSMUSG00000078532	ENSMUSG00000078532.9	Nkain1	3.177988398	2.24E-07	4.06E-05	17	40	60	5	4	10
ENSMUSG00000041695	ENSMUSG00000041695.2	Kcnj2	3.784456996	2.45E-07	4.33E-05	174	366	253	20	18	76
ENSMUSG00000028017	ENSMUSG00000028017.7	Egf	3.715088698	2.53E-07	4.4E-05	31	116	98	2	16	13
ENSMUSG00000021200	ENSMUSG00000021200.14	Asb2	3.589275022	2.55E-07	4.4E-05	378	749	741	61	58	149
ENSMUSG00000021373	ENSMUSG00000021373.16	Cap2	2.974759785	2.84E-07	4.85E-05	420	619	709	99	85	195
ENSMUSG00000040118	ENSMUSG00000040118.15	Cacna2d1	2.670474192	3.03E-07	5.1E-05	623	1006	1095	164	144	303
ENSMUSG00000010064	ENSMUSG00000010064.15	Slc38a3	4.011723698	3.36E-07	5.6E-05	71	138	101	4	13	16
ENSMUSG00000060180	ENSMUSG00000060180.12	Myh13	7.700228233	3.4E-07	5.6E-05	8	33	24	0	0	0
ENSMUSG00000047591	ENSMUSG00000047591.5	Mafa	3.319866058	3.59E-07	5.84E-05	68	175	230	24	14	32
ENSMUSG00000006221	ENSMUSG00000006221.7	Hspb7	5.535288185	3.78E-07	6.09E-05	604	1478	1728	46	44	155
ENSMUSG00000032845	ENSMUSG00000032845.15	Alpk2	7.056443014	4.1E-07	6.53E-05	121	243	256	1	0	13
ENSMUSG00000024210	ENSMUSG00000024210.2	Ip6k3	4.794259105	4.26E-07	6.71E-05	171	391	182	3	4	43
ENSMUSG00000031636	ENSMUSG00000031636.7	Pdlim3	3.368436867	4.34E-07	6.77E-05	406	881	806	67	78	258
ENSMUSG00000021061	ENSMUSG00000021061.15	Sptb	4.477222791	4.42E-07	6.82E-05	540	915	1486	57	65	112
ENSMUSG00000026100	ENSMUSG00000026100.6	Mstn	4.914795098	4.49E-07	6.84E-05	32	77	74	0	0	10
ENSMUSG00000110547	ENSMUSG00000110547.1	Gm29773	5.793180119	4.53E-07	6.84E-05	13	43	24	0	2	1

ENSMUSG00000085348	ENSMUSG00000085348.1	Myhas	5.040639645	5.04E-07	7.53E-05	30	150	113	0	1	12
ENSMUSG00000026308	ENSMUSG00000026308.8	Klhl30	3.895562299	5.4E-07	7.98E-05	118	206	204	12	19	34
ENSMUSG00000061462	ENSMUSG00000061462.17	Obscn	6.235084794	5.58E-07	8.17E-05	2151	4491	6715	12	52	306
ENSMUSG00000034055	ENSMUSG00000034055.16	Phka1	2.356189719	6.61E-07	9.57E-05	562	870	1107	165	153	353
ENSMUSG00000021579	ENSMUSG00000021579.4	Lrrc14b	3.661605064	7.13E-07	0.00010226	193	368	340	16	15	81
ENSMUSG00000030554	ENSMUSG00000030554.16	Synm	1.885395875	7.62E-07	0.00010725	2426	4811	4947	1280	1178	2008
ENSMUSG00000025754	ENSMUSG00000025754.11	Agbl1	8.06931816	7.55E-07	0.00010725	11	21	39	0	0	0
ENSMUSG00000025241	ENSMUSG00000025241.16	Fyco1	1.545551591	8.08E-07	0.0001126	769	1075	1383	484	330	586
ENSMUSG00000086298	ENSMUSG00000086298.1	Gm11716	3.675865171	8.23E-07	0.00011357	29	58	70	2	5	10
ENSMUSG00000028464	ENSMUSG00000028464.16	Tpm2	4.112577848	8.37E-07	0.00011438	12597	22476	24672	939	1177	3763
ENSMUSG00000070424	ENSMUSG00000070424.12	Art5	5.580992102	8.57E-07	0.00011609	33	52	84	1	0	7
ENSMUSG00000034353	ENSMUSG00000034353.14	Ramp1	2.996964908	9.04E-07	0.00012019	165	243	289	16	24	64
ENSMUSG00000104453	ENSMUSG00000104453.1	Gm37829	3.561810064	9.03E-07	0.00012019	105	202	155	6	27	23
ENSMUSG00000071342	ENSMUSG00000071342.5	Lsmem1	4.659480505	9.32E-07	0.0001228	39	106	115	0	4	13
ENSMUSG00000038777	ENSMUSG00000038777.19	Sema6c	3.514841091	9.55E-07	0.00012468	85	160	255	17	12	33
ENSMUSG00000027805	ENSMUSG00000027805.16	Pfn2	2.193477606	1.02E-06	0.00013159	283	491	555	113	101	178
ENSMUSG00000048416	ENSMUSG00000048416.15	Mlf1	5.107412622	1.03E-06	0.00013159	337	671	509	2	20	49

ENSMUSG00000032816	ENSMUSG00000032816.15	Igdcc4	3.851126472	1.09E-06	0.00013859	46	106	156	13	8	15
ENSMUSG00000053025	ENSMUSG00000053025.13	Sv2b	8.387782481	1.22E-06	0.0001539	10	67	53	0	0	1
ENSMUSG00000069372	ENSMUSG00000069372.3	Ctxn3	5.11590608	1.23E-06	0.0001539	36	36	96	1	0	5
ENSMUSG00000087410	ENSMUSG00000087410.7	2310065F04Rik	4.481359091	1.31E-06	0.00016237	50	29	52	0	1	3
ENSMUSG00000029066	ENSMUSG00000029066.12	Mrpl20	-0.730415209	1.41E-06	0.00017024	4988	5102	6025	7726	6166	8711
ENSMUSG00000039661	ENSMUSG00000039661.14	Dusp26	2.132437342	1.4E-06	0.00017024	113	150	276	42	35	72
ENSMUSG00000032648	ENSMUSG00000032648.14	Pygm	4.758152298	1.39E-06	0.00017024	5625	9663	10108	148	241	1251
ENSMUSG00000068699	ENSMUSG00000068699.12	Flnc	4.232559982	1.53E-06	0.00018352	706	1617	2201	150	123	285
ENSMUSG00000044086	ENSMUSG00000044086.8	Lmod3	5.327788673	1.62E-06	0.00018908	191	597	639	10	5	58
ENSMUSG00000052374	ENSMUSG00000052374.15	Actn2	4.988338959	1.62E-06	0.00018908	1298	2465	3830	176	124	301
ENSMUSG00000034295	ENSMUSG00000034295.9	Fhod3	2.435493256	1.62E-06	0.00018908	112	247	151	60	42	82
ENSMUSG00000024617	ENSMUSG00000024617.16	Camk2a	5.06322839	1.63E-06	0.00018908	223	554	481	3	11	50
ENSMUSG00000079428	ENSMUSG00000079428.8	Tceal7	5.843575318	1.75E-06	0.00020086	10	53	6	0	0	3
ENSMUSG00000019933	ENSMUSG00000019933.7	Mrln	4.137022564	1.79E-06	0.00020374	44	66	77	0	4	12
ENSMUSG00000038205	ENSMUSG00000038205.12	Prkab2	2.057350454	1.9E-06	0.00021165	333	483	591	117	105	173
ENSMUSG00000045667	ENSMUSG00000045667.14	Smtnl2	3.116988322	1.89E-06	0.00021165	142	407	620	43	24	133

ENSMUSG00000047419	ENSMUSG00000047419.5	Cmya5	5.786865609	1.89E-06	0.00021165	2984	5802	7909	33	65	524
ENSMUSG00000027010	ENSMUSG00000027010.16	Slc25a12	2.307480108	1.92E-06	0.00021225	544	960	854	224	227	263
ENSMUSG00000041329	ENSMUSG00000041329.13	Atp1b2	1.246779913	1.95E-06	0.00021466	342	810	479	265	270	405
ENSMUSG00000024049	ENSMUSG00000024049.14	Myom1	4.27596099	2.03E-06	0.00022092	1611	2802	3132	136	137	483
ENSMUSG00000071317	ENSMUSG00000071317.4	Bves	3.450964786	2.14E-06	0.00023168	77	136	120	6	13	35
ENSMUSG00000006542	ENSMUSG00000006542.13	Prkag3	4.66620635	2.33E-06	0.00024903	39	75	105	0	2	9
ENSMUSG00000017817	ENSMUSG00000017817.11	Jph2	2.951632923	2.34E-06	0.00024903	947	2577	2764	307	296	664
ENSMUSG00000031972	ENSMUSG00000031972.5	Acta1	5.542313682	2.36E-06	0.00025012	31934	66872	46841	43	983	5451
ENSMUSG00000074001	ENSMUSG00000074001.3	Klhl40	5.657400338	2.44E-06	0.00025627	151	493	476	1	9	34
ENSMUSG00000062694	ENSMUSG00000062694.7	Cav3	4.175077479	2.48E-06	0.00025893	39	124	109	1	5	18
ENSMUSG00000021589	ENSMUSG00000021589.13	Rhobtb3	1.145519159	2.66E-06	0.00027499	188	251	173	97	75	143
ENSMUSG00000037989	ENSMUSG00000037989.15	Wnk2	3.889968407	2.7E-06	0.00027752	111	292	274	8	14	72
ENSMUSG00000026950	ENSMUSG00000026950.17	Neb	5.934492024	2.77E-06	0.00028255	3981	7249	8323	14	115	571
ENSMUSG00000038170	ENSMUSG00000038170.15	Pde4dip	3.799166413	2.87E-06	0.00029082	3556	5895	9261	583	442	1072
ENSMUSG00000022441	ENSMUSG00000022441.17	Efcab6	7.765870065	2.93E-06	0.00029539	21	25	71	0	0	0
ENSMUSG00000107585	ENSMUSG00000107585.1	3300002P13Rik	5.514818943	3.01E-06	0.00030116	11	33	44	0	0	3
ENSMUSG00000026062	ENSMUSG00000026062.12	Slc9a2	3.7914926	3.07E-06	0.00030461	68	138	168	3	11	29

ENSMUSG00000109237	ENSMUSG00000109237.1	9130214F15Rik	-2.125582668	3.19E-06	0.00031496	144	49	140	125	211	380
ENSMUSG00000021798	ENSMUSG00000021798.14	Ldb3	4.511008879	3.49E-06	0.00034133	1438	3402	3250	115	118	549
ENSMUSG00000056900	ENSMUSG00000056900.13	Usp13	4.932390884	3.53E-06	0.00034341	589	1055	1017	10	24	132
ENSMUSG00000013936	ENSMUSG00000013936.12	Myl2	7.349701283	3.87E-06	0.00037421	150	521	1264	11	5	19
ENSMUSG00000026817	ENSMUSG00000026817.14	Ak1	1.852675843	4.07E-06	0.00038686	2012	3355	3272	1159	826	969
ENSMUSG00000038764	ENSMUSG00000038764.14	Ptpn3	2.580692454	4.08E-06	0.00038686	118	239	287	50	51	51
ENSMUSG00000057280	ENSMUSG00000057280.15	Musk	5.050089562	4.11E-06	0.00038686	46	45	26	0	0	6
ENSMUSG00000002007	ENSMUSG00000002007.5	Srpk3	3.923216243	4.09E-06	0.00038686	31	53	100	7	3	11
ENSMUSG00000028023	ENSMUSG00000028023.16	Pitx2	4.986623664	4.27E-06	0.00039946	37	98	138	0	2	14
ENSMUSG00000031543	ENSMUSG00000031543.18	Ank1	4.548760904	4.45E-06	0.00041345	416	959	1057	27	26	141
ENSMUSG00000091712	ENSMUSG00000091712.2	Sec14l5	3.742374885	4.53E-06	0.00041831	18	66	86	5	3	12
ENSMUSG00000002500	ENSMUSG00000002500.15	Rpl3l	5.242542603	4.8E-06	0.00043835	623	1128	1334	5	22	115
ENSMUSG00000054034	ENSMUSG00000054034.10	Tceal5	3.717471853	4.81E-06	0.00043835	19	61	33	6	3	8
ENSMUSG00000019848	ENSMUSG00000019848.14	Popdc3	4.712024592	5.06E-06	0.00045851	39	71	150	0	2	14
ENSMUSG00000051890	ENSMUSG00000051890.13	Klhdc1	1.578750596	5.42E-06	0.00048789	52	94	122	32	25	40
ENSMUSG00000022525	ENSMUSG00000022525.13	Plaat1	4.410164085	5.94E-06	0.00053154	61	121	106	0	2	21

ENSMUSG00000026418	ENSMUSG00000026418.16	Tnni1	8.196223125	6.38E-06	0.00056735	261	890	1753	0	7	16
ENSMUSG00000035934	ENSMUSG00000035934.16	Pknox2	2.611066608	6.56E-06	0.00057672	72	130	141	18	16	47
ENSMUSG00000031312	ENSMUSG00000031312.5	Itgb1bp2	5.237574616	6.57E-06	0.00057672	147	231	208	1	8	22
ENSMUSG00000049134	ENSMUSG00000049134.15	Nrap	5.962706242	6.65E-06	0.00058096	1378	3040	4427	11	46	269
ENSMUSG00000071540	ENSMUSG00000071540.4	3425401B19Rik	6.583713954	6.82E-06	0.00059192	324	1009	1250	0	13	42
ENSMUSG00000025429	ENSMUSG00000025429.8	Pstpip2	3.273670783	6.91E-06	0.00059614	26	25	28	3	3	3
ENSMUSG00000029685	ENSMUSG00000029685.15	Asb15	5.496449299	7.01E-06	0.00060099	185	265	206	0	6	20
ENSMUSG00000025932	ENSMUSG00000025932.14	Eya1	3.165359263	7.11E-06	0.00060644	50	108	73	10	2	28
ENSMUSG00000031204	ENSMUSG00000031204.3	Asb12	4.637482476	7.29E-06	0.00061807	20	43	49	0	2	5
ENSMUSG00000030672	ENSMUSG00000030672.12	Mylpf	5.413431213	7.47E-06	0.00062942	2746	5146	3669	11	71	417
ENSMUSG00000025537	ENSMUSG00000025537.12	Phkg1	4.34524471	7.86E-06	0.00065812	359	696	703	9	19	103
ENSMUSG00000040350	ENSMUSG00000040350.16	Trim7	3.226368162	7.97E-06	0.00066643	42	101	95	11	6	29
ENSMUSG00000091898	ENSMUSG00000091898.8	Tnnc1	7.145657569	8.5E-06	0.00070372	357	1067	2141	8	29	19
ENSMUSG00000042717	ENSMUSG00000042717.5	Ppp1r3a	5.454438762	8.62E-06	0.00071012	296	556	551	2	5	53
ENSMUSG00000023153	ENSMUSG00000023153.9	Tmem52	3.313577844	8.97E-06	0.00073269	91	132	118	10	9	30
ENSMUSG00000038763	ENSMUSG00000038763.12	Alpk3	5.001510141	9E-06	0.00073269	368	856	1372	11	38	109
ENSMUSG00000003476	ENSMUSG00000003476.16	Crhr2	3.966904058	9.58E-06	0.00077567	24	54	75	2	3	10

ENSMUSG00000053093	ENSMUSG00000053093.16	Myh7	8.098417297	9.68E-06	0.0007798	1789	6012	10678	2	76	84
ENSMUSG00000051747	ENSMUSG00000051747.14	Ttn	6.000302383	1.01E-05	0.00081041	9701	16118	24083	15	221	1647
ENSMUSG00000001027	ENSMUSG00000001027.7	Scn4a	6.075533192	1.02E-05	0.00081485	488	1032	1241	1	10	72
ENSMUSG00000051910	ENSMUSG00000051910.13	Sox6	0.967347294	1.07E-05	0.00084813	454	425	663	250	187	317
ENSMUSG00000021451	ENSMUSG00000021451.16	Sema4d	2.70582275	1.09E-05	0.00085805	121	254	302	48	35	86
ENSMUSG00000040666	ENSMUSG00000040666.18	Sh3bgr	4.210624182	1.13E-05	0.00088507	385	742	924	18	31	116
ENSMUSG00000013419	ENSMUSG00000013419.7	Zfp651	1.407122307	1.19E-05	0.00092555	284	553	706	206	208	276
ENSMUSG00000031461	ENSMUSG00000031461.4	Myom2	5.872381887	1.2E-05	0.00093135	1587	3026	2640	6	29	290
ENSMUSG00000032495	ENSMUSG00000032495.8	Lrrc2	5.413025874	1.21E-05	0.0009339	287	371	464	4	6	53
ENSMUSG00000042404	ENSMUSG00000042404.16	Dennd4b	1.452583113	1.25E-05	0.0009585	239	415	521	146	146	224
ENSMUSG00000043154	ENSMUSG00000043154.15	Ppp2r3a	1.434229524	1.26E-05	0.0009585	1134	1366	1481	640	480	682
ENSMUSG00000060600	ENSMUSG00000060600.15	Eno3	4.90039787	1.26E-05	0.0009585	4043	9798	8779	68	185	1181
ENSMUSG00000044461	ENSMUSG00000044461.6	Shisa2	2.907163262	1.29E-05	0.00097231	103	202	183	19	28	63
ENSMUSG00000061603	ENSMUSG00000061603.8	Akap6	2.4774756	1.35E-05	0.00100616	87	184	188	43	24	62
ENSMUSG00000031376	ENSMUSG00000031376.15	Atp2b3	6.779997207	1.35E-05	0.00100616	21	14	23	0	0	1
ENSMUSG00000024924	ENSMUSG00000024924.14	Vldlr	1.226389917	1.36E-05	0.00101424	1470	1672	2843	956	462	971
ENSMUSG00000050211	ENSMUSG00000050211.14	Pla2g4e	4.928103637	1.43E-05	0.00105832	18	31	45	0	0	5

ENSMUSG00000027022	ENSMUSG00000027022.13	Xirp2	6.09365212	1.46E-05	0.00107272	2637	4961	5064	3	55	339
ENSMUSG00000067081	ENSMUSG00000067081.12	Asb18	5.08220573	1.49E-05	0.00108784	11	31	61	0	1	4
ENSMUSG00000029158	ENSMUSG00000029158.9	Yipf7	5.837837223	1.52E-05	0.00110684	96	160	201	0	3	14
ENSMUSG00000038239	ENSMUSG00000038239.11	Hrc	5.35238276	1.54E-05	0.001 1117	749	1765	1822	11	25	203
ENSMUSG00000079243	ENSMUSG00000079243.3	Xirp1	4.516636547	1.54E-05	0.001 1117	228	450	990	77	41	84
ENSMUSG00000042155	ENSMUSG00000042155.3	Klhl23	2.311778943	1.66E-05	0.001 1887	92	258	213	41	36	82
ENSMUSG00000024381	ENSMUSG00000024381.15	Bin1	2.031719644	1.68E-05	0.00119884	565	1149	1340	257	221	498
ENSMUSG00000047485	ENSMUSG00000047485.6	Klhl34	6.500218733	1.72E-05	0.00121912	50	84	176	0	0	7
ENSMUSG00000020169	ENSMUSG00000020169.4	Best3	6.529990301	1.75E-05	0.001 2388	8	35	9	0	1	0
ENSMUSG00000112739	ENSMUSG00000112739.1	Gm20597	4.864932881	1.77E-05	0.00124311	8	38	27	0	0	5
ENSMUSG00000101086	ENSMUSG00000101086.2	Gm28651	7.36783655	1.86E-05	0.00129974	5	26	17	0	0	0
ENSMUSG00000028584	ENSMUSG00000028584.3	Lrrc38	5.149221353	2.12E-05	0.00147622	26	41	70	0	0	5
ENSMUSG00000023092	ENSMUSG00000023092.16	Fhl1	2.318193103	2.14E-05	0.00148315	5010	10074	11217	3420	1709	4038
ENSMUSG00000044951	ENSMUSG00000044951.15	Mylk4	6.264947646	2.2E-05	0.00151534	1590	3157	2915	0	35	96
ENSMUSG00000043155	ENSMUSG00000043155.4	Hpdl	-0.855643548	2.27E-05	0.00155815	199	158	332	284	228	362
ENSMUSG00000049551	ENSMUSG00000049551.2	Fzd9	3.812157813	2.31E-05	0.00157218	75	138	254	9	12	37

ENSMUSG00000051627	ENSMUSG00000051627.3	H1f4	2.857572306	2.31E-05	0.00157218	23	44	67	10	4	10
ENSMUSG00000004085	ENSMUSG00000004085.14	Map3k20	1.44520797	2.37E-05	0.00160668	669	1009	1248	436	346	586
ENSMUSG00000018893	ENSMUSG00000018893.15	Mb	4.872415714	2.4E-05	0.00161599	3985	4618	7794	154	111	808
ENSMUSG00000097354	ENSMUSG00000097354.7	2310001H17Rik	1.513392129	2.41E-05	0.00161656	52	63	66	23	17	30
ENSMUSG00000050315	ENSMUSG00000050315.13	Synpo2	2.628444329	2.43E-05	0.00162353	661	1383	1780	290	227	466
ENSMUSG00000027887	ENSMUSG00000027887.11	Sypl2	4.784285685	2.44E-05	0.00162359	307	884	767	10	15	118
ENSMUSG00000078815	ENSMUSG00000078815.8	Cacng6	5.68463646	2.53E-05	0.00167649	109	254	371	0	3	20
ENSMUSG00000026208	ENSMUSG00000026208.9	Des	2.231423417	2.59E-05	0.0017039	6983	9936	15147	2687	1999	5146
ENSMUSG00000039376	ENSMUSG00000039376.13	Synpo2l	4.536661153	2.8E-05	0.00183475	100	316	616	13	18	49
ENSMUSG00000044788	ENSMUSG00000044788.10	Fads6	1.991085887	2.81E-05	0.00183753	51	110	119	28	15	45
ENSMUSG00000055489	ENSMUSG00000055489.8	Ano5	5.294997415	2.89E-05	0.00187851	150	272	255	0	3	27
ENSMUSG00000079278	ENSMUSG00000079278.1	Tmem233	5.633775869	3.17E-05	0.0020494	98	219	221	0	1	17
ENSMUSG00000097317	ENSMUSG00000097317.1	NA	3.131685545	3.38E-05	0.00217628	27	70	64	7	10	10
ENSMUSG00000025813	ENSMUSG00000025813.14	Homer2	3.543089703	3.52E-05	0.00225456	45	146	244	12	24	29
ENSMUSG00000080850	ENSMUSG00000080850.1	Gm12439	3.3194476	3.58E-05	0.00227399	22	27	36	5	2	7
ENSMUSG00000021622	ENSMUSG00000021622.3	Ckmt2	5.486230368	3.57E-05	0.00227399	1063	2188	2617	10	37	213
ENSMUSG00000085272	ENSMUSG00000085272.7	Sbk3	2.944379035	3.64E-05	0.00230223	41	64	39	5	10	18

ENSMUSG00000051456	ENSMUSG00000051456.4	Hspb3	4.275455291	3.65E-05	0.00230223	13	27	38	0	3	4
ENSMUSG00000033182	ENSMUSG00000033182.12	Kbtbd12	4.760706328	3.7E-05	0.00231866	147	117	607	7	17	6
ENSMUSG00000030852	ENSMUSG00000030852.17	Tacc2	2.408171527	3.81E-05	0.00237733	1827	2153	2097	611	629	873
ENSMUSG00000027313	ENSMUSG00000027313.3	Chac1	2.560540971	3.89E-05	0.002 4143	123	114	57	11	25	16
ENSMUSG00000046480	ENSMUSG00000046480.6	Scn4b	3.893707792	3.9E-05	0.002 4143	555	1265	1381	80	31	247
ENSMUSG00000060913	ENSMUSG00000060913.6	Trim55	6.506569832	3.94E-05	0.00243196	58	172	209	0	0	10
ENSMUSG00000042045	ENSMUSG00000042045.6	Sln	6.941598771	3.96E-05	0.00243196	34	95	84	1	0	3
ENSMUSG00000051067	ENSMUSG00000051067.8	Lingo3	5.129217356	3.99E-05	0.00243929	12	22	50	0	0	4
ENSMUSG00000009207	ENSMUSG00000009207.15	Lnpk	1.130588272	4.05E-05	0.00246608	145	196	186	89	62	120
ENSMUSG00000037736	ENSMUSG00000037736.18	Limch1	1.173619815	4.14E-05	0.00251164	324	374	418	183	123	281
ENSMUSG00000047343	ENSMUSG00000047343.4	Mettl21c	9.076425269	4.21E-05	0.002 5303	12	39	146	0	0	0
ENSMUSG00000024302	ENSMUSG00000024302.16	Dtna	2.466056186	4.2E-05	0.002 5303	100	246	183	41	38	71
ENSMUSG00000052430	ENSMUSG00000052430.15	Bmpr1b	4.69264117	4.26E-05	0.00254844	23	24	13	1	1	2
ENSMUSG00000042828	ENSMUSG00000042828.12	Trim72	5.285555156	4.4E-05	0.002 6253	505	780	926	4	9	104
ENSMUSG00000020475	ENSMUSG00000020475.3	Pgam2	4.621015124	4.48E-05	0.00265886	1409	3280	2825	18	70	408
ENSMUSG00000054477	ENSMUSG00000054477.15	Kcnn2	5.583410012	4.51E-05	0.00266869	16	27	17	1	0	1
ENSMUSG00000064179	ENSMUSG00000064179.13	Tnnt1	5.471015144	4.55E-05	0.002 682	371	806	1434	25	43	47

ENSMUSG00000035105	ENSMUSG00000035105.5	Egln3	1.599303581	4.64E-05	0.00272477	624	633	830	206	216	518
ENSMUSG00000072720	ENSMUSG00000072720.9	Myo18b	6.371235705	4.73E-05	0.00275221	720	1169	1547	0	14	77
ENSMUSG00000060548	ENSMUSG00000060548.13	Tnfrsf19	4.626633491	4.72E-05	0.00275221	14	35	111	0	0	9
ENSMUSG00000059741	ENSMUSG00000059741.13	Myl3	6.778789332	5.02E-05	0.00290854	290	626	1568	36	10	15
ENSMUSG00000051000	ENSMUSG00000051000.17	Fam160a1	1.787591014	5.43E-05	0.00313632	261	363	364	178	99	117
ENSMUSG00000026971	ENSMUSG00000026971.15	Itgb6	3.86183052	5.48E-05	0.00314392	14	53	71	0	6	8
ENSMUSG00000009471	ENSMUSG00000009471.4	Myod1	6.445026891	5.49E-05	0.00314392	10	15	38	0	0	1
ENSMUSG00000025216	ENSMUSG00000025216.9	Lbx1	3.494506902	5.74E-05	0.00327673	22	51	77	2	4	12
ENSMUSG00000062077	ENSMUSG00000062077.14	Trim54	5.547194682	5.8E-05	0.00329888	374	796	1112	2	10	85
ENSMUSG00000065990	ENSMUSG00000065990.12	Aurkaip1	-0.546967691	5.87E-05	0.00332419	2417	2548	3729	3263	2896	4423
ENSMUSG00000063296	ENSMUSG00000063296.5	Tmem117	3.109281086	5.9E-05	0.003299	28	62	31	4	2	12
ENSMUSG00000025938	ENSMUSG00000025938.16	Slco5a1	5.149406386	5.99E-05	0.00335334	56	187	236	0	7	17
ENSMUSG00000024059	ENSMUSG00000024059.10	Clip4	4.247873324	5.98E-05	0.00335334	305	651	795	10	28	113
ENSMUSG00000052920	ENSMUSG00000052920.14	Prkg1	1.999021771	6.11E-05	0.00340745	39	98	113	30	23	39
ENSMUSG00000030089	ENSMUSG00000030089.15	Slc41a3	1.982483503	6.59E-05	0.00365164	126	169	148	46	51	64
ENSMUSG00000030470	ENSMUSG00000030470.15	Csrp3	6.07656592	6.6E-05	0.00365164	237	730	1305	2	11	107

ENSMUSG00000034127	ENSMUSG00000034127.15	Tspan8	3.619527455	6.79E-05	0.00374093	78	114	106	1	6	31
ENSMUSG00000056328	ENSMUSG00000056328.14	Myh1	6.431403631	7.03E-05	0.00386042	8367	15915	9917	1	192	742
ENSMUSG00000028116	ENSMUSG00000028116.13	Myoz2	6.256895638	7.14E-05	0.00390556	213	461	1088	3	4	57
ENSMUSG00000034768	ENSMUSG00000034768.4	Asb16	5.08483207	7.52E-05	0.00409972	89	200	236	0	6	21
ENSMUSG00000007877	ENSMUSG00000007877.2	Tcap	5.406277005	7.81E-05	0.00422268	4644	7297	8752	7	145	617
ENSMUSG00000000552	ENSMUSG00000000552.10	Zfp385a	1.99625876	7.8E-05	0.00422268	437	889	1161	259	231	436
ENSMUSG00000046818	ENSMUSG00000046818.7	Ddit4l	3.941883824	8.09E-05	0.00432929	150	225	438	10	6	54
ENSMUSG00000052934	ENSMUSG00000052934.14	Fbxo31	1.370110794	8.09E-05	0.00432929	932	810	883	447	293	505
ENSMUSG00000031962	ENSMUSG00000031962.6	Cdh15	3.86339806	8.04E-05	0.00432929	16	43	58	1	3	9
ENSMUSG00000071708	ENSMUSG00000071708.11	Sms	1.13105918	8.41E-05	0.00448266	267	424	403	164	181	243
ENSMUSG00000059149	ENSMUSG00000059149.17	Mfsd4a	2.765834524	8.49E-05	0.00450853	27	35	68	9	1	12
ENSMUSG00000026429	ENSMUSG00000026429.9	Ube2t	3.453029775	8.53E-05	0.00451052	14	24	10	0	3	3
ENSMUSG00000027470	ENSMUSG00000027470.9	Mylk2	5.074484419	8.58E-05	0.00452244	994	1371	1640	2	38	151
ENSMUSG00000027692	ENSMUSG00000027692.16	Tnik	1.980740709	8.82E-05	0.00462884	53	96	81	33	21	32
ENSMUSG00000040653	ENSMUSG00000040653.6	Ppp1r14c	4.856139222	8.85E-05	0.00462884	103	216	152	5	0	25
ENSMUSG00000035296	ENSMUSG00000035296.14	Sgcg	4.788850788	9.06E-05	0.00472459	314	328	483	5	5	46
ENSMUSG00000016349	ENSMUSG00000016349.10	Eef1a2	5.414738206	9.2E-05	0.00478045	1818	3968	5078	7	69	424

ENSMUSG00000020333	ENSMUSG00000020333.17	Acsl6	3.717280189	9.61E-05	0.00497456	23	31	31	4	1	5
ENSMUSG00000073600	ENSMUSG00000073600.3	Prob1	2.521281005	9.81E-05	0.00505918	145	226	478	33	64	111
ENSMUSG00000021250	ENSMUSG00000021250.13	Fos	2.27376459	0.0001045	0.00537109	137	377	180	183	76	97
ENSMUSG00000045776	ENSMUSG00000045776.3	Lrtm1	2.355223819	0.00011403	0.00584023	152	120	88	38	26	32
ENSMUSG00000051980	ENSMUSG00000051980.13	Casr	5.476185285	0.00011454	0.00584576	15	24	29	0	0	2
ENSMUSG00000042903	ENSMUSG00000042903.8	Foxo4	0.818373352	0.00011766	0.00599835	1025	1180	1758	820	555	887
ENSMUSG00000066705	ENSMUSG00000066705.7	Fxyd6	2.550102861	0.00011901	0.00603145	155	214	328	37	28	99
ENSMUSG00000039873	ENSMUSG00000039873.4	Neurl2	1.66227757	0.00012144	0.00613274	55	66	77	27	23	29
ENSMUSG00000038403	ENSMUSG00000038403.10	Hjv	4.99490861	0.00013013	0.006549	770	1488	2043	3	38	165
ENSMUSG00000026407	ENSMUSG00000026407.17	Cacna1s	5.674644078	0.00013169	0.00656195	1222	2206	2433	1	26	205
ENSMUSG00000026564	ENSMUSG00000026564.9	Dusp27	4.414218256	0.00013133	0.00656195	84	184	306	21	2	32
ENSMUSG00000033152	ENSMUSG00000033152.13	Podxl2	2.146244874	0.00013175	0.00656195	58	152	185	25	34	53
ENSMUSG00000034220	ENSMUSG00000034220.7	Gpc1	2.168649202	0.00013458	0.00665735	586	785	1061	283	165	303
ENSMUSG00000025161	ENSMUSG00000025161.16	Slc16a3	2.547956589	0.00013442	0.00665735	177	309	468	63	93	69
ENSMUSG00000026459	ENSMUSG00000026459.5	Myog	6.506581723	0.00014757	0.00727487	3	11	34	0	0	1
ENSMUSG00000036879	ENSMUSG00000036879.15	Phkb	1.081442822	0.00015003	0.00737111	1241	1216	1870	599	534	890
ENSMUSG00000073375	ENSMUSG00000073375.2	Lrrc30	4.981616962	0.00015081	0.007 3844	154	235	220	0	5	26

ENSMUSG00000079110	ENSMUSG00000079110.11	Capn3	4.755639914	0.00015267	0.00745068	84	171	242	2	1	30
ENSMUSG00000075307	ENSMUSG00000075307.3	Klhl41	5.393424842	0.0001559	0.00758264	955	1894	2360	3	19	232
ENSMUSG00000025777	ENSMUSG00000025777.8	Gdap1	6.427627849	0.00016517	0.00796985	14	27	19	0	0	1
ENSMUSG00000007122	ENSMUSG00000007122.11	Casq1	5.294434339	0.00016457	0.00796985	1784	4155	2714	2	70	309
ENSMUSG00000027257	ENSMUSG00000027257.13	Pacsin3	1.637646576	0.00016606	0.00796985	479	813	1018	317	257	358
ENSMUSG00000084939	ENSMUSG00000084939.2	Gm830	5.523094515	0.00016606	0.00796985	5	30	54	0	0	6
ENSMUSG00000051373	ENSMUSG00000051373.5	Plpp7	2.518294034	0.00016821	0.00804614	101	303	303	28	43	97
ENSMUSG00000023232	ENSMUSG00000023232.17	Serinc2	2.750809927	0.00017075	0.00814073	56	147	173	12	22	59
ENSMUSG00000090066	ENSMUSG00000090066.2	1110002E22Rik	5.081799102	0.0001732	0.00823085	68	286	550	1	11	36
ENSMUSG00000000296	ENSMUSG00000000296.8	Tpd52l1	1.173361059	0.00017451	0.00826602	111	156	205	84	48	107
ENSMUSG00000080935	ENSMUSG00000080935.3	Got2-ps1	2.559790291	0.00017587	0.00830323	76	93	106	38	9	34
ENSMUSG00000020067	ENSMUSG00000020067.8	Mypn	5.172813289	0.0001772	0.00833851	455	797	1155	2	18	123
ENSMUSG00000067653	ENSMUSG00000067653.12	Ankrd23	3.373891656	0.00017944	0.00841703	11	25	35	4	1	6
ENSMUSG00000039960	ENSMUSG00000039960.5	Rhou	1.378097049	0.00018288	0.00855071	534	686	805	336	171	398
ENSMUSG00000085779	ENSMUSG00000085779.1	Atcayos	5.402326134	0.00018615	0.00867532	233	644	331	0	10	48
ENSMUSG00000039601	ENSMUSG00000039601.16	Rcan2	2.131634721	0.00019309	0.00897011	237	450	392	143	92	160
ENSMUSG00000068614	ENSMUSG00000068614.7	Actc1	4.960173384	0.00020361	0.00939828	73	347	30	34	23	26

ENSMUSG00000005628	ENSMUSG00000005628.12	Tmod4	4.68546482	0.00020347	0.00939828	495	837	918	3	13	120
ENSMUSG00000002808	ENSMUSG00000002808.7	Epdr1	2.219466225	0.000211	0.00970871	292	506	516	188	71	182
ENSMUSG00000028496	ENSMUSG00000028496.17	Mllt3	1.284604348	0.00021267	0.00975458	143	229	325	93	76	162
ENSMUSG00000069601	ENSMUSG00000069601.14	Ank3	1.58005066	0.0002154	0.00984842	268	471	424	197	158	252
ENSMUSG00000022565	ENSMUSG00000022565.15	Plec	1.033344159	0.00021778	0.00992588	2097	3545	3345	2143	1771	2133
ENSMUSG00000022215	ENSMUSG00000022215.6	Fitm1	4.944367115	0.00021894	0.00994762	174	341	381	0	10	37
ENSMUSG00000035606	ENSMUSG00000035606.8	Ky	5.139543656	0.00022108	0.00998252	50	257	333	3	0	24
ENSMUSG00000009097	ENSMUSG00000009097.9	Tbx1	4.128567821	0.00022098	0.00998252	15	14	32	1	0	3
ENSMUSG00000030592	ENSMUSG00000030592.18	Ryr1	5.824564161	0.00022638	0.0101582	3140	5635	7781	1	72	479
ENSMUSG00000087579	ENSMUSG00000087579.7	Hectd2os	2.50226262	0.00022571	0.0101582	47	55	59	13	12	17
ENSMUSG00000030785	ENSMUSG00000030785.8	Cox6a2	5.003679605	0.00022854	0.01022381	541	834	1219	7	9	144
ENSMUSG00000110613	ENSMUSG00000110613.1	Lncbate1	-0.676138147	0.00022948	0.0102342	960	953	1607	1412	1195	1677
ENSMUSG00000020908	ENSMUSG00000020908.14	Myh3	4.458658265	0.00024768	0.01101188	6	25	17	0	1	4
ENSMUSG00000040694	ENSMUSG00000040694.3	Apobec2	5.319338559	0.0002503	0.01109437	984	2837	2861	2	49	284
ENSMUSG00000096146	ENSMUSG00000096146.2	Kcnj11	2.41034779	0.00025165	0.01112	164	338	431	93	54	142
ENSMUSG00000063821	ENSMUSG00000063821.6	Dupd1	4.704303819	0.00025705	0.01132445	30	36	68	0	0	7

ENSMUSG00000032411	ENSMUSG00000032411.15	Tfdp2	0.721265516	0.00026616	0.01169001	372	431	454	302	238	355
ENSMUSG00000032114	ENSMUSG00000032114.9	Slc37a4	0.987957669	0.00026739	0.01170857	206	287	175	103	105	158
ENSMUSG00000081752	ENSMUSG00000081752.3	Sms-ps	1.179123368	0.00026867	0.017292	82	136	130	61	46	80
ENSMUSG00000021898	ENSMUSG00000021898.14	Asb14	4.990751069	0.00027581	0.01200491	79	117	188	0	2	18
ENSMUSG00000027861	ENSMUSG00000027861.13	Casq2	3.894333396	0.00027788	0.01205879	71	170	225	21	9	42
ENSMUSG00000040705	ENSMUSG00000040705.2	A930016O22Rik	4.187781059	0.00029706	0.01285248	124	198	179	0	10	28
ENSMUSG00000026202	ENSMUSG00000026202.13	Tuba4a	1.201270375	0.00030426	0.01312502	2731	5199	3578	2393	2089	2728
ENSMUSG00000025229	ENSMUSG00000025229.15	Pitx3	2.368223163	0.00031911	0.01372472	21	60	23	9	10	13
ENSMUSG00000038670	ENSMUSG00000038670.11	Mybpc2	5.267258177	0.0003223	0.01377978	4525	8207	7483	5	107	872
ENSMUSG00000034457	ENSMUSG00000034457.10	Eda2r	1.612858468	0.00032212	0.01377978	32	79	39	15	30	24
ENSMUSG00000073557	ENSMUSG00000073557.11	Ppp1r12b	1.388405468	0.00032483	0.01380689	850	1442	1396	623	501	914
ENSMUSG00000032503	ENSMUSG00000032503.18	Arpp21	4.023286954	0.00032443	0.01380689	25	37	35	0	0	11
ENSMUSG00000030739	ENSMUSG00000030739.18	Myh14	1.334698876	0.00033381	0.01414703	299	409	641	162	171	233
ENSMUSG00000037111	ENSMUSG00000037111.9	Setd7	1.0176644	0.00033814	0.01428881	872	1279	1422	661	500	922
ENSMUSG00000030727	ENSMUSG00000030727.12	Rabep2	1.023681168	0.00034454	0.01447453	262	300	276	115	161	186
ENSMUSG00000031519	ENSMUSG00000031519.3	Asb5	5.398381387	0.0003441	0.01447453	542	882	960	1	5	105
ENSMUSG00000031672	ENSMUSG00000031672.8	Got2	1.611157188	0.00035399	0.0148288	1433	1869	1915	919	615	966

ENSMUSG00000087382	ENSMUSG00000087382.7	Ctcflos	-0.97626704	0.00035772	0.0149418	1016	704	1506	1638	1315	1273
ENSMUSG00000024411	ENSMUSG00000024411.9	Aqp4	4.812016869	0.0003673	0.01529778	84	228	155	0	3	28
ENSMUSG00000033044	ENSMUSG00000033044.12	Dhrs7c	5.072825055	0.00038113	0.01582846	202	452	361	0	6	48
ENSMUSG00000013076	ENSMUSG00000013076.17	Amotl1	0.970774549	0.00038351	0.01588154	2103	2892	3712	1599	1381	1945
ENSMUSG00000002104	ENSMUSG00000002104.11	Rapsn	3.105063723	0.00039634	0.01636488	45	70	96	6	4	28
ENSMUSG00000039347	ENSMUSG00000039347.7	Atp6v0e2	1.198573603	0.00039744	0.01636488	124	193	181	92	51	111
ENSMUSG00000011148	ENSMUSG00000011148.14	Adssl1	0.982635637	0.00040045	0.01644226	2038	2573	2937	1585	1037	1462
ENSMUSG00000020598	ENSMUSG00000020598.16	Nrcam	2.765356218	0.0004058	0.01661494	21	23	22	3	4	7
ENSMUSG00000020216	ENSMUSG00000020216.13	Jsrp1	4.621498374	0.00040791	0.01665413	443	675	986	2	16	115
ENSMUSG00000042359	ENSMUSG00000042359.18	Osbpl6	1.152494773	0.00041658	0.01696058	97	214	142	92	87	113
ENSMUSG00000033751	ENSMUSG00000033751.5	Gadd45gip1	-0.684552997	0.00044897	0.01822807	882	725	1071	862	889	1507
ENSMUSG00000015850	ENSMUSG00000015850.11	Adamtsl4	1.85565809	0.00045037	0.01823364	117	230	186	80	54	100
ENSMUSG00000030887	ENSMUSG00000030887.4	Pdzd9	-2.362404955	0.00046217	0.01864632	8	7	8	26	19	24
ENSMUSG00000116056	ENSMUSG00000116056.1	Gm4544	3.677640219	0.00046314	0.01864632	12	45	35	1	1	12
ENSMUSG00000045620	ENSMUSG00000045620.7	Odf3l1	-1.698470377	0.00047386	0.01902535	22	3	26	21	19	19

ENSMUSG00000003528	ENSMUSG00000003528.14	Slc25a1	-0.985399026	0.00048968	0.01960615	4809	3778	9272	5703	5924	10488
ENSMUSG00000027077	ENSMUSG00000027077.7	Smtnl1	5.555659241	0.00049393	0.01972173	325	750	977	0	12	84
ENSMUSG00000037656	ENSMUSG00000037656.9	Slc20a2	1.062171786	0.00049634	0.01976358	796	828	1515	419	421	610
ENSMUSG00000044499	ENSMUSG00000044499.11	Hs3st5	3.8142973	0.00049817	0.01978195	12	25	23	0	1	5
ENSMUSG00000042254	ENSMUSG00000042254.14	Cilp	2.759350483	0.00050313	0.01992429	42	137	48	41	7	18
ENSMUSG00000096944	ENSMUSG00000096944.1	NA	3.255607958	0.00050798	0.02006176	5	27	24	2	1	5
ENSMUSG00000087543	ENSMUSG00000087543.1	Gm16576	1.594042844	0.00051521	0.02029195	24	44	62	18	12	24
ENSMUSG00000020836	ENSMUSG00000020836.15	Coro6	2.142860894	0.00052774	0.02072913	235	326	523	101	84	212
ENSMUSG00000038502	ENSMUSG00000038502.16	Ptov1	-0.909161577	0.00053084	0.02079465	1271	1461	2190	3186	1504	3664
ENSMUSG00000072591	ENSMUSG00000072591.10	Fzd10os	3.786860785	0.00053572	0.02087285	11	18	25	4	2	0
ENSMUSG00000034898	ENSMUSG00000034898.16	Filip1	1.08228777	0.00053523	0.02087285	250	430	401	167	170	302
ENSMUSG00000087478	ENSMUSG00000087478.1	4930506C21Rik	-1.786182178	0.00005412	0.02102981	30	12	23	41	27	36
ENSMUSG00000006457	ENSMUSG00000006457.3	Actn3	5.320169174	0.00005454	0.02113644	8313	16685	18658	6	216	1673
ENSMUSG00000097705	ENSMUSG00000097705.1	Gm26740	5.251657122	0.00054729	0.02115298	4	10	11	0	1	0
ENSMUSG00000070385	ENSMUSG00000070385.12	Ampd1	5.304237404	0.00054995	0.021994	578	1429	1266	0	37	123

ENSMUSG00000039395	ENSMUSG00000039395.8	Mreg	1.24427495	0.00055887	0.02148616	262	790	253	321	134	395
ENSMUSG00000041616	ENSMUSG00000041616.9	Nppa	-16.43183362	0.00056938	0.02183207	0	0	0	29	0	0
ENSMUSG00000057606	ENSMUSG00000057606.14	Colq	4.704879584	0.000576	0.02202779	8	16	17	0	2	2
ENSMUSG00000032267	ENSMUSG00000032267.8	Usp28	1.378660348	0.0005815	0.02217943	150	193	292	115	74	140
ENSMUSG00000038086	ENSMUSG00000038086.4	Hspb2	2.296342836	0.00059607	0.02261628	41	120	145	24	22	42
ENSMUSG00000022512	ENSMUSG00000022512.2	Cldn1	-1.003149047	0.00059452	0.02261628	1555	1008	1278	1937	1586	3171
ENSMUSG00000021094	ENSMUSG00000021094.10	Dhrs7	-0.856762568	0.00059778	0.02262184	1478	1337	2988	1918	1885	3471
ENSMUSG00000045761	ENSMUSG00000045761.15	Togaram2	3.596040233	0.00060599	0.02287309	38	43	32	0	1	13
ENSMUSG00000026173	ENSMUSG00000026173.15	Plcd4	5.062782614	0.00061615	0.02319584	25	80	97	0	0	10
ENSMUSG00000026409	ENSMUSG00000026409.14	Pfkfb2	1.130773038	0.00063228	0.02374164	74	93	96	37	44	60
ENSMUSG00000006526	ENSMUSG00000006526.13	Stimate	-0.525196989	0.00064468	0.02414448	1069	1019	1692	1335	1205	1646
ENSMUSG00000070576	ENSMUSG00000070576.4	Mn1	1.117669283	0.00065646	0.02452252	250	519	493	267	187	260
ENSMUSG00000027004	ENSMUSG00000027004.3	Frzb	2.758452672	0.00066627	0.02482514	11	23	13	3	0	11
ENSMUSG00000031737	ENSMUSG00000031737.11	Irx5	1.897306433	0.00067381	0.02497753	39	110	107	32	25	49
ENSMUSG00000007033	ENSMUSG00000007033.4	Hspa1l	2.928687323	0.00067262	0.02497753	62	144	218	50	16	17

ENSMUSG00000028542	ENSMUSG00000028542.17	Slc6a9	1.299685883	0.00068134	0.02514844	27	73	36	18	26	33
ENSMUSG00000043126	ENSMUSG00000043126.5	D830039M14Rik	5.250660642	0.00068189	0.02514844	3	26	34	0	2	0
ENSMUSG00000031885	ENSMUSG00000031885.14	Cbfb	0.636388178	0.00068678	0.02523913	644	1031	898	555	514	783
ENSMUSG00000020715	ENSMUSG00000020715.9	Ern1	0.621082468	0.00068783	0.02523913	275	412	392	272	226	307
ENSMUSG00000041476	ENSMUSG00000041476.12	Smpx	5.466976096	0.00069725	0.025 5202	256	438	514	0	3	53
ENSMUSG00000006057	ENSMUSG00000006057.15	Atp5g1	1.701562421	0.00070347	0.02568291	412	622	474	234	217	256
ENSMUSG00000051985	ENSMUSG00000051985.12	Igfn1	5.652905279	0.00070882	0.02581332	7	16	3	0	0	1
ENSMUSG00000090942	ENSMUSG00000090942.1	F830016B08Rik	3.18888332	0.00072096	0.02618946	8	42	87	3	8	8
ENSMUSG00000079434	ENSMUSG00000079434.8	Neu2	3.630891351	0.00074458	0.02697984	22	90	53	0	2	21
ENSMUSG00000073535	ENSMUSG00000073535.5	Gm5532	4.006718999	0.00076158	0.02715655	32	42	64	4	7	10
ENSMUSG00000026630	ENSMUSG00000026630.9	Batf3	-1.969114375	0.00075305	0.02715655	10	18	5	60	39	62
ENSMUSG00000103114	ENSMUSG00000103114.1	Gm32200	-3.370463426	0.0007618	0.02715655	91	1	49	90	51	7
ENSMUSG00000029438	ENSMUSG00000029438.9	Bcl7a	0.621252822	0.00076042	0.02715655	142	213	202	125	101	168
ENSMUSG00000030996	ENSMUSG00000030996.8	Art1	5.284964233	0.00076257	0.02715655	369	610	641	0	7	72
ENSMUSG00000002032	ENSMUSG00000002032.17	Tmem25	2.138140889	0.00075835	0.02715655	10	14	18	2	3	5
ENSMUSG00000044938	ENSMUSG00000044938.8	Klhl31	4.603847098	0.00075667	0.02715655	324	488	586	1	9	101

ENSMUSG00000034472	ENSMUSG00000034472.13	Rasd2	1.839873947	0.00077945	0.02768965	44	132	112	24	38	82
ENSMUSG00000026211	ENSMUSG00000026211.17	Obsl1	1.269995226	0.00078435	0.02779536	158	321	241	154	146	156
ENSMUSG00000032418	ENSMUSG00000032418.15	Me1	-1.213122347	0.00079791	0.02820716	7238	8571	10764	13717	11523	24148
ENSMUSG00000034460	ENSMUSG00000034460.9	Six4	2.662181893	0.00080769	0.02848325	33	60	109	9	20	18
ENSMUSG00000055214	ENSMUSG00000055214.15	Pld5	5.604964382	0.00081408	0.02863894	1	30	14	0	0	2
ENSMUSG00000087523	ENSMUSG00000087523.1	Gm12319	3.547261228	0.00081 73	0.02868258	14	39	38	1	0	13
ENSMUSG00000020061	ENSMUSG00000020061.17	Mybpc1	6.041575293	0.00082041	0.02872239	3390	6059	6008	0	53	435
ENSMUSG00000021506	ENSMUSG00000021506.7	Pitx1	4.097719284	0.00083667	0.029 1506	10	26	34	0	0	5
ENSMUSG00000060459	ENSMUSG00000060459.13	Kng2	-0.80212852	0.00083475	0.029 1506	1401	968	2206	1792	1213	2018
ENSMUSG00000034780	ENSMUSG00000034780.6	B3galt1	2.423637558	0.00084876	0.02950102	40	47	38	13	7	22
ENSMUSG00000037490	ENSMUSG00000037490.5	Slc2a12	1.328312633	0.00085881	0.02977883	42	63	80	20	14	44
ENSMUSG00000074121	ENSMUSG00000074121.3	Ntf5	4.182904602	0.00087662	0.030 3238	9	20	24	1	1	2
ENSMUSG00000034648	ENSMUSG00000034648.9	Lrrn1	2.69776486	0.00088211	0.03044119	22	18	19	2	7	3
ENSMUSG00000021768	ENSMUSG00000021768.15	Dusp13	4.56570657	0.00009038	0.03111561	93	204	286	0	5	34
ENSMUSG00000028861	ENSMUSG00000028861.13	Mrps15	-0.596058069	0.00092561	0.03179083	772	661	929	823	900	1209

ENSMUSG00000048807	ENSMUSG00000048807.2	Slc35e4	0.912379507	0.00092929	0.03184183	203	405	349	153	208	273
ENSMUSG00000041688	ENSMUSG00000041688.16	Amot	1.809216892	0.00093176	0.03185113	180	381	411	154	111	171
ENSMUSG00000039103	ENSMUSG00000039103.12	Nexn	2.971451057	0.00094434	0.03220531	1046	1152	1156	130	205	387
ENSMUSG00000023927	ENSMUSG00000023927.15	Satb1	1.427434386	0.00095783	0.03258853	103	183	200	73	71	74
ENSMUSG00000027605	ENSMUSG00000027605.18	Acss2	-1.105513386	0.00097615	0.03313434	1098	1240	2293	2070	1672	3008
ENSMUSG00000019787	ENSMUSG00000019787.9	Trdn	5.020183479	0.00099791	0.03379359	1213	2071	2146	1	27	272
ENSMUSG00000026500	ENSMUSG00000026500.6	Cox20	-0.649426137	0.00102122	0.03450246	565	455	725	674	575	790
ENSMUSG00000041920	ENSMUSG00000041920.14	Slc16a6	2.030244835	0.00104595	0.03525584	32	44	45	14	14	15
ENSMUSG00000012350	ENSMUSG00000012350.15	Ehf	2.521648087	0.00105602	0.03551251	1	123	1	9	17	37
ENSMUSG00000035923	ENSMUSG00000035923.4	Myf6	4.617361712	0.00105912	0.03553428	44	60	206	0	2	16
ENSMUSG00000023805	ENSMUSG00000023805.16	Synj2	0.992537557	0.00107643	0.03603195	314	556	332	274	178	281
ENSMUSG00000020173	ENSMUSG00000020173.17	Cobl	2.500830607	0.00109342	0.03651632	54	95	67	10	8	46
ENSMUSG00000030399	ENSMUSG00000030399.2	Ckm	5.06387753	0.00110845	0.03684818	21797	37798	39359	12	658	4278
ENSMUSG00000059734	ENSMUSG00000059734.6	Ndufs8	-0.578095816	0.001106	0.03684818	4004	4787	5710	5993	5628	7002
ENSMUSG00000048277	ENSMUSG00000048277.15	Syngr2	0.718785384	0.00114432	0.03795354	563	846	895	483	472	632

ENSMUSG00000044433	ENSMUSG00000044433.16	Camsap3	-0.944731735	0.00114759	0.03797526	107	78	147	168	166	181
ENSMUSG00000031239	ENSMUSG00000031239.5	Itm2a	1.423673185	0.00116203	0.03836537	285	566	245	258	177	164
ENSMUSG00000048096	ENSMUSG00000048096.7	Lmod1	1.45174582	0.00121222	0.03984105	469	938	896	343	282	625
ENSMUSG00000056116	ENSMUSG00000056116.18	H2-T22	-0.699405148	0.00121066	0.03984105	941	1215	1375	1971	1360	2082
ENSMUSG00000061360	ENSMUSG00000061360.8	Phf5a	-0.521933027	0.00123619	0.0404456	1757	2029	2646	2569	2044	3806
ENSMUSG00000023809	ENSMUSG00000023809.9	Rps6ka2	1.181336823	0.00123486	0.0404456	211	434	473	190	171	241
ENSMUSG00000000708	ENSMUSG00000000708.14	Kat2b	0.617794523	0.00123982	0.04047287	831	887	1229	673	448	739
ENSMUSG00000029095	ENSMUSG00000029095.17	Ablim2	1.458691541	0.00128169	0.04146613	59	106	162	31	41	52
ENSMUSG00000002910	ENSMUSG00000002910.11	Arrdc2	1.44368776	0.00127678	0.04146613	240	202	127	60	88	95
ENSMUSG00000037940	ENSMUSG00000037940.17	Inpp4b	1.558146142	0.00127506	0.04146613	65	170	171	49	45	106
ENSMUSG00000000901	ENSMUSG00000000901.16	Mmp11	-0.786857689	0.00127938	0.04146613	85	97	137	173	114	219
ENSMUSG00000021520	ENSMUSG00000021520.4	Uqcrb	-0.436571113	0.00129046	0.04165682	8498	8198	9883	10056	8006	12380
ENSMUSG00000078716	ENSMUSG00000078716.9	Tmem8b	1.082927368	0.00129612	0.04174656	86	169	239	74	78	102
ENSMUSG00000039474	ENSMUSG00000039474.13	Wfs1	1.13787334	0.0013181	0.04224706	322	303	521	144	146	250

ENSMUSG00000007030	ENSMUSG00000007030.8	Vwa7	3.242895174	0.0013204	0.04224706	7	18	28	2	5	1
ENSMUSG00000024236	ENSMUSG00000024236.18	Svil	1.454575073	0.00131727	0.04224706	800	1378	1251	573	508	771
ENSMUSG00000038422	ENSMUSG00000038422.2	Hdhd3	-0.797011938	0.00133289	0.04250462	322	225	427	350	315	452
ENSMUSG00000037443	ENSMUSG00000037443.13	Cep85	0.889869923	0.00133725	0.04250462	203	290	364	171	159	213
ENSMUSG00000097404	ENSMUSG00000097404.1	Gm10814	4.428323063	0.00133657	0.04250462	4	11	7	1	0	0
ENSMUSG00000044177	ENSMUSG00000044177.4	Wfikkn2	2.117426986	0.00135941	0.04311448	35	63	38	11	14	28
ENSMUSG00000028949	ENSMUSG00000028949.13	Smarcd3	1.01666097	0.00140772	0.04454902	409	572	786	291	247	348
ENSMUSG00000004798	ENSMUSG00000004798.14	Ulk2	0.598276072	0.00141871	0.04479892	863	1042	1265	702	520	940
ENSMUSG00000021748	ENSMUSG00000021748.9	Pdhb	-0.603407946	0.00142529	0.04490912	10471	9812	14254	14328	9755	17157
ENSMUSG00000045064	ENSMUSG00000045064.4	Zc2hc1c	2.523438892	0.00144021	0.04528073	22	24	23	5	1	9
ENSMUSG00000034161	ENSMUSG00000034161.8	Scx	4.048621379	0.00145441	0.04562807	15	22	44	1	0	9
ENSMUSG00000063564	ENSMUSG00000063564.13	Col23a1	1.149417134	0.00148265	0.04640036	45	66	82	18	23	46
ENSMUSG00000021069	ENSMUSG00000021069.17	Pygl	-0.97394291	0.00148543	0.04640036	3240	1760	5461	3420	3324	6608
ENSMUSG00000084929	ENSMUSG00000084929.1	Foxo6os	3.974077215	0.00149678	0.04645478	8	69	40	0	0	12
ENSMUSG00000073409	ENSMUSG00000073409.12	H2-Q6	-1.727496924	0.00149391	0.04645478	327	216	141	639	670	508

ENSMUSG00000095597	ENSMUSG00000095597.2	Rps7-ps3	-0.615270984	0.0014963	0.04645478	2737	3498	3855	4265	3816	5160
ENSMUSG00000022450	ENSMUSG00000022450.6	Ndufa6	-0.581432919	0.00151562	0.04693897	5917	6837	8451	8284	8403	9972
ENSMUSG00000041220	ENSMUSG00000041220.10	Elovl6	-0.960639196	0.00152732	0.04715677	12868	12070	22448	18872	16287	26057
ENSMUSG00000056228	ENSMUSG00000056228.10	Cars2	-0.954131879	0.00152916	0.04715677	11234	12692	8793	18029	19604	23424
ENSMUSG00000025141	ENSMUSG00000025141.2	Myadml2	5.492895303	0.00156073	0.04802819	60	149	201	0	0	20
ENSMUSG00000036833	ENSMUSG00000036833.16	Pnpla7	0.790577419	0.00156695	0.04811625	250	271	368	212	137	201
ENSMUSG00000019088	ENSMUSG00000019088.13	Dnase1l1	0.998784508	0.00157024	0.04811625	227	314	298	112	164	182
ENSMUSG00000021838	ENSMUSG00000021838.17	Samd4	1.519070105	0.00161879	0.04949952	214	384	282	166	150	152

Appendix C: RNA-Seq normalized counts for 4-day cold exposure (*Prkd1*^{BKO} cold v. *Prkd1*$^{fl/fl}$ cold) (significantly changed genes only: p_{adj}<0.05)

KO_cold__vs__WT_cold-DESeq2-results-all-data													
ensemblid	gene_ symbol	Log 2-Fold Change	p-value	padj	KO_cold / 8047-MC-0013	KO_cold / 8047-MC-0014	KO_cold / 8047-MC-0015	KO_cold / 8047-MC-0016	WT_cold / 8047-MC-0009	WT_cold / 8047-MC-0010	WT_cold / 8047-MC-0011	WT_cold / 8047-MC-0012
ENSMUSG00000035151.12	Elmod2	1.084466554	4.1776E-15	7.8518E-11	1032.561118	887.4283882	967.89298	847.8859741	378.1722193	359.082145	509.548088	519.073194
ENSMUSG00000028328.13	Tmod1	-3.118659213	4.50294E-13	4.23164E-09	135.1791998	61.20195781	67.873379	40.49861868	1296.469335	606.182487	465.147632	273.131371
ENSMUSG00000025216.9	Lbx1	-3.604289509	7.43474E-12	4.65786E-08	4.159359994	5.276030846	4.648861576	1.723345476	83.09613788	42.5715945	42.2861483	19.7742169
ENSMUSG00000017817.11	Jph2	-2.449085284	1.43723E-11	6.75321E-08	453.3702393	124.514328	235.2323957	261.0868396	2211.374771	1438.17952	1434.55758	779.845679
ENSMUSG00000034768.4	Asb16	-3.241235226	3.04404E-11	9.91868E-08	23.91631996	9.496855522	5.578633891	9.478400117	232.3300182	84.2177196	97.2581412	39.5484338
ENSMUSG00000037989.15	Wnk2	-2.959853652	3.16638E-11	9.91868E-08	49.91231993	9.496855522	37.1908926	25.85018214	488.40179	189.721236	182.887592	90.2198646
ENSMUSG00000032648.14	Pygm	-3.469627452	1.07894E-10	2.89694E-07	986.8081585	215.2620585	254.7576143	260.2251669	8426.626717	4446.88069	4134.52815	2008.3189
ENSMUSG00000001604.14	Tcea3	-2.746272802	6.25381E-10	1.46925E-06	42.63343994	14.77288637	17.66567399	17.23345476	344.2554284	92.5469446	113.115447	65.5020935
ENSMUSG00000072720.9	Myo18b	-4.981641971	1.10879E-09	2.08397E-06	101.9043198	8.441649353	11.15726778	7.755054641	2288.535471	684.84739	807.665433	292.905588

ENSMUSG00000030433.15	Sbk2	-1.980970006	1.01633E-09	2.08397E-06	303.6332795	276.4640163	148.7635704	205.0781116	1697.535388	726.493515	783.350898	474.581206
ENSMUSG00000038663.7	Fsd2	-2.011119102	1.43193E-09	2.44665E-06	167.4142398	83.36128736	107.8535886	67.21047356	749.5610805	304.479448	291.774424	367.058901
ENSMUSG00000090799.2	Klhl33	-2.141217614	2.15071E-09	3.36854E-06	258.9201596	104.4654107	166.4292444	124.0808743	1042.941322	708.909595	765.379285	364.587124
ENSMUSG00000032523.11	Hhatl	-4.786579648	2.51502E-09	3.37641E-06	4.159359994	0	0	0.861672738	59.3543842	29.6150223	30.6574576	13.5947741
ENSMUSG00000079055.10	Slc8a3	-3.467783423	2.50802E-09	3.37641E-06	20.79679997	6.331237015	10.22749547	3.446690952	237.4175368	91.6214751	85.6294504	32.1331025
ENSMUSG00000002688.8	Prkd1	-1.398953941	3.07739E-09	3.85598E-06	248.5217596	208.9308215	245.4598912	250.7467667	516.3831425	636.722979	655.435299	708.164143
ENSMUSG00000021061.15	Sptb	-3.684897874	4.42976E-09	5.20358E-06	169.4939197	14.77288637	55.78633891	43.94530963	1757.737692	662.636123	831.979969	396.720227
ENSMUSG00000038201.10	Kcna7	-3.105187349	7.31041E-09	8.08231E-06	17.67727997	6.331237015	17.66567399	3.446690952	218.7633018	64.7828612	70.8292985	30.8972139
ENSMUSG00000068699.12	Flnc	-4.01766588	9.00127E-09	9.39883E-06	256.8404796	68.58840099	157.1315213	117.1874924	5580.160035	2079.52984	1549.78734	503.006642
ENSMUSG00000039376.13	Synpo2l	-4.235598738	1.03353E-08	1.02238E-05	69.6692799	6.331237015	14.87635704	9.478400117	1091.27275	300.77757	338.289187	154.48607
ENSMUSG00000031962.6	Cdh15	-6.789539423	1.3318E-08	1.25156E-05	1.039839998	0	0	0	72.92110059	28.6895528	21.1430742	6.17944278

ENSMUSG00000024210.2	Ip6k3	-4.574327249	1.40216E-08	1.25494E-05	6.239039991	0	5.578633891	6.893381903	262.0072103	98.0997612	66.6006836	22.245994
ENSMUSG00000028017.7	Egf	-2.034942404	1.9039E-08	1.62654E-05	44.71311993	15.82809254	30.6824864	29.29687309	229.7862588	103.652578	101.486756	56.8508736
ENSMUSG00000029158.9	Yipf7	-6.105838918	2.39528E-08	0.00001875 8	1.039839998	0	1.85954463	0	133.9713243	20.3603278	37.0003798	7.41533134
ENSMUSG00000033182.12	Kbtbd12	-2.58094808	2.389E-08	0.00001875 8	43.67327993	21.10412338	26.03362482	32.74356404	382.4118182	156.404336	148.001519	50.6714308
ENSMUSG00000045761.15	Togaram2	-4.70181935	2.54954E-08	1.91674E-05	6.239039991	0	0.929772315	0	115.3170893	24.0622056	26.4288427	13.5947741
ENSMUSG00000006221.7	Hspb7	-5.310091394	2.77056E-08	1.95607E-05	76.94815989	15.82809254	10.22749547	18.0951275	3663.013425	498.828031	478.89063	156.957847
ENSMUSG00000049641.14	Vgll2	-5.504389247	2.91406E-08	1.95607E-05	10.39839998	0	1.85954463	0	366.3013425	62.9319223	69.7721448	48.1996537
ENSMUSG00000033196.17	Myh2	-6.116820916	2.81243E-08	1.95607E-05	726.8481589	18.99371104	39.98020955	8.616727379	40122.7158	6991.92166	5961.28976	2041.68789
ENSMUSG00000042529.14	Kcnj12	-2.80530491	4.40958E-08	0.00002762 6	18.71711997	8.441649353	13.94658473	5.170036428	158.5609978	60.155514	63.4292225	38.3125452
ENSMUSG00000020882.17	Cacnb1	-1.412436739	4.3238E-08	0.00002762 6	169.4939197	138.2320082	204.5499093	169.7495294	685.9670974	379.442473	394.318333	354.700016
ENSMUSG00000038170.15	Pde4dip	-2.02191672	5.45046E-08	3.30456E-05	3009.296956	1765.359921	2183.105396	2046.472753	17840.23205	6442.19281	7719.33638	4564.13644

ENSMUSG00000038763.12	Alpk3	-3.580044662	5.8746E-08	3.45041E-05	99.82463985	37.98742209	61.3649728	66.34880082	1983.284352	448.852681	558.177158	184.147395
ENSMUSG00000021451.16	Sema4d	-1.81241386	6.99569E-08	3.98436E-05	63.43023991	33.76659741	27.89316945	33.60523678	167.8881153	193.423114	118.401215	74.1533134
ENSMUSG00000026308.8	Klhl30	-3.765046415	7.9958E-08	4.36856E-05	23.91631996	3.165618507	5.578633891	3.446690952	271.3343278	90.6960057	83.515143	40.7843224
ENSMUSG00000050211.14	Pla2g4e	-4.758303238	8.13513E-08	4.36856E-05	7.278879989	0	0	1.723345476	142.4505221	47.1989417	37.0003798	12.3588856
ENSMUSG00000104453.1	Gm37829	-1.797538815	8.4285E-08	4.40038E-05	43.67327993	15.82809254	26.03362482	25.85018214	163.6485164	62.0064529	69.7721448	90.2198646
ENSMUSG00000085272.7	Sbk3	-2.239082324	9.57531E-08	4.63126E-05	20.79679997	8.441649353	18.5954463	13.78676381	117.0129289	94.3978835	43.3433021	34.6048796
ENSMUSG00000000031.16	H19	-4.231030269	9.41253E-08	4.63126E-05	496.0036793	132.9559773	72.52224058	38.77527321	8897.222192	2314.59908	1759.10377	923.208752
ENSMUSG00000047591.5	Mafa	-2.634603333	9.60996E-08	4.63126E-05	46.79279993	10.55206169	13.94658473	4.30836369	155.1693187	170.286378	99.3724486	39.5484338
ENSMUSG00000060913.6	Trim55	-5.035592771	1.29314E-07	5.92794E-05	12.47807998	0	0.929772315	0	250.9842532	72.1866168	77.1722207	30.8972139
ENSMUSG00000052374.15	Actn2	-4.359045024	1.26709E-07	5.92794E-05	348.3463995	137.176802	68.80315132	106.8474195	9121.073012	1872.22469	1998.02051	572.216402
ENSMUSG00000026778.13	Prkcq	-2.729177619	1.47779E-07	0.00006206 8	27.03583996	17.93850488	20.45499093	12.92509107	319.6657549	78.6649029	82.4579893	35.8407681

ENSMUSG00000016349.10	Eef1a2	-4.732204405	1.50211E-07	0.00006206 8	307.7926395	32.71139124	13.94658473	7.755054641	4960.33068	2077.67891	1770.73246	809.507004
ENSMUSG00000020067.8	Mypn	-4.391609502	1.51761E-07	0.00006206 8	111.2628798	7.386443184	18.5954463	3.446690952	1571.195342	620.064529	504.262319	250.885377
ENSMUSG00000051980.13	Casr	-5.06486709	1.42078E-07	0.00006206 8	1.039839998	0	0	1.723345476	39.00430962	20.3603278	28.5431501	7.41533134
ENSMUSG00000041731.13	Pgm5	-1.379036135	1.54855E-07	0.00006206 8	32.23503995	14.77288637	27.89316945	28.43520035	76.31277969	62.9319223	72.9436059	56.8508736
ENSMUSG00000031137.17	Fgf13	-2.179081995	1.55211E-07	0.00006206 8	10.39839998	4.220824677	9.297723151	13.78676381	62.7460633	44.4225334	27.4859964	37.0766567
ENSMUSG00000035606.8	Ky	-4.285257274	1.78701E-07	6.88459E-05	44.71311993	1.055206169	1.85954463	3.446690952	346.7991877	243.398464	269.574196	129.768298
ENSMUSG00000021798.14	Ldb3	-4.091459953	1.79487E-07	6.88459E-05	315.0715195	37.98742209	55.78633891	51.70036428	4909.455493	1258.63845	1244.26992	433.796883
ENSMUSG00000057003.12	Myh4	-4.33254769	1.92545E-07	7.23776E-05	9392.874706	178.3298426	716.8544549	59.45541892	87888.58044	55586.4713	42388.6923	22608.1094
ENSMUSG00000028197.4	Col24a1	-3.592475129	2.12929E-07	7.84707E-05	5.199199992	0	1.85954463	1.723345476	50.87518646	27.7640834	19.0287668	6.17944278
ENSMUSG00000071540.4	3425401B19Rik	-4.773884787	2.34288E-07	8.46817E-05	128.9401598	2.110412338	17.66567399	8.616727379	2357.216973	776.468865	826.6942	337.397576
ENSMUSG00000060600.15	Eno3	-2.711452114	2.71306E-07	9.62114E-05	971.2105586	303.8993767	352.3837074	377.4126592	6935.983754	2763.45176	2252.79455	1176.56591

ENSMUSG00000060548.13	Tnfrsf19	-3.81857407	2.89529E-07	0.0001007772	7.278879989	0	0	0.861672738	50.02726668	21.2857973	25.371689	13.5947741
ENSMUSG00000031791.8	Tmem38a	-2.775027621	3.22798E-07	0.0001103039	247.4819196	108.6862354	105.9940439	139.5909835	2373.327448	708.909595	664.949683	369.530678
ENSMUSG00000042828.12	Trim72	-4.06283863	3.57554E-07	0.0001200004	89.42623987	6.331237015	13.01681241	19.81847297	1287.990137	383.144351	346.746416	127.296521
ENSMUSG00000040653.6	Ppp1r14c	-2.625962815	4.04719E-07	0.0001290001	20.79679997	3.165618507	6.508406206	7.755054641	85.6398972	42.5715945	67.6578374	38.3125452
ENSMUSG00000010461.15	Eya4	-3.535282752	4.0495E-07	0.0001290001	9.358559986	2.110412338	1.85954463	1.723345476	95.81493449	47.1989417	21.1430742	6.17944278
ENSMUSG00000081194.1	Gm8424	-6.146683575	4.036E-07	0.0001290001	1.039839998	0	0	0	46.63558759	19.4348584	13.7429982	2.47177711
ENSMUSG00000028464.16	Tpm2	-3.368356842	4.40886E-07	0.0001295997	2148.309437	414.6960245	670.3658392	666.9346992	21816.97579	7117.78551	7715.10777	3626.09702
ENSMUSG00000030319.8	Cand2	-2.100967569	4.28072E-07	0.0001295997	53.03183992	50.64989612	54.85656659	49.9770188	401.0660532	248.951281	165.973132	76.6250905
ENSMUSG00000030852.17	Tacc2	-1.222773345	4.40566E-07	0.0001295997	1250.927518	989.7833866	1280.296478	1453.641909	4415.118265	2423.80448	2799.34302	1971.24225
ENSMUSG00000021200.14	Asb2	-3.157095372	4.413E-07	0.0001295997	62.39039991	9.496855522	32.54203103	25.85018214	736.8422839	165.659031	155.401595	102.57875
ENSMUSG00000064372.1	mt-Tp	1.260718084	4.20228E-07	0.0001295997	1160.461438	1675.667397	1519.247963	2444.565557	643.5711087	661.710654	857.351658	676.03104

ENSMUSG00000009210.10	Prr29	-3.089082681	4.6922E-07	0.00013567 7	9.358559986	5.276030846	0.929772315	0	52.57102601	35.1678389	19.0287668	19.7742169
ENSMUSG00000046818.7	Ddit4l	-3.443880173	4.97553E-07	0.00013957 5	28.07567996	9.496855522	5.578633891	3.446690952	227.2424995	144.373234	104.658217	25.9536597
ENSMUSG00000038204.13	Asb10	-2.734689736	4.97114E-07	0.00013957 5	14.55775998	10.55206169	11.15726778	2.585018214	155.1693187	37.0187778	31.7146113	30.8972139
ENSMUSG00000028584.3	Lrrc38	-4.97220287	5.19927E-07	0.00014370 6	8.318719988	0	0	0	150.0818	50.9008195	35.9432261	16.0665512
ENSMUSG00000029386.15	NA	-0.841109749	5.32641E-07	0.00014508 7	103.9839998	94.96855522	100.41541	87.02894653	150.0818	177.690134	179.7163	185.383283
ENSMUSG00000008658.16	Rbfox1	-3.438818065	5.6008E-07	0.00015038 2	31.19519995	7.386443184	5.578633891	1.723345476	260.3113707	95.3233529	90.9152189	45.7278766
ENSMUSG00000032503.18	Arpp21	-4.856843861	5.87713E-07	0.00015557 8	4.159359994	0	2.789316945	0	109.3816509	50.9008195	31.7146113	6.17944278
ENSMUSG00000027077.7	Smtnl1	-5.003010635	6.61612E-07	0.00017270 8	64.4700799	9.496855522	0.929772315	2.585018214	1728.90842	267.46067	372.118105	107.522304
ENSMUSG00000001333.9	Sync	-2.372770186	6.75897E-07	0.00017367	25.99599996	11.60726786	17.66567399	24.9885094	234.8737775	72.1866168	71.8864522	35.8407681
ENSMUSG00000055027.17	Smyd1	-3.344123767	6.83776E-07	0.00017367	70.70911989	48.53948378	32.54203103	12.06341833	1021.743328	273.938956	252.659736	111.22997
ENSMUSG00000001027.7	Scn4a	-4.276909695	6.93672E-07	0.00017383 4	142.4580798	2.110412338	27.89316945	6.893381903	1683.968672	716.313351	716.750215	354.700016

ENSMUSG00000024059.10	Clip4	-4.271972779	7.11297E-07	0.00017590 6	30.15535996	0	10.22749547	5.170036428	519.7748216	133.2676	173.373208	50.6714308
ENSMUSG00000019194.15	Scn1b	-1.177386793	8.70352E-07	0.00021244 5	868.2663987	720.7058135	602.4924602	928.8832115	2730.301673	1763.01929	1305.58483	1255.66277
ENSMUSG00000032643.12	Fhl3	-1.605609352	8.91733E-07	0.00021487 3	316.1113595	180.4402549	173.8674229	210.2481481	1046.333001	723.717107	622.663534	284.254368
ENSMUSG00000034040.16	Galnt17	-1.419001597	1.05653E-06	0.00025136	22.87647997	9.496855522	36.26112029	24.12683666	78.00861923	70.3356779	59.2006077	40.7843224
ENSMUSG00000062077.14	Trim54	-4.752662473	1.10655E-06	0.00025996 9	58.23103991	12.66247403	3.71908926	0	1238.81079	285.970059	311.860344	166.844955
ENSMUSG00000031972.5	Acta1	-4.686210288	1.37934E-06	0.00031648 8	2532.010396	235.3109757	205.4796816	61.17876439	43277.82528	15094.4067	13762.027	5968.10584
ENSMUSG00000046997.5	Spsb4	-6.48315151	1.38201E-06	0.00031648 8	0	0	0	0	22.89383391	14.8075111	23.2573816	2.47177711
ENSMUSG00000020216.13	Jsrp1	-4.084445423	1.39763E-06	0.00031648 8	53.03183992	10.55206169	5.578633891	2.585018214	785.173711	180.466542	170.201747	75.3892019
ENSMUSG00000022525.13	Plaat1	-4.28873352	1.44271E-06	0.00032280 6	5.199199992	0	0	0	61.89814352	13.8820417	14.8001519	4.94355422
ENSMUSG00000041779.5	Tram2	-0.852293736	1.47285E-06	0.00032567 3	120.6214398	75.97484418	127.3788072	104.2624013	191.629869	216.55985	205.087819	159.429624
ENSMUSG00000041889.7	Shisa4	-2.235975747	1.60637E-06	0.00034390 1	45.75295993	15.82809254	26.03362482	24.12683666	242.5050554	132.342131	102.54391	46.9637651

ENSMUSG00000048416.15	Mlf1	-3.178111618	1.61018E-06	0.00034390 1	33.27487995	5.276030846	2.789316945	7.755054641	220.4591413	98.0997612	81.4008356	40.7843224
ENSMUSG00000062694.7	Cav3	-4.214686509	1.58597E-06	0.00034390 1	7.278879989	0	0.929772315	0	84.79197743	26.8386139	23.2573816	12.3588856
ENSMUSG00000028927.6	Padi2	-3.593054728	1.63778E-06	0.00034586 5	159.0955198	22.15932955	23.24430788	25.85018214	1479.620006	478.467703	587.777462	229.875271
ENSMUSG00000075307.3	Klhl41	-4.424726933	1.78407E-06	0.00037257 3	115.4222398	6.331237015	8.367950836	12.06341833	2054.509613	371.113248	424.975791	197.742169
ENSMUSG00000064179.13	Tnnt1	-4.627391291	1.89372E-06	0.00039112 5	61.35055991	11.60726786	17.66567399	4.30836369	1561.020304	322.063367	337.232033	121.117079
ENSMUSG00000024617.16	Camk2a	-2.828292434	1.9295E-06	0.00039418 4	96.70511986	17.93850488	26.03362482	17.23345476	508.7518646	256.355036	214.602203	138.419518
ENSMUSG00000052135.8	Foxo6	-2.112021645	2.13916E-06	0.00043231 8	22.87647997	6.331237015	42.76952649	23.26516392	144.9942814	108.279925	63.4292225	96.3993074
ENSMUSG00000006457.3	Actn3	-4.053596859	2.23993E-06	0.00044786 6	1047.118878	79.14046268	62.29474511	17.23345476	8272.305318	4155.35781	5097.59518	2491.55133
ENSMUSG00000031376.15	Atp2b3	-5.753076882	2.31112E-06	0.00045723 7	0	0	0	0	17.80631526	11.1056333	6.34292225	2.47177711
ENSMUSG00000056900.13	Usp13	-3.939035631	2.40693E-06	0.00046769 4	45.75295993	10.55206169	6.508406206	8.616727379	749.5610805	131.416661	158.573056	51.9073194
ENSMUSG00000021250.13	Fos	-2.122313973	2.41374E-06	0.00046769 4	148.6971198	30.6009789	39.98020955	71.51883725	172.1277142	356.305737	234.688123	503.006642

ENSMUSG00000043795.9	Prr33	-4.837885527	2.59307E-06	0.00049731 4	17.67727997	0	0.929772315	0	300.1636001	84.2177196	102.54391	38.3125452
ENSMUSG00000028023.16	Pitx2	-2.786382076	2.70815E-06	0.00051413 7	23.91631996	5.276030846	4.648861576	8.616727379	137.3630034	68.484739	63.4292225	21.0101055
ENSMUSG00000070424.12	Art5	-2.939826128	2.85515E-06	0.00053662 5	20.79679997	4.220824677	5.578633891	3.446690952	166.1922758	34.2423695	34.8860724	22.245994
ENSMUSG00000087410.7	231006 5F04Rik	-3.459525257	0.00000325 1	0.00060497 5	11.43823998	3.165618507	0.929772315	0	78.00861923	33.3169	44.4004558	9.88710845
ENSMUSG00000057719.10	Sh3rf2	-4.014185147	3.29398E-06	0.00060696 5	13.51791998	2.110412338	0	0	126.3400464	45.3480028	47.5719169	27.1895482
ENSMUSG00000027832.5	Ptx3	-4.996790322	3.39378E-06	0.00061928 3	2.079679997	0	0	3.446690952	19.50215481	147.149642	2.11430742	11.122997
ENSMUSG00000027253.15	Lrp4	-1.547828302	3.44507E-06	0.00062259 8	40.55375994	22.15932955	50.20770502	44.80698237	219.6112215	92.5469446	81.4008356	66.737982
ENSMUSG00000026582.6	Sele	-2.671982104	3.54734E-06	0.00063497 4	2.079679997	1.055206169	8.367950836	4.30836369	26.28551 3	23.1367361	8.45722967	45.7278766
ENSMUSG00000049134.15	Nrap	-5.051257522	3.6501E-06	0.00064720 5	319.2308795	6.331237015	26.03362482	1.723345476	6966.508866	1605.68949	2329.96677	805.799339
ENSMUSG00000063296.5	Tmem117	-5.611504373	3.7734E-06	0.00066281 4	1.039839998	0	0	0	29.6771921	11.1056333	7.40007596	8.65121989
ENSMUSG00000009471.4	Myod1	-6.152038375	3.84666E-06	0.00066942 5	1.039839998	1.055206169	0	0	104.2941322	20.3603278	12.6858445	1.23588856

ENSMUSG00000032549.7	Rab6b	4.156213561	3.97638E-06	0.00067941 9	880.7444787	1179.720497	68.80315132	1421.760018	62.7460633	51.826289	41.2289946	43.2560995
ENSMUSG00000024049.14	Myom1	-1.91592153	3.97319E-06	0.00067941 9	461.6889593	364.0461283	329.1393995	498.0468425	3129.671887	982.848551	1266.47014	851.527215
ENSMUSG00000050315.13	Synpo2	-1.846032183	4.08376E-06	0.00069061 1	562.5534392	418.9168491	438.8525327	449.7931692	3122.888529	1395.60792	1378.52844	824.337667
ENSMUSG00000010064.15	Slc38a3	-3.406788967	4.11849E-06	0.00069061 1	63.43023991	17.93850488	17.66567399	11.20174559	743.625642	158.255275	187.116206	76.6250905
ENSMUSG00000063142.15	Kcnma1	-4.676689637	4.15211E-06	0.00069061 1	9.358559986	1.055206169	0.929772315	0	200.1090667	34.2423695	34.8860724	14.8306627
ENSMUSG00000030592.18	Ryr1	-4.86722627	4.43164E-06	0.00073063 8	583.3502391	4.220824677	62.29474511	4.30836369	9671.372946	3515.85842	4017.18409	1882.25827
ENSMUSG00000030401.16	Rtn2	-1.836117279	4.62622E-06	0.00075608 5	152.8564798	113.9622663	75.31155752	91.33731022	758.0402782	271.162548	321.374727	194.034503
ENSMUSG00000026950.17	Neb	-4.499746139	4.86876E-06	0.00078666 4	857.8679987	42.20824677	74.38178521	43.94530963	14441.7696	3486.2434	3913.58303	1192.63246
ENSMUSG00000027499.12	Pkia	-2.823401605	4.90327E-06	0.00078666 4	65.5099199	23.21453572	25.10385251	20.68014571	546.9082544	155.478867	161.744517	85.2763104
ENSMUSG00000002500.15	Rpl3l	-3.749451871	4.93888E-06	0.00078666 4	145.5775998	11.60726786	15.80612936	13.78676381	1479.620006	463.660192	412.289946	152.014292
ENSMUSG00000074121.3	Ntf5	-4.14659467	5.16647E-06	0.00081599 9	2.079679997	2.110412338	0	0	36.46055029	18.5093889	9.51438338	3.70766567

ENSMUSG00000047419.5	Cmya5	-4.048265106	6.07139E-06	0.00095093 2	498.0833593	20.04891721	49.2779327	63.76378261	6228.818662	1480.75111	1945.16282	783.553345
ENSMUSG00000007122.11	Casq1	-4.202031422	6.36776E-06	0.000981	193.4102397	7.386443184	13.94658473	7.755054641	1945.975882	996.730593	824.579893	322.566913
ENSMUSG00000028841.14	Cnksr1	-4.277885542	6.3635E-06	0.000981	6.239039991	0	1.85954463	2.585018214	151.7776396	25.9131445	22.2002279	6.17944278
ENSMUSG00000070639.5	Lrrc8b	0.740705256	6.53423E-06	0.00099846 2	585.4299191	667.9455051	666.6467499	764.3037185	330.688712	339.647287	511.662395	427.61744
ENSMUSG00000032495.8	Lrrc2	-3.189257163	6.60856E-06	0.00100167 6	27.03583996	12.66247403	11.15726778	17.23345476	385.8034973	69.4102084	123.686984	40.7843224
ENSMUSG00000038777.19	Sema6c	-1.92347858	7.30985E-06	0.00109038 6	106.0636798	28.49056657	78.10087447	66.34880082	516.3831425	223.963606	195.573436	121.117079
ENSMUSG00000025089.15	Gfra1	-3.227622543	7.3054E-06	0.00109038 6	51.99199992	54.87072079	33.47180334	24.9885094	1223.548234	85.143189	161.744517	75.3892019
ENSMUSG00000026100.6	Mstn	-4.030041828	7.66803E-06	0.00112316 4	2.079679997	2.110412338	0.929772315	0	50.87518646	17.5839195	9.51438338	1.23588856
ENSMUSG00000034648.9	Lrrn1	-3.313377276	7.63572E-06	0.00112316 4	9.358559986	2.110412338	4.648861576	2.585018214	116.1650091	27.7640834	34.8860724	4.94355422
ENSMUSG00000002007.5	Srpk3	-2.492324161	7.70887E-06	0.00112316 4	32.23503995	5.276030846	13.94658473	21.54181845	243.3529752	76.813964	47.5719169	42.0202109
ENSMUSG00000022357.2	Klhl38	-2.791222061	7.77034E-06	0.00112341 1	10.39839998	1.055206169	4.648861576	3.446690952	68.68150172	12.9565722	34.8860724	17.3024398

ENSMUSG00000069601.14	Ank3	-1.21109765	8.25786E-06	0.00118478 2	222.5257597	178.3298426	208.2689986	226.6199301	774.9986737	465.511131	341.460648	350.99235
ENSMUSG00000026564.9	Dusp27	-4.011072943	8.65325E-06	0.00123210 5	37.43423994	0	6.508406206	3.446690952	388.3472566	169.360909	145.887212	56.8508736
ENSMUSG00000031596.15	Slc7a2	-1.489425054	8.93432E-06	0.00126256	33.27487995	20.04891721	30.6824864	46.53032785	154.3213989	91.6214751	71.8864522	48.1996537
ENSMUSG00000030399.2	Ckm	-3.870772713	9.61484E-06	0.00134858 9	2172.225757	330.2795309	120.870401	16.37178202	19378.35852	7541.65051	7922.30989	3769.4601
ENSMUSG00000079243.3	Xirp1	-4.424308061	1.01004E-05	0.00144062	92.54575986	0	29.75271408	29.29687309	2035.007458	652.455959	410.175639	155.721958
ENSMUSG00000030409.15	Dmpk	-0.700921666	1.15323E-05	0.00158946 7	1887.309597	1487.840698	2090.128164	1955.135442	3481.558593	3369.63425	2354.28131	2856.13845
ENSMUSG00000021536.7	Adcy2	-3.49706175	1.15859E-05	0.00158946 7	13.51791998	2.110412338	0.929772315	5.170036428	178.9110724	22.2112667	31.7146113	9.88710845
ENSMUSG00000003476.16	Crhr2	-3.427094827	1.26159E-05	0.00171823 3	19.75695997	1.055206169	2.789316945	11.20174559	220.4591413	56.4536362	71.8864522	24.7177711
ENSMUSG00000061462.17	Obscn	-4.273582549	1.31425E-05	0.00177706 8	1047.118878	17.93850488	73.45201289	24.12683666	11736.0576	3824.96522	4616.59025	2303.69627
ENSMUSG00000033044.12	Dhrs7c	-3.74833513	1.35231E-05	0.00181548 2	23.91631996	4.220824677	3.71908926	0	239.9612961	67.5592695	88.8009115	27.1895482
ENSMUSG00000020475.3	Pgam2	-3.789171598	1.39854E-05	0.00186421 8	238.1233596	18.99371104	15.80612936	10.34007286	1923.082048	923.618507	771.722207	292.905588

ENSMUSG00000030554.16	Synm	-0.875199714	1.46638E-05	0.00194088 8	1721.975037	1306.345237	1774.93535	1238.223724	3842.772417	2044.36201	2790.88579	2401.33146
ENSMUSG00000079110.11	Capn3	-3.234587213	1.47989E-05	0.00194506 6	45.75295993	4.220824677	11.15726778	7.755054641	375.62846	108.279925	125.801291	35.8407681
ENSMUSG00000038239.11	Hrc	-4.256016423	1.53354E-05	0.00200158 8	322.3503995	7.386443184	20.45499093	9.478400117	3920.781036	1393.75699	1080.41109	472.109428
ENSMUSG00000051067.8	Lingo3	-3.87505269	1.56371E-05	0.00202689 3	4.159359994	0	0	0	30.52511187	15.7329806	6.34292225	3.70766567
ENSMUSG00000030672.12	Mylpf	-3.042833067	1.58333E-05	0.00203826 6	194.4500797	65.42278249	35.33134797	21.54181845	1444.855295	583.045751	416.518561	161.901401
ENSMUSG00000034295.9	Fhod3	-1.281776484	1.66347E-05	0.00212686 8	51.99199992	55.92592696	53.92679428	61.17876439	227.2424995	118.460089	98.3152949	96.3993074
ENSMUSG00000026418.16	Tnni1	-4.901074713	1.70177E-05	0.00216112 8	40.55375994	8.441649353	1.85954463	3.446690952	1144.691695	167.50997	266.402735	38.3125452
ENSMUSG00000072591.10	Fzd10os	-5.282030747	1.72778E-05	0.00217943 2	1.039839998	0	0	0	27.98135255	9.25469446	6.34292225	1.23588856
ENSMUSG00000027887.11	Sypl2	-1.782100353	0.00001764 7	0.00221117 3	176.7727997	124.514328	103.204727	165.4411657	886.9240839	428.492353	420.747176	222.45994
ENSMUSG00000027868.11	Tbx15	-1.689649226	1.79384E-05	0.00222328	141.4182398	85.4716997	123.6597179	131.8359289	779.2382726	335.019939	290.71727	149.542515
ENSMUSG00000102676.1	Gm37435	-5.987487342	1.85793E-05	0.00223844 8	0	0	0	0	37.30847007	1.85093889	4.22861483	1.23588856

ENSMUSG00000028834.13	Trim63	-4.109035444	1.84948E-05	0.00223844 8	36.39439995	8.441649353	1.85954463	0	486.7059504	118.460089	139.54429	55.614985
ENSMUSG00000029769.16	Ccdc136	-2.112346141	1.83299E-05	0.00223844 8	6.239039991	3.165618507	10.22749547	8.616727379	64.44190285	23.1367361	14.8001519	19.7742169
ENSMUSG00000032060.10	Cryab	-2.779999317	1.83677E-05	0.00223844 8	523.0395192	491.7260748	252.8980697	253.3317849	6868.998091	1692.68362	1233.69838	648.841492
ENSMUSG00000031382.14	Asb11	-3.620990376	1.84167E-05	0.00223844 8	21.83663997	4.220824677	2.789316945	0.861672738	245.8967345	37.0187778	48.6290706	29.6613253
ENSMUSG00000107585.1	330000 2P13Rik	-5.078812915	0.00002148 7	0.00257228 7	1.039839998	0	0	0	18.65423503	9.25469446	7.40007596	3.70766567
ENSMUSG00000001508.15	Sgca	-3.691826513	2.25755E-05	0.00266859 6	28.07567996	0	4.648861576	2.585018214	266.2468091	75.8884945	75.0579133	35.8407681
ENSMUSG00000087095.2	Emx2os	-5.546536472	2.25594E-05	0.00266859 6	0	0	0	0	19.50215481	4.62734723	7.40007596	1.23588856
ENSMUSG00000029683.7	Lmod2	-4.514395866	2.34232E-05	0.00273440 6	146.6174398	8.441649353	8.367950836	0.861672738	2343.650256	569.163709	586.720308	249.649488
ENSMUSG00000031519.3	Asb5	-3.129446554	2.33708E-05	0.00273440 6	15.59759998	5.276030846	0.929772315	1.723345476	128.0358859	30.5404917	29.6003038	13.5947741
ENSMUSG00000039601.16	Rcan2	-1.70631265	2.41523E-05	0.00280211 4	47.83263993	56.98113313	47.41838807	58.59374618	378.1722193	116.60915	111.001139	80.3327562
ENSMUSG00000078815.8	Cacng6	-4.03117977	2.44849E-05	0.00282327 3	19.75695997	1.055206169	0.929772315	0	215.3716227	52.7517584	62.3720688	21.0101055

ENSMUSG00000044086.8	Lmod3	-2.644788028	0.00002465 1	0.00282509 4	181.9719997	62.25716398	45.55884344	49.11534606	1174.368887	372.964187	390.089719	179.203841
ENSMUSG00000007877.2	Tcap	-4.202920038	2.59257E-05	0.00293538 5	848.5094387	103.4102046	46.48861576	8.616727379	11608.86963	2527.45706	3138.68936	1265.54988
ENSMUSG00000007030.8	Vwa7	-1.946172183	2.57704E-05	0.00293538 5	8.318719988	3.165618507	12.0870401	8.616727379	57.65854465	21.2857973	26.4288427	18.5383283
ENSMUSG00000050069.3	Grem2	-1.9741362	2.61058E-05	0.00293807	7.278879989	7.386443184	11.15726778	4.30836369	49.17934691	24.0622056	27.4859964	16.0665512
ENSMUSG00000031543.18	Ank1	-1.424338504	2.66513E-05	0.00296397 5	259.9599996	109.7414416	260.3362482	304.1704765	1009.024531	704.282248	481.004937	312.679805
ENSMUSG00000063821.6	Dupd1	-5.289839811	2.65911E-05	0.00296397 5	1.039839998	0	0.929772315	0	40.70014917	14.8075111	13.7429982	6.17944278
ENSMUSG00000033065.14	Pfkm	-0.99536024	2.73065E-05	0.00301897 6	2705.663676	2364.717025	1955.311179	1989.602352	7266.672466	3474.2123	3732.80975	3495.09284
ENSMUSG00000038403.10	Hjv	-4.112276983	2.74913E-05	0.00302089 7	132.0596798	12.66247403	6.508406206	0.861672738	1436.376098	497.902562	510.605241	180.439729
ENSMUSG00000029361.18	Nos1	-1.200776035	2.76559E-05	0.00302089 7	126.8604798	56.98113313	80.89019141	70.65716451	295.9240012	184.16842	114.172601	174.260286
ENSMUSG00000031204.3	Asb12	-5.075606025	2.78061E-05	0.00302089 7	2.079679997	0	0	0	37.30847007	11.1056333	11.6286908	4.94355422
ENSMUSG00000039103.12	Nexn	-2.50205025	2.83854E-05	0.00304859 7	240.2030396	100.2445861	126.4490349	94.78400117	1800.981601	584.89669	552.89139	240.998268

ENSMUSG00000037139.15	Myom3	-1.683488381	2.83248E-05	0.00304859 7	422.1750394	291.2369027	272.4232883	224.8965846	1904.427813	743.151965	634.292225	604.349504
ENSMUSG00000036856.4	Wnt4	-2.240405432	2.93595E-05	0.00308274 7	8.318719988	5.276030846	0	0	12.71879661	22.2112667	11.6286908	13.5947741
ENSMUSG00000079278.1	Tmem233	-3.6249538	2.92543E-05	0.00308274 7	27.03583996	2.110412338	0.929772315	0	153.4734791	86.0686584	89.8580652	37.0766567
ENSMUSG00000030996.8	Art1	-4.06354378	2.92365E-05	0.00308274 7	64.4700799	1.055206169	5.578633891	1.723345476	670.7045415	250.80222	204.030666	87.7480875
ENSMUSG00000030730.12	Atp2a1	-4.41151298	2.88852E-05	0.00308274 7	4132.324154	72.80922567	249.1789804	19.81847297	43186.24994	21379.2697	19958.0049	10686.7283
ENSMUSG00000058975.7	Kcnc1	-4.736940293	2.95437E-05	0.00308485 6	13.51791998	0	0	0	230.6341786	50.9008195	57.0863003	16.0665512
ENSMUSG00000021768.15	Dusp13	-3.697821431	2.98572E-05	0.00310036 7	54.07167992	6.331237015	4.648861576	0.861672738	499.4247471	120.311028	168.08744	63.0303164
ENSMUSG00000085614.1	1700123M08Rik	-1.559914184	3.19781E-05	0.00330235 7	8.318719988	5.276030846	8.367950836	8.616727379	20.35007458	25.9131445	21.1430742	23.4818826
ENSMUSG00000042686.5	Jph1	-1.475798808	3.22487E-05	0.00331210 2	273.4779196	148.7840698	202.6903647	209.3864753	944.5826286	569.163709	501.090858	304.028585
ENSMUSG00000038132.6	Rbm24	-3.673375453	3.26391E-05	0.00333398	49.91231993	1.055206169	6.508406206	8.616727379	522.318581	127.714784	138.487136	51.9073194
ENSMUSG00000027016.17	Zfp385b	-2.443529112	3.38361E-05	0.00343756 2	5.199199992	4.220824677	4.648861576	4.30836369	53.41894578	12.9565722	11.6286908	21.0101055

ENSMUSG00000049551.2	Fzd9	-2.625306826	0.00003433 7	0.0034697	22.87647997	14.77288637	3.71908926	5.170036428	183.1506712	30.5404917	32.771765	37.0766567
ENSMUSG00000031099.16	Smarca1	-1.560814515	3.58729E-05	0.00360551 9	6.239039991	7.386443184	13.01681241	9.478400117	37.30847007	25.9131445	22.2002279	21.0101055
ENSMUSG00000026062.12	Slc9a2	-2.909879359	3.63867E-05	0.00363770 6	4.159359994	5.276030846	7.438178521	9.478400117	123.796287	36.0933084	35.9432261	2.47177711
ENSMUSG00000033152.13	Podxl2	-1.232546414	3.74624E-05	0.00371620 3	61.35055991	89.69252438	41.83975418	56.8704007	238.2654566	136.969478	132.144214	75.3892019
ENSMUSG00000024471.12	Myot	-4.586945743	3.75674E-05	0.00371620 3	168.4540797	18.99371104	13.01681241	0	3353.522707	587.673098	658.606761	212.572832
ENSMUSG00000038670.11	Mybpc2	-3.999984404	3.96229E-05	0.00387871 3	641.581279	18.99371104	56.71611122	5.170036428	4867.059504	3017.95586	2409.2533	1260.60633
ENSMUSG00000059741.13	Myl3	-4.233314464	0.00003947 4	0.00387871 3	54.07167992	8.441649353	1.85954463	14.64843654	910.6658376	240.622056	250.545429	81.5686447
ENSMUSG00000051456.4	Hspb3	-4.910692407	3.99279E-05	0.00388831 8	1.039839998	1.055206169	0	0	40.70014917	4.62734723	7.40007596	4.94355422
ENSMUSG00000035934.16	Pknox2	-1.846747151	4.12533E-05	0.00399667 7	37.43423994	16.88329871	47.41838807	23.26516392	245.8967345	101.801639	57.0863003	43.2560995
ENSMUSG00000021373.16	Cap2	-2.555825216	4.16143E-05	0.00401098 3	62.39039991	30.6009789	51.13747733	29.29687309	625.7647934	126.789314	182.887592	82.8045333
ENSMUSG00000017300.9	Tnnc2	-3.760501269	4.28492E-05	0.00410893 5	637.421919	91.80293671	31.61225871	12.92509107	5988.009446	1685.27986	1969.47736	839.16833

ENSMUSG00000054477.15	Kcnn2	-2.529937115	0.00004391 4	0.00418966 4	7.278879989	1.055206169	0.929772315	2.585018214	28.82927233	12.0311028	15.8573056	9.88710845
ENSMUSG00000097317.1	NA	-2.602836139	4.92547E-05	0.00467546 5	7.278879989	5.276030846	0	8.616727379	72.07318081	17.5839195	23.2573816	14.8306627
ENSMUSG00000051747.14	Ttn	-4.561073678	5.12829E-05	0.00481189 1	2439.464636	39.04262826	116.2215394	15.51010928	36829.3954	10086.6915	10928.855	3766.98832
ENSMUSG00000030470.15	Csrp3	-4.906142572	0.00005146	0.00481189 1	53.03183992	9.496855522	0.929772315	0	1393.132189	242.472995	210.373588	50.6714308
ENSMUSG00000031461.4	Myom2	-4.482073629	0.00005131 1	0.00481189 1	178.8524797	3.165618507	6.508406206	0.861672738	2464.054864	797.754662	634.292225	331.218133
ENSMUSG00000068697.7	Myoz1	-3.691364187	0.00005175 5	0.00481552 5	222.5257597	43.26345293	14.87635704	1.723345476	1834.050472	725.568045	730.493213	353.464127
ENSMUSG00000027010.16	Slc25a12	-1.774407209	0.00005245 1	0.00484112 2	159.0955198	119.2382971	90.18791456	84.44392832	847.9197743	276.715364	267.459888	154.48607
ENSMUSG00000053025.13	Sv2b	-5.598989398	5.28988E-05	0.00484112 2	0	0	0	0	21.19799436	2.77640834	5.28576854	4.94355422
ENSMUSG00000038086.4	Hspb2	-2.086244312	5.30604E-05	0.00484112 2	19.75695997	10.55206169	9.297723151	16.37178202	134.8192441	47.1989417	30.6574576	23.4818826
ENSMUSG00000085779.1	Atcayos	-4.005891583	5.28446E-05	0.00484112 2	44.71311993	0	7.438178521	4.30836369	602.8709595	132.342131	127.915599	40.7843224
ENSMUSG00000024222.16	Fkbp5	-1.426248289	5.35565E-05	0.00486277 4	660.298399	528.6582907	667.5765222	609.2026257	3027.073594	825.518746	677.635527	2096.06699

ENSMUSG00000032366.15	Tpm1	-1.443750342	5.58308E-05	0.00499005 2	2311.564317	1766.415127	1377.922571	1497.587219	8380.839049	4107.2334	3901.95434	2522.44854
ENSMUSG00000053093.16	Myh7	-5.947103627	5.54124E-05	0.00499005 2	632.2227191	3.165618507	33.47180334	0	27588.7657	5736.98509	6785.86966	1146.90458
ENSMUSG00000022759.14	Lrrc74b	-2.029907103	0.0000556	0.00499005 2	7.278879989	2.110412338	3.71908926	1.723345476	19.50215481	16.65845	15.8573056	6.17944278
ENSMUSG00000007033.4	Hspa1l	-2.743872074	5.60203E-05	0.00499005 2	9.358559986	17.93850488	6.508406206	2.585018214	147.5380407	25.9131445	57.0863003	9.88710845
ENSMUSG00000030091.17	Nup210	-1.469437171	5.69206E-05	0.00504632 9	41.59359994	23.21453572	40.90998186	24.12683666	123.796287	109.205395	65.5435299	59.3226507
ENSMUSG00000005628.12	Tmod4	-2.690586003	5.73539E-05	0.00506087 7	101.9043198	28.49056657	27.89316945	19.81847297	645.2669482	214.708911	210.373588	76.6250905
ENSMUSG00000052698.15	Tln2	-0.508999883	5.90193E-05	0.00518349 5	1381.947358	1184.996528	1669.871078	1340.76278	1901.884054	1797.26166	2277.10909	1963.82692
ENSMUSG00000070385.12	Ampd1	-3.820378722	5.94466E-05	0.00519674	114.3823998	8.441649353	4.648861576	1.723345476	961.541024	370.187778	375.289567	113.701747
ENSMUSG00000040705.2	A930016O22Rik	-3.616022754	6.05259E-05	0.00526659 8	3.119519995	0	1.85954463	0	35.61263052	13.8820417	3.17146113	6.17944278
ENSMUSG00000025537.12	Phkg1	-2.514566253	6.14007E-05	0.00531809 6	289.0755196	16.88329871	86.4688253	88.75229201	1300.708934	471.063948	548.662775	427.61744
ENSMUSG00000028116.13	Myoz2	-5.128418901	6.25177E-05	0.00539000 4	22.87647997	6.331237015	0	0	757.1923584	102.727108	134.258521	21.0101055

ENSMUSG00000019787.9	Trdn	-4.391544973	0.00006304 7	0.00541081 5	135.1791998	4.220824677	3.71908926	0.861672738	1803.52536	476.616765	553.948543	182.911506
ENSMUSG00000032816.15	Igdcc4	-3.058427042	6.33697E-05	0.00541379 1	43.67327993	7.386443184	24.17408019	17.23345476	474.8350736	156.404336	113.115447	24.7177711
ENSMUSG00000025754.11	Agbl1	-5.007682656	6.63087E-05	0.00563924 1	1.039839998	1.055206169	0	0	31.37303165	13.8820417	16.9144593	0
ENSMUSG00000038418.7	Egr1	-1.5829269	6.78432E-05	0.00574375 1	727.8879989	319.7274692	397.9425509	491.1534606	595.2396815	2175.77867	833.037122	2198.64574
ENSMUSG00000028396.5	231000 2L09Rik	-4.092042601	7.25303E-05	0.00611303 2	12.47807998	4.220824677	0	0	186.5423503	38.8697167	43.3433021	11.12299 7
ENSMUSG00000025813.14	Homer 2	-2.260406395	7.28863E-05	0.00611561 9	16.63743998	16.88329871	15.80612936	20.68014571	217.0674622	34.2423695	41.2289946	42.0202109
ENSMUSG00000027022.13	Xirp2	-4.586540992	7.33178E-05	0.00612448 4	410.7367994	3.165618507	35.33134797	2.585018214	6821.514584	1704.71472	1754.87516	569.744624
ENSMUSG00000021822.3	Plau	-0.798844619	7.48965E-05	0.00622867 1	240.2030396	206.8204091	181.3056014	193.876366	381.5638984	501.60444	281.202887	262.008374
ENSMUSG00000108322.1	543043 1A17Rik	-3.783577237	8.23403E-05	0.00681756 3	8.318719988	1.055206169	1.85954463	0.861672738	94.96701472	14.8075111	14.8001519	39.5484338
ENSMUSG00000031312.5	Itgb1bp 2	-2.888054954	8.53927E-05	0.00703927 9	41.59359994	6.331237015	6.508406206	5.170036428	228.0904193	86.0686584	84.5722967	39.5484338
ENSMUSG00000021579.4	Lrrc14b	-1.553033003	8.77012E-05	0.00719801 1	83.18719988	91.80293671	66.01383437	70.65716451	449.3974804	148.075111	237.859584	76.6250905

ENSMUSG00000029470.15	P2rx4	0.58095421	8.90132E-05	0.00727392 4	658.218719	846.2753476	629.4558573	728.9751363	393.4347753	516.411951	411.232793	595.698284
ENSMUSG00000031636.7	Pdlim3	-3.026568925	8.96754E-05	0.00729241 6	87.34655987	7.386443184	34.40157566	46.53032785	864.03025	247.100342	236.802431	82.8045333
ENSMUSG00000006435.15	Neurl1a	-1.413362241	9.00155E-05	0.00729241 6	186.1313597	88.63731821	73.45201289	131.8359289	585.0646443	301.703039	233.63097	155.721958
ENSMUSG00000060180.12	Myh13	-6.791601067	9.06875E-05	0.00731533	0	0	0	0	51.72310623	11.1056333	15.8573056	0
ENSMUSG00000020333.17	Acsl6	-2.548119024	9.13498E-05	0.00733725 9	7.278879989	2.110412338	0.929772315	3.446690952	33.0688712	26.8386139	13.7429982	4.94355422
ENSMUSG00000039891.6	Txlnb	-1.194883387	9.40517E-05	0.00752213 4	675.895999	751.3067924	804.2530526	875.4595017	2951.608734	1097.60676	1872.21922	1190.16068
ENSMUSG00000006542.13	Prkag3	-2.791573863	9.58779E-05	0.00763570 3	29.11551996	2.110412338	3.71908926	6.893381903	135.6671639	76.813964	53.9148391	21.0101055
ENSMUSG00000020173.17	Cobl	-2.052728868	9.76276E-05	0.00774223 7	15.59759998	3.165618507	10.22749547	9.478400117	82.24821811	31.4659612	27.4859964	17.3024398
ENSMUSG00000025172.2	Ankrd2	-3.560949282	9.83435E-05	0.00776624 3	69.6692799	66.47798865	40.90998186	37.91360047	1745.018895	337.796348	357.317954	95.1634188
ENSMUSG00000043126.5	D830039M14Rik	-2.853295555	0.00010346 2	0.00813624 3	5.199199992	0	1.85954463	0	24.58967345	7.40375557	12.6858445	3.70766567
ENSMUSG00000061723.18	Tnnt3	-3.910873233	0.00010448 8	0.00818272 3	1789.564637	236.3661819	81.81996373	10.34007286	17868.2134	5406.5925	5983.48999	2596.60186

ENSMUSG00000071342.5	Lsmem1	-3.257243954	0.00010902 8	0.00850280 1	0	2.110412338	0	2.585018214	25.43759323	8.32922501	8.45722967	2.47177711
ENSMUSG00000069372.3	Ctxn3	-3.488831793	0.00011501 8	0.00893293 1	3.119519995	3.165618507	0	0	36.46055029	15.7329806	10.5715371	3.70766567
ENSMUSG00000031722.10	Hp	-1.302033071	0.00011618 7	0.00898657	3538.575515	6426.20557	2552.225005	3799.976774	15334.62912	13586.8169	6730.89766	4577.73121
ENSMUSG00000022237.17	Ankrd33b	-1.301935105	0.00011709 8	0.00901994 3	116.4620798	155.1153069	146.9040258	177.504584	569.8020883	228.590953	374.232413	296.613253
ENSMUSG00000021898.14	Asb14	-4.443882873	0.00012119 4	0.00929728 6	13.51791998	0	0	0	184.8465108	37.9442473	58.143454	8.65121989
ENSMUSG00000027692.16	Tnik	-1.427054111	0.00012273 2	0.00933909 8	29.11551996	34.82180358	39.05043723	33.60523678	165.344356	68.484739	74.0007596	58.0867621
ENSMUSG00000091712.2	Sec14l5	-2.681994991	0.00012264 2	0.00933909 8	46.79279993	2.110412338	13.01681241	15.51010928	289.9885628	87.9195973	72.9436059	44.491988
ENSMUSG00000061816.15	Myl1	-1.337836499	0.00012600 8	0.00954971 6	1481.771998	1029.881221	883.2836993	754.8253184	4544.84999	2253.5181	2024.44935	1663.506
ENSMUSG00000101655.1	2310040G24Rik	-1.395098394	0.00012728 3	0.00960757 5	25.99599996	25.32494806	11.15726778	15.51010928	85.6398972	25.9131445	46.5147632	44.491988
ENSMUSG00000025141.2	Myadml2	-3.503675299	0.00013000 6	0.00977381 7	14.55775998	2.110412338	6.508406206	0	155.1693187	42.5715945	53.9148391	8.65121989
ENSMUSG00000025129.2	Ppp1r27	-4.150450581	0.00013068 9	0.00978604 6	14.55775998	3.165618507	0	0	224.6987402	28.6895528	44.4004558	12.3588856

ENSMUSG00000027470.9	Mylk2	-4.034258939	0.00013705 4	0.01022195 3	311.9519995	6.331237015	23.24430788	1.723345476	3138.999004	809.785765	1204.09807	467.165874
ENSMUSG00000030089.15	Slc41a3	-1.059214096	0.00014688	0.01091150 2	66.5497599	41.1530406	59.50542817	43.94530963	158.5609978	93.472414	106.772525	79.0968676
ENSMUSG00000010492.10	Uckl1os	-3.284735606	0.00014757 6	0.01092006 3	22.87647997	0	9.297723151	2.585018214	216.2195424	41.6461251	59.2006077	19.7742169
ENSMUSG00000028975.16	Pex14	0.515558076	0.00014828 9	0.01092975 9	4941.319673	6797.638142	4526.13163	5214.84341	3105.930133	4035.04678	3920.98311	3964.73049
ENSMUSG00000038764.14	Ptpn3	-1.410762006	0.00014921 9	0.01095536 5	73.82863989	47.48427761	51.13747733	80.99723736	303.5552792	129.565722	123.686984	116.173524
ENSMUSG00000074001.3	Klhl40	-4.371274403	0.00015491 7	0.01132945 4	54.07167992	1.055206169	1.85954463	0.861672738	864.03025	168.435439	118.401215	42.0202109
ENSMUSG00000021622.3	Ckmt2	-4.751377114	0.00015676 2	0.01141992 2	151.8166398	5.276030846	8.367950836	0	3295.016243	558.058076	501.090858	97.6351959
ENSMUSG00000113178.1	Mylf-ps	-1.321155419	0.00015806 9	0.01147066 1	402.4180794	301.7889644	245.4598912	227.4816028	1273.575501	633.94657	606.806229	423.909775
ENSMUSG00000026494.12	Kif26b	-2.744264424	0.00016407 6	0.01186081 1	2.079679997	2.110412338	1.85954463	0	12.71879661	10.1801639	10.5715371	4.94355422
ENSMUSG00000099906.2		-4.372826914	0.00016740 8	0.01205533 5	8.318719988	0	0.929772315	0	150.9297198	10.1801639	16.9144593	9.88710845
ENSMUSG00000032845.15	Alpk2	-4.414592011	0.00016848 2	0.01208631 2	37.43423994	2.110412338	0	0	481.6184318	173.062786	132.144214	51.9073194

ENSMUSG00000020061.17	Mybpc1	-4.70822925	0.00017211	0.01229965 1	635.3422391	3.165618507	30.6824864	1.723345476	11089.94273	2602.42008	2932.54439	855.234881
ENSMUSG00000005320.9	Fgfr4	-2.742517716	0.00017508 4	0.01246479 3	3.119519995	0	1.85954463	0.861672738	10.17503729	7.40375557	13.7429982	7.41533134
ENSMUSG00000013936.12	Myl2	-4.819060602	0.00018208 4	0.01291420 5	46.79279993	3.165618507	0.929772315	0	1006.480772	174.913725	201.916358	48.1996537
ENSMUSG00000022215.6	Fitm1	-3.858340264	0.00018545 7	0.01310400 5	21.83663997	4.220824677	0	0	232.3300182	59.2300445	62.3720688	19.7742169
ENSMUSG00000064337.1	mt-Rnr1	0.776684016	0.00018827 7	0.01325346 5	278426.5181	511447.8781	357615.5362	315731.5396	193639.4389	148325.914	284443.063	227685.277
ENSMUSG00000042451.12	Mybph	-3.655224291	0.00019435 9	0.01352952 4	28.07567996	0	5.578633891	5.170036428	144.9942814	268.386139	45.4576095	28.4254368
ENSMUSG00000027895.9	Kcnc4	-1.109326582	0.00019334 3	0.01352952 4	69.6692799	59.09154547	39.05043723	54.28538249	139.058843	106.428986	116.286908	116.173524
ENSMUSG00000040694.3	Apobec2	-4.125951051	0.00019367 3	0.01352952 4	152.8564798	11.60726786	13.01681241	0	2005.330266	441.448926	487.34786	160.665512
ENSMUSG00000009075.2	Cabp7	-3.146366094	0.00019543 8	0.01355446	3.119519995	1.055206169	0.929772315	0	13.56671639	15.7329806	8.45722967	4.94355422
ENSMUSG00000068130.11	Zfp442	-2.02968678	0.00020469 9	0.01414453 1	6.239039991	2.110412338	2.789316945	1.723345476	15.26255594	13.8820417	7.40007596	14.8306627
ENSMUSG00000055489.8	Ano5	-3.791579021	0.00022316 2	0.01536382 6	17.67727997	0	0.929772315	0	163.6485164	36.0933084	37.0003798	17.3024398

ENSMUSG00000048003.12	Catsper4	-5.848030342	0.00022807 7	0.01555413 6	0	0	0	0	35.61263052	1.85093889	3.17146113	0
ENSMUSG00000006675.10	P4htm	-0.760952391	0.00022763 2	0.01555413 6	55.11151992	46.42907144	46.48861576	42.22196416	78.85653901	80.5158418	76.115067	86.5121989
ENSMUSG00000056328.14	Myh1	-4.337388371	0.00023006 4	0.01555413 6	2352.118076	35.87700975	93.90700383	10.34007286	26594.1558	9840.51662	10914.0549	3029.16285
ENSMUSG00000021597.16	Slf1	-0.637555307	0.00022996 8	0.01555413 6	85.26687987	87.58211204	81.81996373	93.0606557	155.1693187	121.236497	124.744138	139.655407
ENSMUSG00000073600.3	Prob1	-1.022845919	0.00022966 9	0.01555413 6	202.7687997	153.0048945	170.1483337	193.876366	654.5940657	301.703039	273.802811	229.875271
ENSMUSG00000066705.7	Fxyd6	-2.063220475	0.00024359 3	0.01640981 2	21.83663997	20.04891721	14.87635704	26.71185488	234.0258577	49.0498806	42.2861483	22.245994
ENSMUSG00000059743.12	Fdps	0.799170314	0.00024690 2	0.01651432 9	198.6094397	184.6610796	209.1987709	216.2798572	108.5337311	100.87617	99.3724486	158.193735
ENSMUSG00000040118.15	Cacna2d1	-1.138190 59	0.00024668 5	0.01651432 9	138.2987198	125.5695341	155.2719766	137.8676381	457.8766781	261.907853	292.831577	210.101055
ENSMUSG00000044938.8	Klhl31	-3.779984703	0.00025924 6	0.01727844 5	43.67327993	4.220824677	1.85954463	0	435.830764	114.758211	91.9723727	37.0766567
ENSMUSG00000065460.1	Mir133a-2	-4.311536816	0.00026137 5	0.01735879	2.079679997	0	0	0	20.35007458	6.47828612	7.40007596	3.70766567
ENSMUSG00000068394.4	Cep152	-0.724171129	0.00026753 3	0.01760020 3	177.8126397	104.4654107	169.2185613	125.8042197	301.0115199	258.205975	189.230514	202.685723

ENSMUSG00000024302.16	Dtna	-2.087524621	0.00026781 9	0.01760020 3	31.19519995	3.165618507	17.66567399	8.616727379	142.4505221	37.9442473	57.0863003	18.5383283
ENSMUSG00000079316.10	Rab9	0.496557553	0.00026727 1	0.01760020 3	2243.974717	3285.912011	2233.313101	2366.153338	1665.314437	1752.83913	2015.99212	1745.07464
ENSMUSG00000112739.1	Gm20597	-2.587129657	0.00027200 9	0.01781327 3	5.199199992	0	13.01681241	0	60.20230397	13.8820417	19.0287668	16.0665512
ENSMUSG00000000183.6	Fgf6	-4.304736953	0.00027528 8	0.01796541 5	1.039839998	0	0	0	6.783358194	8.32922501	6.34292225	1.23588856
ENSMUSG00000005716.16	Pvalb	-3.129468318	0.00029328 2	0.01907347 1	419.0555194	103.4102046	29.75271408	6.031709165	2072.315928	1196.63199	1147.01177	465.929986
ENSMUSG00000042717.5	Ppp1r3a	-4.41506426	0.00029582 3	0.01917240 1	25.99599996	0	0	0	335.7762306	72.1866168	106.772525	35.8407681
ENSMUSG00000027107.3	Chrna1	-3.979159113	0.00030412 9	0.01964297 1	1.039839998	0	2.789316945	0	42.39598871	11.1056333	5.28576854	1.23588856
ENSMUSG00000041688.16	Amot	-1.435209991	0.00030761 4	0.01980003 6	176.7727997	75.97484418	116.2215394	112.8791287	568.9541685	254.504098	286.488655	191.562726
ENSMUSG00000057606.14	Colq	-3.080024591	0.00031040 3	0.01991131 5	4.159359994	0	0	1.723345476	19.50215481	17.5839195	5.28576854	6.17944278
ENSMUSG00000100410.1	2310020H05Rik	-3.936489685	0.00032939 9	0.02105802 7	3.119519995	1.055206169	0	0	39.85222939	6.47828612	11.6286908	2.47177711
ENSMUSG00000042895.6	Abra	-4.079023001	0.00033378 6	0.02126615 8	56.15135992	2.110412338	0.929772315	0.861672738	674.0962206	133.2676	146.944366	56.8508736

ENSMUSG00000028785.13	Hpca	-2.73677576	0.00033516 7	0.02128198	7.278879989	3.165618507	7.438178521	6.031709165	22.89383391	124.012906	8.45722967	3.70766567
ENSMUSG00000026251.13	Chrnd	-4.771525964	0.00034927	0.02210277 7	1.039839998	0	0	0	15.26255594	12.0311028	4.22861483	0
ENSMUSG00000110547.1	Gm29773	-4.022808738	0.00035172	0.02210893 5	5.199199992	0	0.929772315	0	61.89814352	22.2112667	12.6858445	0
ENSMUSG00000011148.14	Adssl1	-0.79157948	0.00035148 7	0.02210893 5	1150.063038	1804.402549	1043.204538	1184.800015	3157.653239	1732.4788	1601.58787	2498.96666
ENSMUSG00000025938.16	Slco5a1	-3.362175516	0.00035397 2	0.02217632	20.79679997	0	5.578633891	1.723345476	181.4548317	36.0933084	50.74337 8	18.5383283
ENSMUSG00000087523.1	Gm12319	-1.682150485	0.00037043 4	0.02313058 7	28.07567996	5.276030846	15.80612936	7.755054641	77.16069946	41.6461251	35.9432261	25.9536597
ENSMUSG00000022508.5	Bcl6	-0.940107803	0.00037380 7	0.02322940 8	1858.194077	2997.840726	2959.465279	2869.370217	4559.264626	4871.67116	5085.96649	5985.40828
ENSMUSG00000025427.14	Rnf165	-2.146989744	0.00037448 8	0.02322940 8	3.119519995	4.220824677	3.71908926	3.446690952	16.11047571	29.6150223	13.7429982	3.70766567
ENSMUSG00000031097.15	Tnni2	-3.55868967	0.00038190 2	0.02361131 3	644.700799	161.4465439	13.94658473	6.893381903	5766.702385	1537.20475	1710.474 7	726.702471
ENSMUSG00000087405.1	Gm14232	1.102317568	0.00039189 4	0.02414967 1	97.74495985	68.58840099	54.85656659	64.62545534	29.6771921	33.3169	28.5431501	42.0202109
ENSMUSG00000040964.16	Arhgef10l	-0.870703283	0.00040426	0.02474939 6	115.4222398	74.91963801	119.0108563	105.124074	248.4404939	229.516423	162.801671	114.937636

ENSMUSG00000042734.6	Ttc9	-2.401702589	0.00040319	0.02474939 6	8.318719988	4.220824677	1.85954463	6.031709165	64.44190285	20.3603278	17.97161 3	3.70766567
ENSMUSG00000073375.2	Lrrc30	-4.329888104	0.00044089	0.02495219 2	16.63743998	0	0	0	241.6571357	43.4970639	30.6574576	14.8306627
ENSMUSG00000058057.5	Mettl7a3	-4.23528723	0.00042315 7	0.02573864 3	0	0	0	0	4.239598871	7.40375557	1.05715371	0
ENSMUSG00000028838.11	Extl1	-1.600711001	0.00042799 4	0.02583804 6	47.83263993	75.97484418	31.61225871	65.48712808	226.3945797	224.889075	162.801671	54.3790965
ENSMUSG00000103183.1	Gm37090	-1.025742224	0.00042773 8	0.02583804 6	56.15135992	20.04891721	63.22451743	61.17876439	93.27117517	102.727108	96.2009875	118.645301
ENSMUSG00000029816.10	Gpnmb	-2.441288312	0.00043023 6	0.02583804 6	79.02783988	121.3487094	58.57565585	188.7063296	532.4936183	1382.65135	469.376247	46.9637651
ENSMUSG00000049173.7	Myoz3	-2.503066698	0.00043029	0.02583804 6	12.47807998	1.055206169	3.71908926	0.861672738	60.20230397	23.1367361	10.5715371	6.17944278
ENSMUSG00000026459.5	Myog	-5.175616425	0.00044728 3	0.02677287 4	3.119519995	0	0	0	87.33573675	9.25469446	9.51438338	2.47177711
ENSMUSG00000046808.17	Atp10d	0.975511635	0.00047564	0.02837987 3	661.338239	603.5779287	773.5705662	924.5748478	376.4763798	223.038136	305.517422	604.349504
ENSMUSG00000027805.16	Pfn2	-1.214954866	0.00047915	0.02849879 8	98.78479985	96.02376139	72.52224058	77.55054641	334.0803911	153.627928	195.573436	114.937636
ENSMUSG00000087579.7	Hectd2os	-2.50419122	0.00048428 9	0.02871361 2	3.119519995	0	3.71908926	5.170036428	37.30847007	9.25469446	5.28576854	17.3024398

ENSMUSG00000074794.10	Arrdc3	-0.630470927	0.00049700 2	0.02937472 2	307.7926395	291.2369027	259.4064759	266.256876	460.4204374	324.839775	374.232413	583.339399
ENSMUSG00000040666.18	Sh3bgr	-1.543094826	0.00050684 2	0.02986237 1	135.1791998	156.170513	56.71611122	91.33731022	677.4878997	217.48532	214.602203	168.080844
ENSMUSG00000053279.7	Aldh1a1	-1.15375735	0.00051742 4	0.03039056 2	114.3823998	150.8944822	89.25814225	152.5160746	553.6916126	222.112667	204.030666	145.83485
ENSMUSG00000042485.7	Mustn1	-0.870114715	0.00054882 2	0.03213427 8	112.3027198	109.7414416	104.1344993	111.1557832	192.4777888	316.51055	152.230134	135.947741
ENSMUSG00000029862.15	Clcn1	-3.828839579	0.00055221 9	0.03223276 8	85.26687987	0	1.85954463	2.585018214	677.4878997	271.162548	231.516662	91.4557532
ENSMUSG00000035923.4	Myf6	-3.558554453	0.00056215 7	0.03271129 2	17.67727997	0	3.71908926	0	156.8651582	53.6772278	25.371689	13.5947741
ENSMUSG00000068614.7	Actc1	-4.074889037	0.00056554 2	0.03280666 3	22.87647997	0	3.71908926	0.861672738	200.1090667	213.783442	26.4288427	19.7742169
ENSMUSG00000029001.15	Fbxo44	0.811964522	0.00059628 8	0.03427286 5	649.899999	813.5639564	394.2234616	717.7733907	345.9512679	356.305737	427.090098	337.397576
ENSMUSG00000087408.10	Cers1	-1.600829881	0.00059516 3	0.03427286 5	6.239039991	5.276030846	4.648861576	4.30836369	15.26255594	16.65845	14.8001519	14.8306627
ENSMUSG00000025429.8	Pstpip2	-1.405219485	0.00059582 3	0.03427286 5	19.75695997	16.88329871	13.94658473	12.92509107	55.9627051	36.0933084	30.6574576	44.491988
ENSMUSG00000044177.4	Wfikkn2	-1.569973088	0.00060360 4	0.03458763 7	7.278879989	11.60726786	8.367950836	11.20174559	48.33142713	17.5839195	25.371689	22.245994

ENSMUSG00000015850.11	Adamtsl4	-1.215215017	0.00061911 7	0.03526155 4	201.7289597	78.08525652	252.8980697	213.694839	814.8509031	378.517003	299.1745	239.76238
ENSMUSG00000020473.13	Aebp1	-1.01037782	0.00061803 5	0.03526155 4	749.7246389	497.0021057	995.7861495	747.0702638	1890.013177	2248.89075	1031.78202	850.291327
ENSMUSG00000016918.15	Sulf1	-0.560730656	0.00063407 2	0.03600415 4	197.5695997	153.0048945	184.0949184	174.9195658	338.3199899	241.547525	220.945125	243.470046
ENSMUSG00000103502.1	933012 1J05Rik	3.83158027	0.00063931 7	0.03609525 9	4.159359994	6.331237015	11.15726778	18.95680023	2.543759323	0	0	0
ENSMUSG00000020598.16	Nrcam	-1.968256948	0.00063951 7	0.03609525 9	3.119519995	4.220824677	10.22749547	2.585018214	33.91679097	23.1367361	6.34292225	14.8306627
ENSMUSG00000016024.9	Lbp	-0.807175387	0.00064659 5	0.03638548	47.83263993	45.37386527	54.85656659	41.36029142	100.9024531	97.1742918	75.0579133	55.614985
ENSMUSG00000045466.18	Zfp956	-0.636596803	0.00065475 5	0.03673466 6	118.5417598	78.08525652	118.081084	102.5390558	200.1090667	149.92605	156.458749	140.891295
ENSMUSG00000022510.14	Trp63	-2.458785381	0.00067419 3	0.03771266 8	19.75695997	0	0.929772315	3.446690952	66.98566217	25.9131445	26.4288427	11.122997
ENSMUSG00000074227.12	Spint2	0.706381741	0.00067656	0.03773277 4	266.1990396	256.4150991	160.8506105	167.1645112	115.3170893	134.19307	116.286908	155.721958
ENSMUSG00000022441.17	Efcab6	-3.725283186	0.00071852 8	0.03995480 6	3.119519995	0	0	0	25.43759323	3.70187778	3.17146113	6.17944278
ENSMUSG00000024236.18	Svil	-0.757433598	0.00073098 7	0.04052773 7	1325.795998	878.9867389	1363.046214	1251.148815	2921.931542	1851.86436	1712.58901	1658.56244

ENSMUSG00000029163.9	Emilin1	-1.011822841	0.00074461 7	0.04116201 3	276.5974396	294.4025212	330.0691719	314.5105493	437.5266035	1197.55746	383.746796	431.325106
ENSMUSG00000032712.16	Resf1	1.131185524	0.00075693 8	0.04172040 1	2965.623676	1585.974872	2963.184368	2602.251669	1174.368887	983.774021	1026.49625	1434.86661
ENSMUSG00000037016.11	Frem2	-3.081661599	0.00079267 6	0.04343538 2	3.119519995	0	2.789316945	0.861672738	28.82927233	9.25469446	13.7429982	4.94355422
ENSMUSG00000032355.16	Mlip	-3.469139074	0.00079186 1	0.04343538 2	42.63343994	3.165618507	2.789316945	0	351.0387866	90.6960057	62.3720688	30.8972139
ENSMUSG00000084929.1	Foxo6os	-3.748811036	0.00080877 3	0.04418860 2	11.43823998	0	0	0	78.00861923	34.2423695	28.5431501	9.88710845
ENSMUSG00000026817.14	Ak1	-0.796496055	0.00081947 7	0.04464369 6	1366.349758	1733.703736	1096.20156	1360.581253	3530.73794	2343.28864	2049.82104	1724.06454
ENSMUSG00000029442.18	Wdr66	-0.953158331	0.00083252 2	0.04522326 8	55.11151992	72.80922567	92.97723151	62.04043713	135.6671639	140.671356	164.915979	106.286416
ENSMUSG00000097574.1	C920006O11Rik	-1.124864686	0.00083792 8	0.04538578 1	25.99599996	10.55206169	14.87635704	21.54181845	37.30847007	32.3914306	31.7146113	59.3226507
ENSMUSG00000036854.14	Hspb6	-1.692888819	0.00084229 5	0.04549120 7	1098.071038	952.8511707	681.523107	792.7389189	5886.259073	2195.21353	2037.1352	1276.67288
ENSMUSG00000025777.8	Gdap1	-2.716784869	0.00084531 7	0.04552360 2	11.43823998	0	1.85954463	0	44.09182826	16.65845	17.97161 3	6.17944278
ENSMUSG00000030785.8	Cox6a2	-3.387027869	0.00085064 6	0.04567969 9	144.5377598	43.26345293	3.71908926	1.723345476	1317.667329	280.417242	306.574576	113.701747

ENSMUSG00000013076.17	Amotl1	-0.599203451	0.00085674 3	0.04574571 4	2894.914556	1807.568168	3396.458267	2909.007163	4764.461212	3787.02097	3823.72496	4302.12806
ENSMUSG00000022636.13	Alcam	-1.22078243	0.00085608 3	0.04574571 4	55.11151992	33.76659741	44.62907112	41.36029142	102.5982927	196.199522	56.0291466	51.9073194
ENSMUSG00000026208.9	Des	-1.175193613	0.00086629 4	0.04612465 2	3148.635515	5459.636719	2586.626581	2485.925849	14674.94753	5715.6993	5787.91656	4712.44306
ENSMUSG00000087038.9	290007 9G21Rik	-4.363872933	0.00089 59	0.04756621 9	0	0	0	0	10.17503729	2.77640834	1.05715371	0
ENSMUSG00000057280.15	Musk	-3.777553362	0.00090232 2	0.04777224	2.079679997	0	0	0.861672738	27.98135255	4.62734723	5.28576854	1.23588856
ENSMUSG00000107451.1	Gm44421	-1.107468083	0.00091275	0.04818859 8	28.07567996	43.26345293	56.71611122	31.02021857	107.6858113	43.4970639	91.9723727	100.106973
ENSMUSG00000029685.15	Asb15	-3.784077699	0.00092804 8	0.04872253 3	44.71311993	0	1.85954463	0	400.2181335	80.5158418	97.2581412	60.5585393
ENSMUSG00000031381.16	Piga	-0.641195164	0.00092588 8	0.04872253 3	63.43023991	39.04262826	55.78633891	56.8704007	98.35869382	73.1120862	82.4579893	81.5686447
ENSMUSG00000043342.9	Hoxd9	-0.8694805	0.00093393 8	0.04875932 1	38.47407994	39.04262826	49.2779327	40.49861868	114.4691695	68.484739	49.6862243	71.6815363
ENSMUSG00000041695.2	Kcnj2	-1.912154119	0.00093188 8	0.04875932 1	31.19519995	3.165618507	11.15726778	15.51010928	110.2295707	42.5715945	56.0291466	19.7742169
ENSMUSG00000097652.2	Mhrt	-4.67568499	0.00094065 5	0.04897400 8	0	0	0	0	11.87087684	3.70187778	2.11430742	0

ENSMUSG00000028033.16	Kcnq5	-1.081814874	0.00095166 2	0.04931139 7	36.39439995	17.93850488	31.61225871	14.64843654	67.83358194	62.9319223	47.5719169	32.1331025
ENSMUSG00000020722.5	Cacng1	-3.440403904	0.00095238 3	0.04931139 7	25.99599996	2.110412338	0.929772315	0	206.8924249	34.2423695	47.5719169	23.4818826
ENSMUSG00000042254.14	Cilp	-2.497365537	0.00095972 1	0.04955484 6	38.47407994	12.66247403	35.33134797	11.20174559	272.1822475	89.7705362	141.658597	46.9637651